



Ludwig-Maximilians-Universität



Sigillum Universitatis Ludovici Maximiliani

Gamma-ray Bursts and their Host Galaxies from Cosmological Simulation

Dissertation der Fakultät für Physik

DISSERTATION OF THE FACULTY OF PHYSICS

der Ludwig-Maximilians-Universität München

AT THE LUDWIG MAXIMILIAN UNIVERSITY OF MUNICH

für den Grad des

FOR THE DEGREE OF

Doctor rerum naturalium

vorgelegt von Maria Angela Campisi

PRESENTED BY



Sigillum Universitatis Ludovici Maximiliani

Prof. Dr. Rashid Sunyaev

(1st REFEREE)

Prof. Dr. Ralf Bender

(2nd REFEREE)

Prof. Dr. Gerhard Buchalla

(HEAD OF THE COMMITTEE)

Date of the oral exam: 4th December 2009

München, August 2009

Contents

Zusammenfassung	5
Abstract	7
1 Introduction	9
2 Gamma-ray Burst	13
2.1 Space missions	14
2.2 Global properties	20
2.2.1 Angular distribution	20
2.2.2 Temporal properties	21
2.3 Spectrum	23
2.4 Afterglow emission	25
2.4.1 Progenitors	27
2.4.2 Energy release	30
2.5 The standard scenario	30
2.5.1 The compactness problem	30
2.5.2 Fireballs	32
2.5.3 Shocks	35
3 Host Galaxies	41
3.1 Chance coincidence of a GRB with galaxy on sky	45
3.1.1 The Galaxy Luminosity Function	46
3.1.2 Morphology and Redshift Dependent LF	47
3.1.3 The Radius-Luminosity Relation	48
3.2 Computation of the Probability	49
3.3 Comparison with observed host galaxies	53

3.3.1 Discussion	57
4 Host Galaxies in Cosmological Simulations	59
4.1 The Simulated Galaxy Catalogues	59
4.2 Identification of LGRB host galaxies	61
4.3 Results	64
4.3.1 The cosmic star formation rate versus the LGRB rate	64
4.3.2 Physical properties of LGRB host galaxies	67
4.3.3 The environment of LGRB host galaxies	73
4.3.4 Descendants of high- z LGRB host galaxies	75
4.4 Discussion and Conclusions	78
5 Redshift Distribution of Long Gamma-ray Burst	83
5.1 Simulated LGRB rate	85
5.1.1 Star Formation History	86
5.2 Observed distribution of LGRBs	88
5.2.1 Beaming effect	88
5.2.2 LGRB luminosity function	89
5.2.3 Best fit: results	90
5.3 LGRB redshift distribution: results	93
5.3.1 Bright and Faint LGRBs	97
5.3.2 Low and High Luminosity LGRBs	99
5.4 Discussion and conclusions	100
6 Conclusions	103
7 Abstract of publications during the PhD project	107

Zusammenfassung

Gamma-ray Bursts (GRBs) gehören zu den energiereichsten Ereignissen im Universum. Aufgrund ihrer sehr großen Leuchtkraft sind sie bereits bis zu Rotverschiebungen von $z \sim 8.3$ beobachtet worden. Die vorliegende Arbeit beschäftigt sich mit einer speziellen Klasse von Gammastrahlungsausbrüchen, den so genannten "Long Gamma-ray Bursts" (LGRBs) sowie mit deren "Muttergalaxien", in welchen diese Ereignisse bisher beobachtet wurden. LGRBs sind durch eine Dauer von mehr als einigen Sekunden gekennzeichnet. Man geht heute davon aus, dass diese Ereignisse mit dem Kollaps schwerer Sterne (mit niedriger Metallizität), wie z. B. Wolf-Rayet Sternen assoziiert sind. Die beobachtbaren Eigenschaften der Muttergalaxien deuten an, dass LGRBs typischerweise in Galaxien mit aktiver Sternentstehung und vorallem in so genannten "irregulären Zwerggalaxien" auftreten. In der vorliegenden Arbeit werden hochaufgelöste N-Teilchen Simulationen mit semianalytischen Modellen zur Sternentstehung mit Galaxiekatalogen kombiniert um einerseits die Eigenschaften der Muttergalaxien von LGRBs und andererseits die Leuchtkraftfunktion (LF) sowie die Detektionsrate bei hohen Rotverschiebungen zu untersuchen. Um Schranken an die Metallizität der Vorläufersterne zu erhalten wurde die Rotverschiebungsentwicklung und verschiedene Modellierungsansätze mit Beobachtungen verglichen. In Übereinstimmung mit Beobachtungen stellt sich für die Eigenschaften der Muttergalaxien heraus, dass diese typischerweise eine niedrige Metallizität ($Z < Z_{\odot}$) haben, dass sie klein ($M < 10^9 M_{\odot}$), blauer und jünger als typische Galaxien sind. Desweiteren sind diese Muttergalaxien gleichmässiger verteilt als typische L_* Galaxien und ihre Nachfolger sind schwere rote Galaxien, welche in Galaxienhaufen mit Halomassen zwischen $10^{13} M_{\odot}$ und $10^{14} M_{\odot}$ zu finden sind. Eine weitere Schlussfolgerung der Arbeit ist es, dass LGRBs, falls sie aus metallarmen Vorläufersternen entstehen, keine guten Indikatoren für die Sternentstehungsrate im Universum sind, da sie bei niedrigen Rotverschiebungen einen immer geringeren Anteil der Sternentstehungsrate repräsentieren.

Darüberhinaus zeigen die Untersuchungen, dass die für LGRBs vorhandenen Modelle mit den Beobachtungen genau dann im Einklang sind, wenn die Vorläufersterne eine Rotverschiebung von $Z < 0.3Z_{\odot}$. Für die Häufigkeit heller Gammastrahlungsausbrüche wird die Voraussage getroffen, dass auf 100 LGRBs zwei bei Rotverschiebungen grösser als sechs eintreten sollten. Ferner zeigen die Simulationen, dass zwei Gruppen von Ausbrüchen mit einer Leuchtkraft von $L \leq (>) 10^{49} \text{erg/s}$ beobachtbar sein sollten, im Einklang mit den Beobachtungen.

Abstract

Gamma-ray bursts (GRBs) are the most energetic explosions in the Universe . Because of their very large luminosity, GRBs represent “cosmological” events, which have been detected up to $z \sim 8.3$, offering exciting possibilities to study astrophysics in extreme conditions. We focus this work in the study of Long Gamma-ray bursts (LGRBs) and their host galaxies. Their duration is longer than a few seconds and the currently favourite hypotheses is that LGRBs originate from the death of massive stars (with low metallicity), such as Wolf-Rayet stars. The observed properties of host galaxies of LGRBs indicate that they are typically found in star-forming galaxies, predominantly irregular dwarf galaxies.

We use galaxy catalogues constructed by combining high-resolution N-body simulations with semi-analytic models of galaxy formation to study: (i) the properties of LGRB host galaxies; (ii) the luminosity function (LF), the comoving rate and the detection rate at high redshift of LGRBs. In both cases, we investigate the redshift (z) evolution and we compare different modeling with observations, imposing different metallicity constraints on the progenitor stars.

Our main findings on the host galaxies’ properties are: they typically have low-metallicity ($Z < 0.5Z_{\odot}$) and they are small ($M < 10^9 M_{\odot}$), bluer and younger than the average galaxy population, in agreement with observational data; hosts galaxies are also less clustered than typical L_* galaxies in the Universe, and their descendents are massive, red and reside in groups of galaxies with halo mass between $10^{13} M_{\odot}$ to $10^{14} M_{\odot}$. Moreover when LGRBs are required to be generated by low-metallicity stars, they trace a decreasing fraction of the cosmic star formation rate at lower redshift, pointing to the conclusion that LGRBs are not good tracers of the star formation rate in the universe.

Our main findings on the LGRBs’ rate are: models where LGRBs are produced by star with $Z < 0.3Z_{\odot}$ and without evolution of the LF are in agreement with the data. We predict to have < 2 bright burst every 100 LGRB at redshift $z > 6$. Finally, dividing the GRB *Swift* sample according to their luminosity, we conclude that two populations of bursts with ridge $L \leq (>) 10^{49} \text{ erg/s}$ are observable, but they are also reproducible by our simulation, assuming the same model for progenitors (collapsar model) and same LF for low and high luminosity bursts.

Chapter 1

Introduction

Gamma-ray bursts (GRBs) are the most luminous explosions in the Universe (Zhang and Mészáros, 2004; Piran, 2005; Mészáros, 2006). As such, they offer exciting possibilities to study astrophysics in extreme conditions, e.g., radiative processes in highly relativistic ejecta (Huang et al., 2000; Fan and Piran, 2008, and references therein). Because of their very large luminosity, GRBs represent cosmological events, which have been detected up to $z \sim 8.3$ (Fernandez-Soto et al., 2009). It has been proposed that some tight correlations among GRB parameters can make them “standard candles” for probing the Universe to the high-redshift regime that supernovae Ia cannot attain (e.g. Ghirlanda et al. 2004a; Dai et al. 2004, Zhang 2007, and references therein. See however Li 2007a,b, 2008a).

It is well-known that the duration distribution of GRBs is bimodal (Kouveliotou et al., 1993), dividing GRBs into two classes: long GRBs (hereafter LGRBs) and short GRBs, depending on whether their durations are longer or shorter than a few seconds. The observed properties of host galaxies of short and long GRBs indicate that they have different progenitors. LGRBs are typically found in star-forming galaxies, predominantly irregular dwarf galaxies (Conselice et al., 2005; Fruchter et al., 2006; Wainwright et al., 2007). In contrast, short GRBs are found in both early-type and late-type galaxies. Many models have been proposed for explaining the origin of these two classes of GRBs. The currently favourite hypotheses are that short GRBs are produced by the merger of compact objects – between two neutron stars or between a neutron star and a black hole (Li and Paczyński, 1998; O’Shaughnessy et al., 2008), while LGRBs originate from the death of massive stars (with low metallicity), such as Wolf-Rayet stars. This scenario for the formation of LGRBs is usually referred to as the “collapsar model” (Yoon et al., 2006,

2008; Woosley and Heger, 2006).

Observational data are consistent with the hypothesis of a LGRB-supernova connection: at least some LGRBs are associated with core-collapse supernovae (Galama et al., 1998; Li, 2006; Woosley and Heger, 2006, and references therein). In addition, all supernovae associated with GRBs are Type Ic, which supports the hypothesis of Wolf-Rayet stars as progenitors of LGRBs. Because of their connection with supernovae, LGRBs are potential tracers of the cosmic star formation history (Totani, 1997; Wijers et al., 1998; Mao and Mo, 1998; Porciani and Madau, 2001). To date, there are 130 GRBs with known redshift and 50 with estimated host galaxy stellar mass (Savaglio et al., 2008). Given the difficulty in detecting and localizing short GRBs, most of the observational studies about host galaxies are for LGRBs, which will be the focus of this work. Studies of the physical properties of GRBs are not easy as they require deep targeted observations at high redshift. In addition, the probability for a chance superposition of GRBs and galaxies on the sky is significant for high- z GRBs, e.g. $\sim 3\%$ for galaxies at $z < 1.5$ (Campisi and Li, 2008).

The observational information gathered so far indicates that most LGRBs are found in faint star forming galaxies dominated by young stellar populations with a sub-solar gas-phase metallicities, although there are a few host galaxies with higher metal content (Prochaska et al., 2004; Wolf and Podsiadlowski, 2007; Fynbo et al., 2006; Price et al., 2007; Savaglio et al., 2003; Savaglio, 2006; Savaglio et al., 2008; Stanek et al., 2006, and references therein).

These accumulating phenomenological evidences provide the motivation guiding the following thesis.

The first part of the analysis concerns a deep investigation of the of host galaxies of LGRBs, using a galaxy catalogue constructed by combining high-resolution N-body simulations with a semi-analytic model of galaxy formation. In particular, we use the models discussed in Wang et al. (2008) for two cosmological models with parameters taken from the first-year and the third-year Wilkinson Microwave Anisotropy Probe (WMAP) (Spergel et al., 2003) measurements. To select candidate host galaxies of LGRBs, we extract from the available semi-analytic galaxy catalogues the information for the age and metallicity of newly formed stars and we adopt the collapsar model. We built

three samples of host galaxies with different metallicity thresholds, and we compare the properties of the selected galaxies with observational data, in particular the data in Savaglio et al. (2008). Compared with previous theoretical studies, the simulations used in our study have the largest volume, and they also allow us to explore the cosmological dependence. Finally, the information available from the semi-analytic catalogues enable us to study the clustering and descendent properties of LGRB hosts.

The performed analysis allows to make interesting predictions of the GRB redshift distribution up to cosmological distances ($z=10$). In the second part of this thesis we have studied the luminosity function (LF), the comoving rate and the detection rate at high redshift of LGRBs in the context of a hierarchical model of galaxy formation. The difference of our work with respect to previous ones is that: 1) we do not use a proportional factor to estimate the LGRB's rate in the Universe but we extrapolate it from our simulated catalog of galaxies, assuming the collapsar model; 2) we take in consideration two scenario together, GRB LF evolution and low metallicity environments. In this way we overlap the error correlated with the LGRB density, deriving robust limits for the LF and for the formation and detection rate of LGRBs at high redshift.

Chapter 2

Gamma-ray Burst

Gamma-ray bursts (GRBs) are fascinating celestial objects. They are, by definition, electromagnetic signals in the γ -ray band (in the spectral domain) with short durations (in the temporal domain). They are, however, unusual in having most of their electromagnetic output in γ -rays, typically at sub-MeV energies (~ 100 keV - 1 MeV), and having most of it concentrated into a brief episode, lasting from a fraction of a second to several tens of seconds. The study of GRBs has been prolific over the past several years. New discoveries on GRBs have been ranked several times as one of the “top-ten scientific breakthroughs of the year” by Science magazine (e.g. #6 in 2003 and #4 in 2005). The topic of GRBs has been extensively reviewed over the years (e.g. Fishman and Meegan (1995); Piran (1999); van Paradijs et al. (2000); Mészáros (2002); Lu et al. (2004); Zhang (2007)).

GRBs were discovered serendipitously in the 1960s by military satellites monitoring for nuclear explosions in verification of the Nuclear Test Ban Treaty. This became public information only several years later, when the announcement of this major discovery was finally reported in 1973. For the next 20 years, hundreds of GRB detections were made, and, frustratingly, they continued to vanish too soon to get an accurate angular position to permit any follow-up observations. During the last two decades, the understanding of GRBs has been revolutionized more by observational progress rather than by theoretical predictions. A first major advance in the comprehension of the GRB phenomenon occurred in 1991 with the launch of the Compton Gamma-Ray Observatory (CGRO). The all-sky survey from the Burst and Transient Experiment (BATSE) on-board CGRO measured about 3000 bursts and showed that they were isotropically distributed, thus suggesting a cosmological origin.

The launch of the NASA’s dedicated GRB mission, Swift (Gehrels and et al (2004)),

has opened a new era for GRB study. Carrying three instruments (Burst Alert Telescope [BAT], Barthelmy et al. (2005), X-Ray Telescope [XRT], Burrows et al. (2005); and UV-Optical Telescope [UVOT], Roming et al. (2005)), Swift is a multi-wavelength observatory that can “swiftly” catch the unpredictable bursts of gamma-rays in the random directions of the sky within less than 100 seconds with all three instruments on target. It allows for the first time detections of multi-wavelength GRB early afterglows in a time domain previously unexplored. In slightly over four years of operation, Swift has fulfilled most of its pre-mission scientific goals in GRB study, and more importantly, brings new surprises and challenges to our understanding of these nature’s most violent and mysterious explosions. The Swift revolution has been summarized in several recent reviews (e.g. Mészáros (2006); Zhang (2007)).

Ever since the establishment of their cosmological nature, GRBs promised to become new probes of cosmology and galaxy evolution. As the numbers of GRB redshifts and detected hosts and afterglows grew, it became possible to use GRBs in new, systematic studies in cosmology.

2.1 Space missions

In these ~ 40 years the major advances in the GRB science coincided with the launch of successful space missions dedicated to their study.

The Burst And Transient Source Experiment (BATSE - Fishman and Meegan (1995)) on board the NASA Compton Gamma Ray Observatory (**CGRO**, 1992-2000) detected up to 3000 GRBs. This large GRB sample showed that: (1) GRBs are of two types: those lasting less than a few seconds (called Short) and those lasting a few tens of seconds (called Long) with the latter being on average softer than the former; (2) GRB emission can vary on very short timescales of even a few milliseconds, thus suggesting that the emission is produced by a relativistically expanding plasma; (3) the isotropic sky distribution suggested that they originate at cosmological distances, although no distance measure was possible, in the BATSE era, due to the large uncertainty (more than 1 degree) of the GRB position based on the BATSE data.

In 1996 the **Beppo-SAX** satellite, the result of an Italian-Dutch collaboration

(Boella et al., 1997), was launched. One of its objectives was the search for the X-ray counterpart of GRBs which was predicted by the theoretical fireball model (Rees and Meszaros, 1994). Beppo-SAX caught the first GRB X-ray counterpart (GRB 970228 - Costa et al. (1997)), so called “GRB afterglow”. The precise localization (with only few arcmin uncertainty) of the GRB X-ray counterpart, allowed also the identification of its optical afterglow. With ground based large optical telescopes the first redshift was directly measured ($z = 0.695$). After this, several other GRB afterglows were found by the Beppo-SAX satellite and their redshifts confirmed their cosmological origin. The great debate between B. Paczynski (who supported the cosmic origin of γ -ray bursts) and D. Lamb (who thought GRBs to lie in the galactic halo of the Milky Way) thus came to an end.

The typical temporal and spectral properties of the X-ray afterglows detected by Beppo-SAX were interpreted as due to the deceleration of the relativistic material, ejected by a newly formed black hole, in the circumburst medium. The study of the afterglow in the Optical/IR from ground, showed that it has temporal and spectral properties similar to those observed in the X-ray band. Beppo-SAX also contributed one of the milestones in the GRB field: the first GRB-SN association of GRB 980425 with the nearby ($z = 0.008$) Type Ic supernova SN1998bw (Galama et al. (1998)). This was the first observational evidence that long GRBs are produced by the core collapse of very massive stars.

Beppo-SAX’s success is due to the possibility to detect GRBs and promptly follow their soft X-ray emission in the energy band down to 2 keV with the Wide Field Cameras (WFC). Despite this advantage most bursts detected by the Beppo-SAX satellite, due to orbit and slew constraints, were observed in the X-ray band starting only few hours after the burst onset. Only in some cases the observations started soon after the trigger. The most famous case is GRB 990123 which showed an extraordinary bright optical emission temporally coincident with the prompt. This was interpreted (Mészáros and Rees (1999)) as the emission from the shock which is propagating backward into the relativistically expanding ejecta. GRB 990123 enforced the importance to observe the burst in the Optical and soft X-ray band as soon as possible.

Partially overlapped to the SAX mission, the international satellite High Energy Transient Explorer (**HETE-II**) with French and Italian participation, dedicated to the

study of GRBs, detected and localized several GRBs from 2001 up to 2004. Together with Beppo-SAX, it contributed to the discovery of a new population of bursts: the X-Ray Flashes (XRF) which have temporal properties of normal GRBs but are much softer (Sakamoto et al. (2005)). The nature of these soft bursts is still debated. HETE-II also discovered another GRB-SN association: GRB 030329 - SN2003dh (Stanek et al. (2003); Hjorth et al. (2003)).

Beppo-SAX and HETE-II also opened the era of extensive observation campaigns in the Optical/NIR and Radio band from ground. Two results are worth mentioning: (1) about 50% of the bursts with detected X-ray afterglow have no Optical counterpart (dubbed “Dark bursts”); (2) the afterglow optical light curve typically shows a steepening at 1-2 days after the burst onset. If the typical break is interpreted as due to the collimation effects of the burst (Frail et al., 2001) it can be used to infer the jet opening angle. The GRB isotropic equivalent energy, estimated for the few bursts with known redshift appeared extreme, i.e. up to 10^{55} erg (note that a solar mass totally converted into radiation corresponds to $M_{\odot}c^2 \simeq 2 \times 10^{54}$ erg). Instead, if GRBs are collimated within a jet opening angle, which can be measured from the optical break time, their true energy is typically 10^{51} erg.

The observational picture of GRBs depicted during the so-called “BATSE and Beppo-SAX era” led to the confirmation of the standard fireball model (e.g. Rees and Meszaros (1994)) which explains GRBs as the result of the formation of black holes through the core collapse of very massive stars. The emission in the γ -ray band is due to the deceleration of the plasma by the external medium. Although several alternatives to this model were proposed, it collected the largest consensus in the scientific community because it could explain several observations. However, some observational facts (e.g. prompt emission spectra; relative energy content of the prompt and afterglow phase) still represented a major issue at the end of 2004 when a new era was beginning.

The INTErnational Gamma-Ray Astrophysics Laboratory (**INTEGRAL**) satellite, a mission of the European Space Agency with contribution from Russia and NASA, was launched in October 2002. Although this mission was not designed to detect GRBs, the large field of view ($\sim 30 \times 30$ degrees) of the coded mask instrument IBIS (Ubertini et al., 2003) and the implementation of a dedicated automatic software for GRB triggering (IBAS

- Mereghetti et al. (2003)) allowed to localize many bursts in the 15–200 keV energy range with an accuracy of a few arcmin. The burst coordinates are then distributed in real time, so that rapid follow-up observation can be performed with ground-based telescopes and other high energy satellites. One of these fast GRB localizations (GRB 031203, which is, by the way, one of the few cases of a nearby GRB associated with a spectroscopically identified SN), followed by a pointed observation with the XMM-Newton X-ray satellite, allowed to discover the first dust scattering X-ray halo around a GRB (Vaughan et al., 2004).

In November 2004 the international *Swift* satellite (Gehrels and et al, 2004) was put in orbit. It is the result of a fruitful collaboration between US, English and Italian institutes and its primary goal was to detect several GRBs and promptly re-point its narrow field instruments (the X-Ray Telescope - XRT which covers the 0.3–10 keV energy range; the UV-Optical Telescope - UVOT) in the burst direction to follow the X-ray and Optical afterglow. The localization of the GRB with the coded mask detector (BAT) with an accuracy of a few arcmin allows, in 90% of cases, the satellite to slew and point the GRB location within 1-3 minutes. The observation with the narrow field instruments refines the GRB position to arcsec level (necessary to search for the optical transient). Finally, the follow up of the burst from ground leads the measurement of its redshift and to study its Optical/NIR afterglow.

In the *Swift* era the observational picture of GRBs dramatically advanced. The observation of the X-ray and optical afterglow starting, in most cases, only a few minutes after the burst explosion revealed an unexpected behavior often in contrast with the predictions of the standard afterglow theory. *Swift*, for the first time, showed that also the elusive class of short GRBs shares some common properties with long events: GRB 050509B (Gehrels et al., 2005) was the first short burst with an associated afterglow. About 8% of the *Swift* bursts with measured redshift are at $z > 5$ with the farthest at $z \sim 8.2$ (Fernandez-Soto et al., 2009; Tanvir et al., 2009; Salvaterra et al., 2009a). This proves that massive stars were already formed at that cosmic epoch. The X-ray observation of *Swift* also suggested the possibility that, previously unexpected, the inner engine of GRBs can be active for thousands of seconds in order to produce the late time flares observed in one third of *Swift* GRBs. In some cases these late time flares can have

an integrated power which is comparable to or even exceeds that of the prompt emission (Burrows et al., 2005). Moreover, *Swift* showed that GRBs and supernovae are intimately connected: GRB 060218, a burst extraordinarily long and with a very soft spectrum, was interpreted as the first detected supernova in the act of exploding (Campana et al., 2006).

The observational discoveries of *Swift*, intriguingly, opened more issues and questions about the nature of GRBs that challenged the standard theoretical interpretation. Several groups are trying either to reconcile the present observational puzzle with the standard model or to formulate a completely new theory for the origin of GRBs. In this context it is mandatory to proceed forward to add new decisive observational results possibly completing one of the major lack of *Swift*, i.e. the study of the prompt/high energy GRB emission. Indeed, while the *Swift*-BAT instrument is fundamental to promptly locate (with a few arcmin precision) GRBs from a large portion of the sky, it cannot provide enough spectral information for most GRBs because of its limited 15–150 keV energy range. Only for about 20% of the burst detected by *Swift*, BAT can properly constrain the prompt emission spectral parameters. For some bursts detected also by other satellites like the IPN **Konus-Wind** or the Japanese **Suzaku**, it is possible to obtain this precious information. It was recently discovered (Amati et al., 2002) that the isotropic energy released by the burst during the prompt phase is correlated with the “color” of the burst, i.e. the peak energy of its νF_ν spectrum which is a good proxy of the characteristic energy of the photons emitted. If the collimation correction is included the large scatter of this correlation is reduced (Ghirlanda et al., 2004b). The importance of the collimation-corrected correlation is twofold: its interpretation could help to understand the still debated physical process responsible for the emission in GRBs and it could be used to standardize the GRB energetics and use them as cosmological probes (Ghirlanda et al., 2004a). However, this is possible only if new bursts with known redshift have also their prompt emission spectral properties well determined.

The near future of GRBs will be dominated by the **Fermi** - Gamma ray Large Area Space Telescope (Fermi - Thompson (2004)) and the Astro-rivelatore Gamma a Immagini Leggero (**AGILE** - Tavani et al. (2006)), both launched in 2008. Already EGRET on board CGRO discovered emission at energies above 30 MeV from GRBs, albeit in only five cases. These cases are still a debated subject: in particular it is unclear if the very

high energy emission belongs to the prompt or to the afterglow. The Large Area Telescope (LAT) on Fermi (30 MeV - 300 GeV) has the possibility to verify these observations and to unveil the nature of the very high energy photons in GRBs. The possible synergy of Fermi, AGILE and *Swift* combined observations hold the promise to provide new diagnostic measurements for studying the broad band prompt and afterglow emission in GRBs.

AGILE has detected GRB 080514B at energies up to $\sim 300\text{MeV}$, and the high-energy emission lasted longer ($> 13\text{s}$) than the low-energy emission ($\sim 7\text{s}$) (Giuliani et al., 2008).

Fermi-LAT is expected to detect ~ 50 bursts per year, a fraction of which (those with position accuracy of < 20 arcmin) could be followed by *Swift* so to refine their position to a few arcsec (if detected by both XRT and UVOT). Also the low energy instrument Gamma Burst Monitor (GBM, 150 keV - 30 MeV) on board Fermi will detect ~ 200 bursts per year, although their localization will be poor (comparable to that of BATSE). This will prevent the follow up with ground based facilities unless the burst also triggered *Swift*. In these cases Fermi will provide a combined GBM+LAT spectrum. The precise number of such cases depends on several factors. The *Swift* and Fermi orbit are very similar and it is expected that about 15% of the time BAT and the LAT pointing will be within 50 deg. The present expectation is for $\sim 8 - 12 \text{ yr}^{-1}$ joint detections, considering the possible pointing strategies optimized to this goal (Gehrels and Cannizzo, 2007).

While most of these hopes will have to wait a bit longer, Fermi has already provided some very interesting initial results during its first half-year of operation. The spectrum of most GRBs detected so far by both the GBM and the LAT is consistent with a single Band function, suggestive of a single dominant emission mechanism in the observed energy range, as is also suggested by the LAT GRB detection rate. Longer lived high-energy emission compared to the low-energy emission (in some cases lasting $> 103\text{s}$) appears to be common in LAT GRBs. Particularly interesting LAT GRBs are GRB 081024B, the first clearly short GRB detected above 1 GeV, and the exceptionally bright and energetic GRB 080916C that provided a wealth of information leading to tight lower limits on the bulk Lorentz factor of the emitting region and the quantum gravity mass. Finally, there is still a lot to look forward to from Fermi.

Future missions dedicated to the study of γ -ray bursts are:

- The POET mission (POLarimeters for Energetic Transients) to be launched in 2012. The main scientific objective will be the measure of the polarization of GRB emission between 2 and 500 keV.
- The Joint Astrophysics Nascent Universe Satellite (JANUS), scheduled for 2012. Its primary objective is to study the very high redshift universe and in particular the re-ionization era either through GRBs at $5 < z < 12$ (and thus reconstructing the star formation rate in this unexplored range) and through QSOs in the $6 < z < 10$ range, to quantify their contribution to the re-ionization.
- The SVOM mission, scheduled for 2012-2013, dedicated to GRBs, with an Italian contribution. Similar to *Swift* (i.e. high energy X-Ray coded mask, soft X-Ray telescope, Optical telescope, fast slewing), it will also host a high energy instrument, similar to BATSE, to better characterize the prompt emission spectrum.

2.2 Global properties

It is quite difficult to summarize the basic features of GRBs. This difficulty is due to the enormous variety displayed by the bursts.

2.2.1 Angular distribution

BATSE observations proved with high level of accuracy that GRBs are isotropically distributed across the sky. Figure 2.1 shows the position of the 2704 bursts detected by BATSE, and it can be seen that their locations are distributed completely isotropically in the sky. Isotropy suggested a cosmological distribution, with no dipole or quadrupole components (Meegan et al., 1992). Furthermore, the number counts distribution of the BATSE bursts displayed a paucity of faint bursts relative to the number expected in an Euclidean space. This provided another piece of evidence for the cosmological origin of the sources (Fenimore et al., 1993). As a result, for the average flux of GRBs at a cosmological distance, the huge total luminosity of $L \sim 10^{51} \text{ erg/s}$ was inferred.

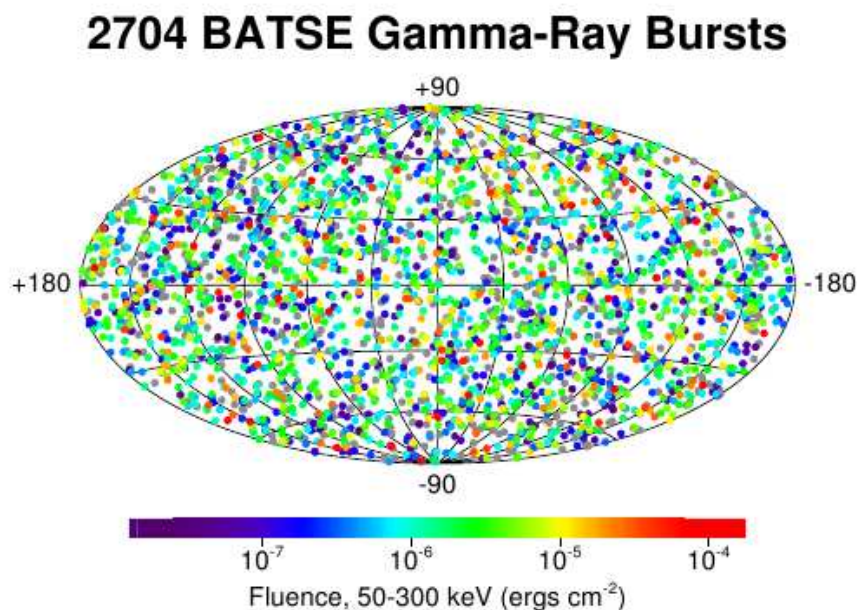


Figure 2.1 Distribution in the sky of 2704 GRBs seen by BATSE. The projection is in Galactic coordinates. Grey levels correspond to different fluences, i.e. the integral of the burst flux over time. Note the very high level of isotropy. This was one of the major results from BATSE. From Paciesas et al. (2000).

2.2.2 Temporal properties

Due to the diversity in the observed properties, it is not possible to define a “typical” event. GRBs exhibit an extremely large variety of time profiles. Their durations span 5 orders of magnitude, while their time histories can have diverse morphologies, from single-peaked to multiple-peaked events with a complicated structure (Fishman and Meegan, 1995). The main temporal properties of GRBs are listed below.

Temporal properties: duration

A “typical” GRB lasts for about 10 s. However, observed durations vary by six orders of magnitude, from few milliseconds to thousands of seconds. A non-negligible fraction of GRB (10-20%) is preceded or followed by emission with a lower flux and separated by the main emission episode by quiescent intervals which can last hundreds of seconds. The definition of duration is not unique. This is due to the fact that the start and end time of a burst strongly depend on its flux and on the value of the background. Burst duration is usually characterized through the T_{90} (or T_{50}) quantity, i.e. the time needed to accumulate from 5% to 95% (from 25% to 75%) of the counts in the energy band of

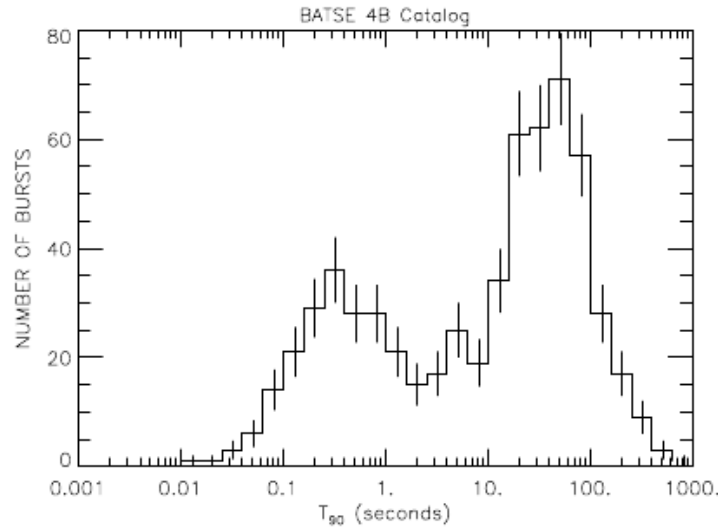


Figure 2.2 Bimodal burst distribution created with the BATSE T₉₀ times from the BATSE 4B Catalog. Light curves used for the calculation of T₉₀ are integrated over all 4 channels ($E > 20$ keV). This kind of distribution led to the conclusion that bursts are divided into "short" and "long" classes. From Paciesas et al. (2000).

the instrument which is being used.

The distribution of bursts is roughly bimodal, see Fig.2.2. Burst T_{90} durations can be divided into two sub-groups: long bursts with $T_{90} > 2$ s and short bursts with $T_{90} < 2$ s (Meegan et al., 1996). The number of short bursts is $\sim 25\%$ of the total. This does not necessarily mean that there are fewer short bursts, as there can be a selection effect of the instruments. For instance BATSE, having an harder trigger than BAT, privileged short bursts with respect to BAT (short bursts tend to be harder than long-soft ones). In fact BAT detected proportionally more long burst than BATSE.

Temporal properties: lightcurves and variability

The bursts have complicated and irregular time profiles which vary drastically from one burst to another. In most bursts, the typical variation takes place on a time-scale δT significantly smaller than the total duration of the burst, T . In a minority of the bursts there is only one peak with no substructure: in this case $\delta T \sim T$. A sub-class of this type of GRBs are the so called "FRED" bursts with a fast rise and exponential decay.

The smaller timescale of variation is usually in the millisecond range and does not vary from the beginning to the end of the burst (Fenimore, 1999). This latter observations imply that the γ -ray radiation cannot come from external shocks (at distances of $\sim 10^{16}$ cm from the engine), in which the slowing of the fireball should produce last pulses lasting longer than the first ones. Moreover, in this case the later the spike the broader. Such correlation has not been observed and thus variability is thought to be due to internal shocks occurring at much smaller distances $\sim 10^{13}$ cm.

2.3 Spectrum

Gamma ray bursts are characterized by emission in the few hundred keV range with a non-thermal spectrum. X-ray emission is weak (in “standard” GRBs) as only a few percent of the energy is emitted below 10 keV. On the other hand, most bursts have a high energy tail which contains a significant amount of energy. GRB 940217, for example, had a high energy tail up to 18 GeV (Hurley et al., 1994). In fact EGRET and COMPTEL observations are consistent with the possibility that all bursts have high energy tail. Fermi has already provided some very interesting initial results during its first half-year of operation. The spectrum of most GRBs detected so far by both the GBM and the LAT is consistent with a single Band function, suggestive of a single dominant emission mechanism in the observed energy range, as is also suggested by the LAT GRB detection rate.

The prompt emission is typically fitted by a Band model (Band et al., 1993), which is a smooth combination of two power laws. The smoothing takes place at an energy $\tilde{E} = (\alpha - \beta)E_0$. The fitting formula, developed for the photon number spectrum $N(\nu)$ is defined through:

$$N(\nu) = N_0 \begin{cases} (h\nu)^\alpha e^{-\frac{h\nu}{E_0}} & h\nu < (\alpha - \beta)E_0 \\ e^{\beta-\alpha}[(\alpha - \beta)E_0]^{\alpha-\beta}(h\nu)^\beta & h\nu > (\alpha - \beta)E_0 \end{cases} \quad (2.1)$$

where α and β represent the spectral indices at low and high energies, respectively. There is no particular theoretical model that predicts this spectral shape. Still, this function provides an excellent fit to most of the observed spectra. For most observed values of α and β , $\nu F_\nu \propto \nu^2 N(\nu)$ peaks at $E_{\text{peak}} = (\alpha + 2)E_0 = [(\alpha + 2)/(\alpha - \beta)]\tilde{E}$ (Piran, 2005).

Typical values found in the observed spectra are $\alpha \approx -1$, $\beta \approx -2.3$ and $E_0 \approx 250 \text{ keV}$. The “typical” energy of the observed radiation is E_{peak} .

The prompt emission often shows a spectral evolution: it is harder at the beginning of the burst (with a typical characteristic photon energy of few MeV) and becomes softer (tens of keV) to the end of the burst. Short events are harder than long bursts. “X-Ray Rich GRBs” and “X-Ray Flashes” (XRFs i.e. long duration GRBs with a soft spectrum) have been widely discussed as forming an apparently new type of transient events with respect to conventional GRBs. Since the discovery of XRF several suggestions for their interpretation have been done. They can be roughly divided into two categories: XRF differ from GRBs extrinsically (different distances or viewing angles) or intrinsically (different physical parameters, different radiation mechanisms, or even different progenitors and central engines).

The prompt emission spectral properties of GRBs with measured redshifts are highly correlated. In particular there exists a positive correlation between the characteristic spectral peak energy (of the νF_ν spectrum) and the isotropic equivalent energy of the prompt phase (Amati et al., 2002). However, both on the observational (Frail et al., 2001) and theoretical (Rhoads, 1997) ground, there are evidences that GRBs are all but isotropic sources. The correct proxy of the GRB energetics should, therefore, account for the collimated nature of these sources. Indeed, by estimating the GRB opening angle from the measurements of the jet break observed in the late optical light curves, the dispersion of the isotropic energy is reduced and a stronger/tighter correlation between the peak energy and the true GRB energy is found (Ghirlanda et al., 2004b, 2007). Several other correlations have been found between spectral and temporal properties of the prompt emission (Reichart and Stephens, 2000; Norris et al., 2000; Firmani et al., 2006). Through these correlation GRBs energetics can be standardized and they can be used to constrain the cosmological parameters (e.g. Ghirlanda et al. (2006)). However, jet breaks are not found for most *Swift* GRBs. E.g. Burrows and Racusin (2006) examine the Swift/X-ray Telescope (XRT) light curves from the first ~ 150 gamma-ray burst (GRB) afterglows. Although they expected to find jet breaks at typical times of 1-2 days after the GRB, they find that these appear to be extremely rare. Typical light curves have a break in the slope at about 104 s, followed by a single power-law decay whose slope is much too shallow to be consistent with expectations for jet breaks. X-ray light

curves typically extend out to ~ 10 days without any further breaks, until they become too faint for the XRT to detect. In some extreme cases, light curves extend out to more than two months without evidence for jet breaks. In agreement with some following studies (e.g. Liang et al. (2008); Willingale et al. (2007); Kocevski and Butler (2008); Evans et al. (2009); Racusin et al. (2009)).

This raises concerns about our understanding of afterglow and jet dynamics, and of GRB energetics.

2.4 Afterglow emission

Afterglows have been detected in the X-ray, the optical/infrared and the radio bands (e.g. Gehrels et al. (2007)). The light curve generally decays as a power law. The afterglow is almost always detected in X-rays, but only half of GRB afterglows have been detected in the optical (others are called “dark” GRBs). In X-ray, the early afterglow often decays very rapidly, more than in the optical band. In a few cases the optical afterglow shows an early rising light curve (e.g. GRB 990123, 060418, 060607 and the “naked eye”¹ GRB 080319B). This rising phase is more common in the, still few, observed radio afterglow. Both the X-ray and optical afterglows often show deviations from the simple power law decay such as steepenings, bumps and wiggles.

Essentially every GRB with an afterglow detection has an underlying host galaxy. The GRB host galaxy properties (magnitude, redshift distribution, morphologies, etc) are typical of normal, faint, star forming galaxies. The GRB afterglow positional offsets with respect to the host galaxy are consistent with GRBs being associated with the star forming regions within their host galaxies.

X-RAY

One of the major discoveries of Swift is the identification of a canonical X-ray afterglow behavior that can be roughly separated into a total of five phases (not necessarily observed in all bursts) which we show in Fig. 2.3.

(1) Steep decay phase (typically smoothly connected to the prompt emission) with a temporal decay slope ~ -3 or steeper, which is observed to last up to $10^2 - 10^3$ s after the

¹ This burst, observed in optical during the prompt emission phase, reached the remarkable magnitude ~ 5.3 . With clean and dark sky, we could have seen it with our own eyes.

burst.

(2) Shallow decay phase with a temporal decay slope ~ -0.5 or flatter extending to $\sim 10^3 - 10^4$ s. At this time the light curve steepens.

(3) A normal decay slope (average value ~ -1.2)

(4) Post Jet break phase following the normal decay phase, typically with a decay slope ~ -2 , (in agreement with the jet model predictions).

(5) X-ray flares appear in nearly 30% of GRB afterglows. Sometimes multiple flares appear in a single GRB, typically have very steep rising and decaying slopes. They occur in both long-duration and short duration GRBs and also in XRFs although only a few have been observed in short GRBs.

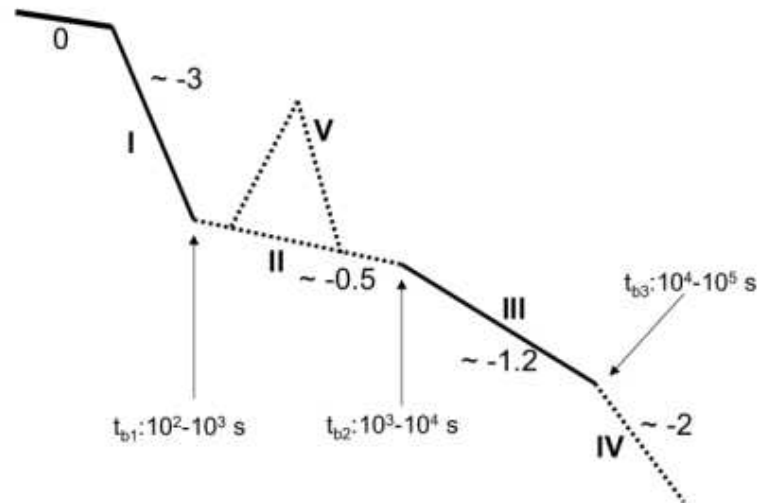


Figure 2.3 Scheme of an X-Ray light curve as seen by *Swift* (Zhang, 2007)

Except for the normal decay and the jet-break phases, all the other three components were not expected in the pre-*Swift* era. As of the time of writing, the steep decay phase and X-ray flares are better understood, while the shallow decay phase is still a mystery.

OPTICAL/IR and RADIO

One of the most intriguing results of the follow up of the optical afterglows in GRBs has been the detection of temporal breaks which are interpreted in the standard GRB scenario as signatures of the collimation of the fireball. This discovery allowed to relax the energetic demand of GRBs which would have a true energy of 10^{51} erg, a factor 100-1000 less than the isotropic value.

Broad-band modeling of the optical/IR to Radio afterglow was possible only for a handful of well observed bursts that turned out to be consistent with the standard afterglow predictions. In some cases, very early optical flashes have been observed (e.g., GRB 990123; GRB 021004, GRB 080319B), which are generally interpreted as emission from the reverse shock as it crosses the fireball.

In the Swift era, UVOT has been promptly observing the optical afterglow starting ~ 100 s after the burst triggers for most GRBs. Ground-based robotic telescopes (e.g., ROTSE-III, PAIRITEL, RAPTOR, P60, TAROT, Liverpool, Faulkes, KAIT, PROMPT, etc.) have promptly observed most targets within their observational constraints. However, the majority of bursts have very dim or undetectable optical afterglows. In only two cases (GRB 060418 and 060607A) the densely-covered early optical afterglow light curves display a round-shaped single bump that could be interpreted as the forward shock emission at the onset of afterglow. In all these cases there is no evidence of a reverse shock component.

Besides these “well behaved” (i.e. understood by the standard model) cases, there are other GRBs with optical flares at later times, and some (e.g. GRB 060313) with properties similar to X-ray flares, which demands a similar interpretation. Interestingly, despite the wide variety of temporal decays observed in the optical afterglows, the luminosity of most GRBs at 12 hours since their explosions seems to be quite universal (Nardini et al., 2006). This result is still unexplained.

2.4.1 Progenitors

A few long GRBs have been firmly associated with SN type Ib/c events (through optical spectroscopic features of SNe emerging in otherwise fading GRB optical afterglows). Other tentative associations are based on red bumps in the optical light curves. The

hosts galaxies of long GRBs appear as irregular dwarf (and spiral in a handful of cases) with moderate/intense star formation signatures. Moreover, GRBs are located in star forming regions within their hosts. These evidence support the idea that the progenitors of long GRBs are single massive stars whose core collapses to a black hole, either directly or after a brief accretion episode. This scenario is referred to as the collapsar or hypernova scenario and is drawn in Fig.2.4.

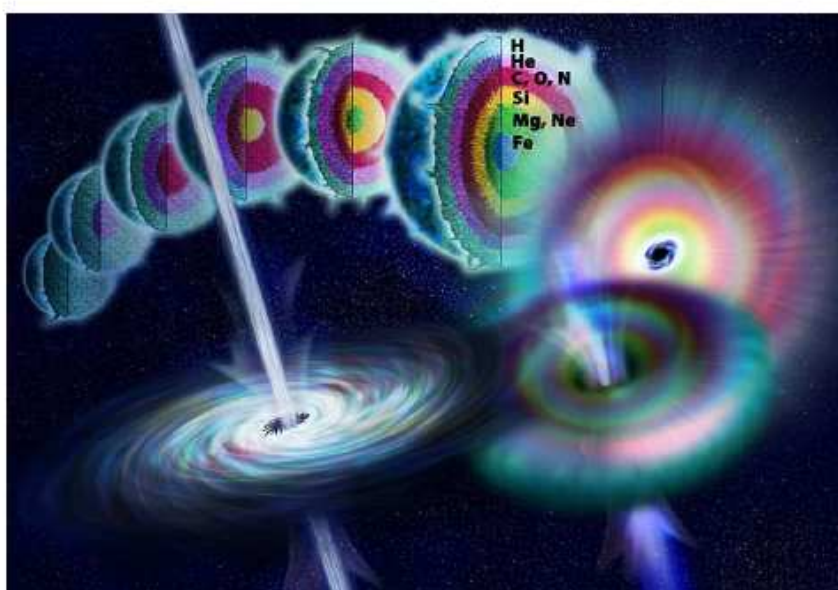


Figure 2.4 Artist's view of a *collapsar* during the phases resulting eventually in a GRB.

Instead, for the class of short GRBs, the progenitor nature is still debated. The most widely speculated candidates are mergers of two compact objects (either two neutron stars or a black hole and a neutron star). Recent population synthesis studies suggest that the durations of the bursts are typically “short” due to the rapid dynamical timescale and the limited materials to fuel the putative black hole at the central engine. The double compact merger scenario would preferentially locate short GRBs in early type galaxies (and possibly in the outskirts due to the long time delay between the formation of the binary system and its final catastrophic end), despite the (still) few localization put short bursts in almost all galaxy types. Both these progenitor types are expected to have, as an end result, the formation of a few solar masses black hole, surrounded by a temporary debris torus whose accretion can provide a sudden release of gravitational energy, sufficient

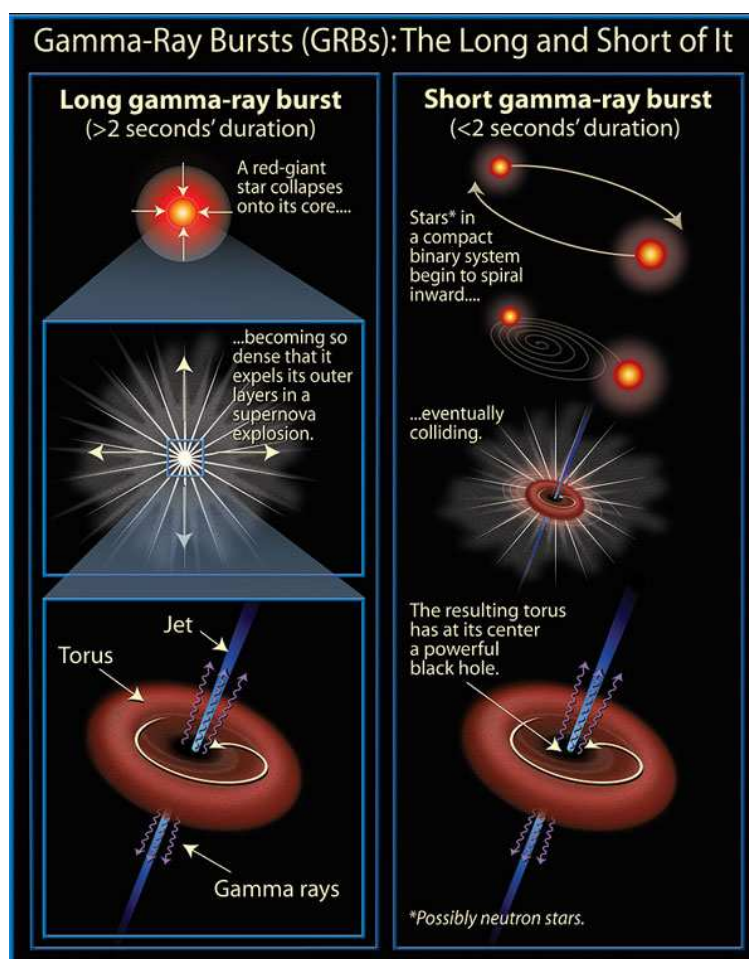


Figure 2.5 Artist's view of the *collapsar model* for Long-GRB and *merger of 2 compact objects* for Short-GRB.

to power a burst. The rotational energy of the spinning black hole is another energy reservoir. An important point is that the overall energetics from these various progenitors need not differ by more than about one order of magnitude. The duration of the burst in this model is related to the fall-back time of matter to form an accretion torus around the BH or the accretion time of the torus for the class of long and short bursts, respectively.

Other promising scenarios include the formation from a stellar collapse of a fast-rotating ultra-high magnetic field neutron star (a "magnetar"), i.e. the cosmological analogous of the few objects observed in our Galaxy to produce sporadic intense outbursts (giant flares) of gamma rays. Magnetars are also thought to be responsible for sporadic intense very short flares like the famous event of Dec 24th 2004 produced by well known galactic object (e.g. Hurley et al. (2005)). After this event, so exceptional that it saturated the detectors of in-orbit satellites, it was proposed that also a fraction of short

GRBs could be the extragalactic equivalent of these giant flares from highly magnetized neutron stars, although this possibility is still an open issue (e.g. Lazzati et al. (2005)).

2.4.2 Energy release

The current interpretation of the energy release in GRBs is that a large amount of gravitational energy (roughly a fraction of a solar mass) is released on short time-scales (seconds or less) in a very small region (tens of kilometers or so) by a catastrophic stellar event, i.e. the collapse of the core of a massive star, or the merger of two remnant compact cores for long and short bursts, respectively. Most of the available energy would escape in the form of thermal neutrinos and a substantial fraction may be emitted as gravitational waves. Only a small fraction of the available energy will lead to the formation of a very high temperature fireball expanding at highly relativistic speeds, which undergoes internal dissipation (Rees and Meszaros, 1992) events leading to gamma-ray prompt emission and it would later develop into a blast wave (Meszaros and Rees, 1993) as it decelerates against the external medium, producing an afterglow which gets progressively weaker.

The nature of the dissipation process is still debated. If “matter dominated” the fireball could develop relativistic shocks which accelerate electrons that radiate in a strong magnetic field through synchrotron. Alternatively, the fireball could be dominated by its magnetic field which can dissipate through, e.g. reconnection events (e.g. Lyutikov (2006)).

2.5 The standard scenario

2.5.1 The compactness problem

The key to unveil γ -ray burst physics lies in the understanding of how they bypass the compactness problem. This problem was realized very early on, in one form by Rudermann (1975) and in another way by Schmidt (1978). Both used it to argue that GRBs could not originate from cosmological distances. Now, we understand that GRB are cosmological and special relativistic effects enable us to overcome this constraint.

The simplest way to the compactness problem is to estimate the average opacity of the high energy gamma-rays to pair production. Consider a typical burst with an observed fluence f . For a source emitting isotropically at a distance D this fluence corresponds to

a total energy release of:

$$E = 4\pi D^2 f \approx 10^{50} \left(\frac{D}{3000 \text{ Mpc}} \right)^2 \left(\frac{f}{10^{-7} \text{ ergcm}^{-2}} \right) \text{ erg} \quad (2.2)$$

Cosmological effects change this equality by numerical factors of order unity that are not important in this discussion. The rapid temporal variability on a time scale $\delta t \approx 10$ ms implies that the source is compact with a size $R < c\delta t \approx 3000$ km. The observed spectrum contains a large fraction of high energy γ -ray photons. These photons (with energy E_1) could interact with lower energy photons (with energy E_2) and produce electron-positron pairs via $\gamma\gamma \rightarrow e^+e^-$ if $\sqrt{E_1 E_2} > m_e c^2$ (up to an angular factor). We denote by g_p the fraction of photon pairs that satisfy this condition. The average optical depth for this process is:

$$\tau_{\gamma\gamma} = g_p \frac{\sigma_T f D^2}{R^2 m_e c^2} \quad (2.3)$$

or:

$$\tau_{\gamma\gamma} = 10^{13} g_p \left(\frac{D}{3000 \text{ Mpc}} \right)^2 \left(\frac{f}{10^{-7} \text{ ergcm}^{-2}} \right) \left(\frac{\delta t}{10 \text{ ms}} \right)^{-2} \quad (2.4)$$

where σ_T is the Thomson cross section. This optical depth is huge. Even if there are no pairs at the very beginning, they will form rapidly and then these pairs will Compton scatter lower energy photons, resulting in a huge optical depth for all photons. However, the observed non-thermal spectrum indicates with certainty that the sources must be optically thin.

The compactness problem is a consequence of the assumption that the size of a source emitting radiation cannot be larger than the smallest observed time scale of variability times the light speed (*causality* constraint). This equation holds only if the emitting source and the observer are at rest with respect to each other.

Relativistic motion

The constraint on the compactness for pair production of GRBs comes from the measurement of (i) the variability time-scale and (ii) the energy of photons. However, both these quantities are modified if the source and the observer are not at rest. Consider a source of radiation that is moving toward an observer with relativistic velocity characterized by a Lorentz factor $\Gamma = 1/\sqrt{1 - v^2/c^2} \gg 1$. Photons with an observed energy $h\nu_{obs}$ have been blue-shifted and their energy at the source was $\approx h\nu_{obs}/\Gamma$. Since the energy at the source is lower, fewer photons have sufficient energy to produce pairs. Now

the observed fraction g_p of photons that could produce pairs is not equal to the fraction of photons that could produce pairs at the source. The latter is smaller by a factor $\Gamma^{-2\tilde{\alpha}}$ (where $\tilde{\alpha}$ is the energy spectral index) than the observed fraction. At the same time, relativistic effects allow the radius from which the radiation is emitted, $R < \Gamma^2 c \delta T$ to be larger than the original estimate, $R < c \delta T$, by a factor of Γ^2 . We have then:

$$\tau_{\gamma\gamma} = \frac{g_p \sigma_T f D^2}{\Gamma^{2\tilde{\alpha}} R^2 m_e c^2}$$

or:

$$\tau_{\gamma\gamma} = 10^{13} \frac{g_p}{\Gamma^{4+2\tilde{\alpha}}} \left(\frac{D}{3000 \text{ Mpc}} \right)^2 \left(\frac{f}{10^{-7} \text{ ergcm}^{-2}} \right) \left(\frac{\delta t}{10 \text{ ms}} \right)^{-2}$$

where the relativistic limit on R was included in the second line. The compactness problem can be resolved if the source is moving relativistically towards us with a Lorentz factor $\Gamma > 10^{13/4+2\tilde{\alpha}} \approx 10^2$. Such extreme relativistic motion is larger than the relativistic motion observed in any other celestial source. Extragalactic super-luminal jets have, for instance, Lorentz factors of $\Gamma \sim 10$, while the known galactic relativistic jets have $\Gamma \sim 2$ or less.

Two possible scenarios can be drawn: (1) a relativistic motion in the dynamical context of fireballs (see next session) and (2) a kinematic solution in which the source moves relativistically and this motion is not necessarily related to the mechanism that produces the burst, i.e. the source as a whole moves toward the observer. However, the latter solution is energetically more demanding since for a solar mass progenitor, moving at $\Gamma = 100$ the total energy required would be $E = \Gamma M_{\odot} c^2 \sim 2 \times 10^{56}$ erg. Moreover, in the first solution the kinetic energy is comparable to the observed energy of the GRBs: in this case the γ -ray emission and the relativistic motion are related and are not two separate phenomena. This is the case if GRBs result from the slowing down of ultra-relativistic matter. This idea was suggested by Meszaros and Rees (1992,1993) in the context of slowing down of the fireball by material of the ISM.

2.5.2 Fireballs

The evolution of a homogeneous fireball can be understood by analogy with the early universe. Consider the rapid release of a huge amount of energy in a small volume. If the temperature is high enough, photons are highly energetic and pairs are formed. The opacity is large, and radiation cannot escape. The initial temperature, at equilibrium is

$T_0 = (L/4\pi r_0^2 \sigma)^{1/4} \sim 10^{10} L_{51}^{1/4} r_{0,7}^{-1/2} \text{ }^\circ\text{K}$, where r_0 is the initial length scale, i.e. some Schwarzschild radii².

Pure fireball

This huge energy content forms a sphere of hot plasma (photons and pairs), i.e. the fireball (see Fig. 2.5.3), which expands and accelerates under its own internal energy pressure, reaching relativistic speed ($\Gamma \gg 1$). If the expansion is adiabatic (i.e. no heat is transferred during the process, so that the internal energy E of the fireball remains constant), the comoving temperature T' and the volume V satisfy $T'V^{1/3} = \text{const}$. Moreover, conservation of energy (as viewed from the observer's frame) requires $E \propto \Gamma T' = \text{const}$ (photons are blueshifted), and by simple algebra we get:

$$\Gamma \propto V^{-1/3} \propto R, \quad (2.5)$$

$$T' \propto \Gamma^{-1} \propto R^{-1}. \quad (2.6)$$

The bigger the expansion, the lower the temperature. When T' reaches 20 keV pairs annihilate and are not replaced by newly created ones⁴. As the scattering optical depth τ scales with the inverse of the distance R , i.e. $\tau \propto R^{-1}$ the opacity, which scales linearly with the optical depth, drops consequently:

$$\tau \propto T', \quad (2.7)$$

and the energy is released in thermal photons. The resulting thermal spectrum has $k_b T \approx 1/3 \times \Gamma T_p$. Note that the observed temperature (cfr. equations 2.1 and 2.2) is approximately equal to the initial temperature.

In this case, the ‘‘pure fireball’’ evaporates, a strong single thermal signal is expected, but **no** afterglow can be produced.

‘‘Dirty’’ fireball

The situation is somewhat different if in addition to e^+e^- pairs, the fireball includes also some baryons (either injected with the original radiation, or present in the atmosphere

²Hereafter the convention $Q = 10^n Q_n$ is adopted in c.g.s units.

³The Lorentz factor for a particle, moving with speed v , is $\Gamma = 1/\sqrt{1 - (v/c)^2}$.

⁴If radiation had a step distribution, the boundary between pair creation and annihilation would be $T_p = m_e c^2 = 511 \text{ keV}$. However assuming a Plank distribution, the photons of the high energy tail can produce pairs also for lower temperatures.

surrounding the initial explosion, or both). This “baryonic loading” can influence the fireball evolution in two ways. First, when the fireball is baryon-loaded the energy distribution among matter and radiation is different. In the radiation-dominated regime, the Lorentz factor, matter density, radiation density, and their ratio scale as:

$$\Gamma \propto R, \quad \rho_{mat} \propto R^{-3}, \quad \rho_{rad} \propto R^{-4}, \quad \rho_{mat}/\rho_{rad} \propto R$$

If, at the point where $T' = T_p \approx 20$ keV, $\rho_{mat} > \rho_{rad}$ (the transition from the radiation dominated phase to the matter dominated one occurs at $\rho_{mat} = 4\rho_{rad}/3$), then a considerable fraction of the energy is not released through photons: it remains to the protons. The baryons are accelerated with the rest of the fireball and convert part of the radiation energy into bulk kinetic energy. The relativistic shell expands with constant thickness (in the observer frame) $\Delta R \sim R_{in}$ equal to the initial radius of the fireball R_{in} . In the observer frame the shell appears contracted due to its high Lorentz factor.

The radiation-dominated regime extends out to a radius where the asymptotic value of the Lorentz factor of the shell reaches, in the matter-dominated regime, the value:

$$\Gamma_{coast} = (4\rho_{rad,0}/3\rho_{mat,0} + 1)\Gamma_0, \quad (2.8)$$

where we label with the subscript 0 the radiation density and the matter density at the time the shell first becomes ultra-relativistic. The acceleration ends and the fireball enters the “coasting” phase. In this regime the dependencies become:

$$\Gamma \rightarrow \text{const}, \quad \rho_{mat} \propto R^{-2}, \quad \rho_{rad} \propto R^{-8/3}$$

At this stage, usually the fireball is still opaque to Thomson scattering and the shell must expand before producing the spectrum that is subsequently observed. The coasting radius is:

$$R_c = \Gamma R_{in} \simeq 10^{11} \Gamma_2 R_{in,9} \text{ cm}. \quad (2.9)$$

Secondly, the electrons associated with this matter increase the opacity, delaying the escape of radiation. Initially, when the local temperature T' is large, the opacity τ_p is dominated by e^+e^- pairs. This opacity τ_p , decreases *exponentially* with decreasing temperature, and falls to unity when $T' = T_p \approx 20$ keV. On the other hand, the opacity

due to matter, τ_b , decreases as R^{-2} , where R is the radius of the fireball. If at the radius where $\tau_p = 1$, τ_b is still > 1 , then the final transition to $\tau = 1$ is delayed and occurs at a lower temperature, and a bigger radius. Independently on the considerations of the above paragraph, at some point the fireball becomes optically thin. The transparency radius is obtained by setting the Thomson scattering optical depth equal to unity:

$$R_\tau = \left(\frac{M\sigma_T}{4\pi m_p} \right)^{1/2} \simeq 2.4 \times 10^{13} E_{51}^{1/2} \Gamma_2^{-1/2} \text{ cm}, \quad (2.10)$$

where m_p is the proton mass, σ_T is Thomson cross section, and M is the mass transported by the fireball. $M = E/(\eta c^2) \sim 10^{-5} E_{52} \eta_2^{-1} M_\odot$ (η is a factor of proportionality of the initial energy to mass ratio). This transition radius has a crucial role in the fireball evolution.

2.5.3 Shocks

We showed in §1.2.1 that the observational evidences result in a need to require the source to be expanding at ultra-relativistic velocity. In §1.2.2 we showed the general properties of the resulting fireball, either in the case of a “pure fireball” made of radiation and leptons, or in the more realistic case of a “dirty fireball” that carries an amount of barions. In the following we review the mechanism which transforms the kinetic energy of the barions, which have been accelerated by the internal pressure of the fireball, into radiation. This shock mechanism has become the most convincingly way to fulfill the observational requirements, both for the prompt phase and the afterglow phase. In Fig. 2.5.3 there is a graphical representation of the different phases of expansion of a fireball, from the energy release in a compact region, through shocks, as far as the interaction with the ISM.

Internal shocks

The prompt phase can be explained through the *internal shock* mechanism. Imagine shells emitted by the central engine at different velocities and thus expanding at different velocities. At some radii the shells will catch up.

To describe the dynamics of this collision we should imagine a source expelling shells of mass m with a bulk Lorentz factor γ , followed by a second shell with mass M , expanding in the same direction with a different Lorentz factor Γ .

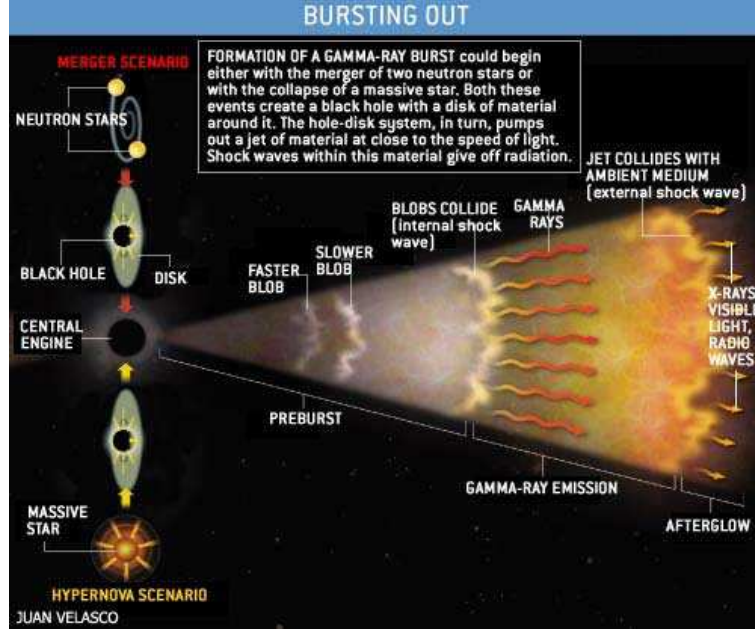


Figure 2.6 Graphic representation of the fireball relativistic expansion. Typical time-scales and radii are also shown.

Assume that $\Gamma > \gamma$: the two shells will eventually catch up and mix in a single shell with mass $M + m$, expanding at a velocity given by the final Lorentz factor Γ_F . Consider that only a fraction of the initial energy is transformed into kinetic energy. We define ε' the energy release in the rest frame of the expanding material.

By applying the laws of conservation of momentum and energy we get to a system of two equations with two unknowns. By some algebra it is possible to retrieve Γ_F and ε' .

$$\begin{cases} M\Gamma + m\gamma = \Gamma_F[M + m + \frac{\varepsilon'}{c^2}] \\ M\sqrt{\Gamma_F^2 - 1} + m\sqrt{\gamma^2 - 1} = [M + m + \frac{\varepsilon'}{c^2}]\sqrt{\Gamma_F^2 - 1}. \end{cases} \quad (2.11)$$

from the first equation in 2.11 we can derive an explicit expression for the energy release ε' as a function of known parameters and of Γ_F .

$$\frac{\varepsilon'}{c^2}\Gamma_F = M\Gamma + m\gamma - m\Gamma_F - M\Gamma_F \quad (2.12)$$

The energy released in the observer frame is the following:

$$\varepsilon^p = \varepsilon'\Gamma_F = Mc^2(\Gamma - \Gamma_F) + mc^2(\gamma - \Gamma_F) \quad (2.13)$$

We now explicit Γ_F as a function of the known variables. We divide the second equation of 2.11 by the first one:

$$\frac{M\sqrt{\Gamma^2 - 1} + m\sqrt{\gamma^2 - 1}}{M\Gamma + m\gamma} = \frac{\sqrt{\Gamma_F^2 - 1}}{\Gamma_F} \quad (2.14)$$

which, squared gives the following:

$$\frac{M^2(\Gamma^2 - 1) + m^2(\gamma^2 - 1) + 2mM\sqrt{(\Gamma^2 - 1)(\gamma^2 - 1)}}{(M\Gamma + m\gamma)^2} = \frac{\Gamma_F^2 - 1}{\Gamma_F^2} \quad (2.15)$$

$$\frac{1}{\Gamma_F^2} = \frac{M^2\Gamma^2 + m^2\gamma^2 + 2mM\Gamma\gamma - M^2\Gamma^2 + M^2 - m^2\gamma^2 + m^2 - 2mM\sqrt{(\gamma^2 - 1)(\Gamma^2 - 1)}}{(M\Gamma + m\gamma)^2}$$

By simple algebra, from the second equation above we get:

$$\frac{1}{\Gamma_F^2} = \frac{m^2 + M^2 + 2Mm\Gamma\gamma - 2mM\sqrt{(\gamma^2 - 1)(\Gamma^2 - 1)}}{(M\Gamma + m\gamma)^2} \quad (2.16)$$

and eventually:

$$\Gamma_F = \frac{(M\Gamma + m\gamma)}{\sqrt{m^2 + M^2 + 2Mm\Gamma\gamma - 2mM\sqrt{(\gamma^2 - 1)(\Gamma^2 - 1)}}} \quad (2.17)$$

The assumption $\Gamma > \gamma \gg 1$ reads a simplification of the square root:

$$\Gamma_F \approx \frac{M\Gamma + m\gamma}{\sqrt{M^2 + m^2}} \quad (2.18)$$

$$\varepsilon^p = \varepsilon' \Gamma_F = Mc^2(\Gamma - \Gamma_F) + mc^2(\gamma - \Gamma_F) \quad (2.19)$$

These two equations can be found in a different form in literature. Consider for instance the β parameter instead of Γ where

$$\Gamma = \frac{1}{\sqrt{1 - \beta^2}}$$

By re-writing the former equations we get:

$$\beta_f = \frac{m\gamma\beta_1 + M\Gamma\beta_2}{m\gamma + m\Gamma} \quad (2.20)$$

By defining the two new parameters:

$$\alpha_\Gamma \equiv \frac{\Gamma}{\gamma}; \quad \alpha_m \equiv \frac{M}{m} \quad (2.21)$$

and using them in equation 2.20 we get (see Lazzati et al. (1999)):

$$\beta_f = \frac{\beta_1 + \alpha_m \alpha_\Gamma \beta_2}{1 + \alpha_m \alpha_\Gamma} \quad (2.22)$$

The emission mechanism during the prompt phase is still debated. According to the standard model there are a number of ultrarelativistic particles moving in intense magnetic fields. The emission is thought to be due to synchrotron emission. Open issues remain, as (i) the low efficiency cannot account properly for the observed radiation, or (ii) the spectral shape during the prompt phase. In the past ten years plenty of new ideas have been proposed, e.g. quasi-thermal comptonization (Ghisellini and Celotti, 1999) or Compton drag (Lazzati et al., 2000).

One of the open problems inside the standard model is that, even if the internal-shock model properly accounts for the light curves of the prompt phase of GRBs, it is not enough efficient to account for the observed luminosity. In the collision between two shells the energy released in photons cannot be much higher than 5-10% of the kinetic energy. The available kinetic energy is the relative energy between the two colliding shells, so the greater the relative velocity, the greater the available energy.

Suppose that the two shells had Lorentz factors $\Gamma \sim 2\gamma$, and the second one was emitted with a time delay $\Delta T \sim R_0/c$. They will collide at a radius (the *internal shock radius*):

$$R_I = 2 \frac{\alpha_\Gamma^2}{\alpha_\Gamma^2 - 1} \gamma^2 c \Delta T = 2.6 \times 10^{13} \Gamma_2^2 R_{0,9} \text{ cm} \quad (2.23)$$

where $\alpha_\Gamma = \Gamma/\gamma = 2$ has been used to derive the numerical estimate. Note that, for typical values, the internal shock radius is larger than the transparency radius give by eq. 2.10, i.e. the shell is already Thomson thin.

External shocks

The final evolution of the fireball takes place when it interacts with the external material (e.g. ISM) which is at rest. The impact of the fireball onto the external material drives a relativistic shock in the same direction. The beginning of this phase is conventionally set to the moment when the initial Lorentz factor has been halved. This happens when the fireball has swept up a mass equal to the rest mass of the fireball itself divided by its Lorentz factor.

If the initial mass of the shell was M_{shell} , moving with a Lorentz factor Γ_s , the mass m needed to halve the initial Lorentz factor is

$$m = \frac{M_{shell}}{\Gamma_s}$$

and the deceleration becomes non-negligible at a radius:

$$R_{ext} = \left(\frac{3E}{4\pi n m_p c^2 \Gamma_s^2} \right)^{\frac{1}{3}} = 6 \times 10^{16} E_{52}^{\frac{1}{3}} \Gamma_2^{-\frac{2}{3}} n_0^{-\frac{1}{3}} \text{ cm} \quad (2.24)$$

the time required to reach the external shock radius is $\approx R_{ext}/c$. In the observer frame (at rest with the ISM) the time is shortened of roughly $2\Gamma_s^2$:

$$t_{ext,obs} \sim \frac{R_{ext}}{2\Gamma_s^2 c} = 100 E_{52}^{\frac{1}{3}} \Gamma_2^{-\frac{8}{3}} n_0^{-\frac{1}{3}} \text{ s} \quad (2.25)$$

Under the assumption for the observer to be at rest with the ISM, by the momentum and energy conservation laws we get a system of two equations (and two unknowns, i.e. $\Gamma(r)$ and ε') where M_{shell} and Γ_s are known. The system reads:

$$\begin{cases} M_{shell}\Gamma_s + m(r) = \Gamma(r)[M_{shell} + m(r) + \frac{\varepsilon'}{c^2}] \\ M\sqrt{\Gamma_s^2 - 1} = [M_{shell} + m(r) + \frac{\varepsilon'}{c^2}] \sqrt{\Gamma^2(r) - 1} \end{cases} \quad (2.26)$$

Dividing the second equation by the first, and squaring the result we get:

$$\frac{M^2(\Gamma_s^2 - 1)}{[M_{shell}\Gamma_s + m(r)]^2} = 1 - \frac{1}{\Gamma(r)^2}$$

i.e.:

$$\frac{1}{\Gamma(r)^2} = \frac{[M_{shell}\Gamma_s + m(r)]^2 - M_{shell}^2(\Gamma_s^2 - 1)}{[M\Gamma_s + m(r)]^2} \quad (2.27)$$

If we invert equation 2.27 we get:

$$\Gamma(r)^2 = \frac{[M_{shell}\Gamma_s + m(r)]^2}{M_{shell}^2\Gamma_s^2 + m(r)^2 + 2mM_{shell}\Gamma_s - M_{shell}^2\Gamma_s^2 + M_{shell}^2} \quad (2.28)$$

which can be written, after some algebra, as:

$$\Gamma(r)^2 = \frac{[M_{shell}\Gamma_s + m(r)]^2}{m(r)^2 + 2mM_{shell}\Gamma_s + M_{shell}^2} \quad (2.29)$$

and eventually:

$$\Gamma(r) = \frac{M_{shell}\Gamma_s + m(r)}{\sqrt{m(r)^2 + 2mM_{shell}\Gamma_s + M_{shell}^2}} \quad (2.30)$$

From the first equation in 2.26 we can derive the following:

$$\frac{\varepsilon'}{c^2}\Gamma(r) = M_{shell}\Gamma_s + m(r) - \Gamma(r)(M_{shell} + m(r)) \quad (2.31)$$

and using equation 2.30 for $\Gamma(r)$, we eventually find the relation for $\varepsilon'(r)$

$$\frac{\varepsilon'(r)}{c^2} = \sqrt{M_{shell}^2 + m(r)^2 + 2\Gamma_s m M_{shell}} - [M_{shell} + m(r)] \quad (2.32)$$

Deceleration and subsequent dissipation convert part of the initial energy of the shell into radiation, producing an emission with a smooth decay in time: the afterglow. In the very last phase of the process, the Lorentz factor of the fireball reaches $\Gamma \approx 1$, and the bulk motion enter the sub-relativistic regime. All the initial internal energy has been released in the shocks so that:

$$\varepsilon \approx \varepsilon' \approx M_{shell} \Gamma_s c^2 \quad (2.33)$$

The *external shock* mechanism is currently the best explanation for a relativistically expanding fireball through the external material. It provides the energy reservoir for the afterglow emission. External shocks cannot be invoked also for the prompt emission, because they cannot account for the rapid variability which is observed in the lightcurves of GRBs. In fact $t_{ext,obs} \gg 10$ ms.

Chapter 3

Host Galaxies

Observation of host galaxies of gamma-ray bursts (GRBs) is very important for understanding the nature of GRBs. Current observations reveal that long duration GRBs occur in star-forming galaxies, consistent with the general belief that long GRBs are produced by the death of massive stars (Conselice et al., 2005; Fruchter et al., 2006; Tanvir and Levan, 2007; Wainwright et al., 2007, and references therein). The discovery of the connection between long GRBs and core-collapse Type Ibc supernovae (Galama et al., 1998; Li, 2006; Woosley and Heger, 2006, and references therein) supports the collapsar model of long GRBs (MacFadyen and Woosley, 1999; MacFadyen et al., 2001).

In contrast, short-duration GRBs are found in both early- and late-type galaxies, similar to the situation of Type Ia supernovae. The rate of star formation in the host galaxies of short GRBs is often lower than that in the hosts of long GRBs (Berger et al. (2006), and references therein). So far no supernovae have been found to be associated with short GRBs.

The difference in the observed host properties for short and long GRBs supports the idea that short and long GRBs have different progenitors (see also Chapter 2). Long GRBs are believed to arise from the death of massive stars (the collapsar model)—most likely the Wolf-Rayet stars since all observed supernovae associated with GRBs are Type Ic, while short GRBs are more likely produced by the merger of compact stars—neutron star-neutron star merger and black hole-neutron star merger (Li & Paczyński 1998; O’Shaughnessy, Kalogera & Belczynski 2007).

To date, there are 130 GRBs with known redshift and 50 with estimated host galaxy stellar mass (Savaglio et al., 2008). Given the difficulty in detecting and localizing short

GRBs, most of the observational studies about host galaxies are for LGRBs, which will be the focus of this work. Studies of the physical properties of GRBs are not easy as they require deep targeted observations at high redshift. In addition, the probability for a chance superposition of GRBs and galaxies on the sky is significant for high- z GRBs, and $\sim 3\%$ for galaxies at $z < 1.5$ (Campisi and Li, 2008). Over 40 LGRBs have been observed with the HST at various times after outburst. The HST is unique in its capability easily to resolve the distant hosts of these objects. Shown in Fig. 3.1 is a mosaic of HST images of the hosts of 42 bursts. These are all LGRBs with public data that had an afterglow detected with better than 3σ significance and a position sufficiently well localized to determine a host galaxy.

The observational information gathered so far indicates that most LGRBs are found in faint star forming galaxies dominated by young stellar populations with a sub-solar gas-phase metallicities, although there are a few host galaxies with higher metal content (Prochaska et al., 2004; Wolf and Podsiadlowski, 2007; Fynbo et al., 2006; Price et al., 2007; Savaglio et al., 2003; Savaglio, 2006; Savaglio et al., 2008; Stanek et al., 2006, and references therein).

In a recent work of Savaglio et al. 2009, is presented a complete study of the largest sample of galaxies hosting GRBs, distributed along the redshift interval $0 < z < 6.3$. GRB hosts can be used as important probes of the cosmic history of galaxy formation and evolution. Most GRBs are associated with the death of young massive stars, which are more common in star-forming galaxies. Therefore, GRBs are an effective tool to detect star-forming galaxies. As shown by recent studies (Glazebrook et al. 2004; Juneau et al. 2005; Borch et al. 2006), the star-formation density in the $z < 1$ universe is carried out by small, faint, low-mass star-forming galaxies, similar to the typical GRB host. Moreover, in the $z \sim 5$ universe, GRB hosts observed with Spitzer are ~ 3 times fainter than the typical spectroscopically confirmed galaxy in the Great Observatories Origins Deep Survey (GOODS; Yan et al. 2006), suggesting that not all star-forming galaxies at these redshifts are detected in deep surveys (Chary, Berger & Cowie, 2007; Yüksel et al. 2008). We consider however, that our view of GRB hosts is still partial, as we mainly detect those at $z < 1.5$. Hosts at higher redshift are harder to observe. It is possible that high- z GRB hosts are more massive than those at low redshift, because star formation could be carried by more-massive galaxies in the remote universe. Future deeper multiband

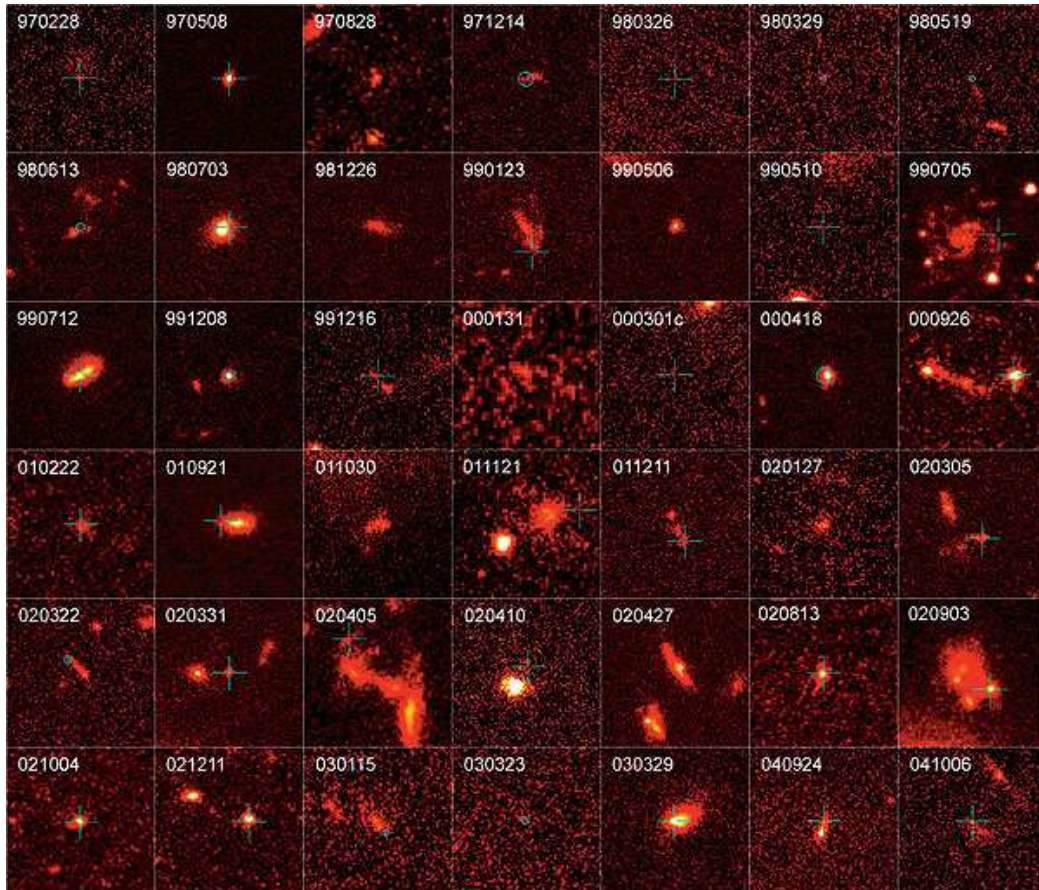


Figure 3.1 From Fruchter et al. 2006: each individual image corresponds to a square region on the sky $3.75''$ on a side. These images were taken with the Space Telescope Imaging Spectrograph (STIS), the Wide-Field and Planetary Camera 2 (WFPC2) and the Advanced Camera for Surveys (ACS) on HST. In cases where the location of the GRB on the host is known to better than $0.15''$ the position of the GRB is shown by a green mark. If the positional error is smaller than the point spread function of the image ($0.07''$ for STIS and ACS, $0.13''$ for WFPC2) the position is marked by a cross-hair; otherwise the positional error is indicated by a circle. The STIS images were all taken in white light (no filter), and in most cases the WFPC2 and ACS images are in the F606W filter (though in a few cases where images in this filter were not available we have used images in F555W or F775W). The STIS and F606W images can be thought of as broad 'V' or visual images, and are, for galaxies exhibiting typical colours of GRB hosts, the single most sensitive settings for these cameras. F555W is close to the ground-based Johnson V band, and F775W corresponds to the ground-based Johnson I band. Owing to the redshifts of the hosts, these images generally correspond to blue or ultraviolet images of the hosts in their rest frame, and thus detect light largely produced by the massive stars in the hosts.

observations of high- z hosts are mandatory to help solve this issue.

In summary, the conclusions in Savaglio et al. (2009) are:

- GRB hosts are generally small star-forming galaxies. The mean stellar mass is similar to the stellar mass of the LMC, $M_* \sim 10^{9.3} M_\odot$. About 83% of the sample has stellar mass in the interval $10^{8.5} - 10^{10.3} M_\odot$. The median SFR = $2.5 M_\odot \text{ yr}^{-1}$ is 5 times higher than in the LMC;
- To estimate SFR, people derived new relations, suitable for GRB hosts. These give the total SFR when $H\alpha$ is not detected, but [OII] or UV are detected. Our SFRs span an interval of more than three orders of magnitudes, from $0.01 M_\odot \text{ yr}^{-1}$ to $36 M_\odot \text{ yr}^{-1}$;
- The dust extinction in the visual band is on average $A_V = 0.53$. The Balmer stellar absorption is generally small, but not negligible. Dust extinction, Balmer absorption and slit-aperture flux loss are considered when measuring SFR;
- The median star-formation rate per unit stellar mass SSFR is $\sim 0.8 \text{ Gyr}^{-1}$, with a small scatter, such that $\text{SFR} \propto M_*$, a somewhat surprising result. The median SSFR is about 5 times higher than in the LMC. A large fraction of GRB hosts are the equivalent of local starbursts;
- Metallicities derived from emission lines in the host galaxies at $z < 1$ are relatively low, likely in the range 1/10 solar to solar;
- Metallicities measured from UV absorption lines in the cold medium of GRB hosts at $z > 2$ (GRB-DLAs) are in a similar range. Combining this with the results for $z < 1$ GRB hosts, we see no significant evolution of metallicity in GRB hosts in the interval $0 < z < 6$;
- The subsample of 6 short-GRB hosts have stellar masses $10^{8.7} M_\odot < M_* < 10^{11.0} M_\odot$ and SSFRs in the range $0.006 - 6 \text{ Gyr}^{-1}$. The suggestion that short-GRB hosts are large quiescent galaxies requires a larger sample to be confirmed;
- There is no clear indication that GRB host galaxies belong to a special population. Their properties are those expected for normal star-forming galaxies, from the local to the most distant universe.

3.1 Chance coincidence of a GRB with galaxy on sky

By the observation of GRB 060614, the association between host galaxy and GRB is changed. This is a long burst with a duration ~ 100 s, with a host galaxy at redshift $z = 0.125$ (Della Valle et al., 2006; Fynbo et al., 2006; Gehrels et al., 2006). For a long GRB that has such a low redshift it is expected that a supernova associated with it should be observed. However, despite extensive observation on its host, no supernova has been found down to limits fainter than any known Type Ic SN and hundreds of times fainter than the archetypal SN 1998bw that accompanied GRB 980425. This challenges the ordinary GRB classification scheme based on GRB durations and the general belief that long GRBs are produced by the core-collapse of massive stars (Zhang, 2006; Watson et al., 2007).

In fact, except its duration, GRB 060614 is much like a short GRB in many aspects. Besides the fact that it has no associated supernova, GRB 060614 has a vanishing spectral lag that is typical of short GRBs (Mangano et al., 2007). Its lightcurve has a very hard and short-duration initial peak, followed by an extended soft emission. Zhang (2007) have shown that if this burst had an eight time smaller total energy, it would have been detected by BATSE as a marginal short-duration GRB, and would have properties in the *Swift* BAT and XRT bands similar to GRB 050724.

GRB 060505 has a duration ~ 4 s and a host galaxy at $z = 0.089$. No supernova has been detected at the location of this burst also (Fynbo et al., 2006; Ofek et al., 2007), so GRB 060505 has also been considered as a long GRB without a supernova. It has been argued that GRB 060505 is indeed a short burst (Ofek et al., 2007; Levesque and Kewley, 2007, see, however, Thöne et al. 2008; McBreen et al. 2008). Models for “long GRBs without supernovae” have been proposed (King, Olsson & Davies 2007).

On the other hand, it has been suggested that GRB 060614 and its host galaxy was just a coincidence rather than a physical association (Cobb et al., 2006). By counting the number of galaxies observed by SMARTS in a field centered on the burst, Cobb et al. (2006) showed that the probability for a chance superposition of GRB 060614 and a galaxy along the line of sight is $\sim 1\%$. This probability is high enough to cause that several cases of chance superposition may have happened for *Swift* GRBs. This conclusion is enforced by a more detailed study by Cobb and Bailyn (2008).

The results of Cobb et al. have raised an important question in identifying GRB host galaxies based only on the superposition of a GRB and a galaxy on the sky (Levan et al., 2007). For a telescope with very high sensitivity, it would observe many galaxies on the sky, then the probability for a GRB to be aligned with a galaxy could be high. Then, unavoidably, some GRB hosts discovered in this approach might be superficial, i.e. they are not physically related to the GRBs. Cobb et al. obtained their results by using galaxy survey data. It is interesting to verify these results with an independent, more theoretical approach.

We calculate the probability for a GRB to be coincident with a galaxy on the sky using galaxy luminosity functions and compare the results with that of Cobb et al. obtained with different ways. Then, we use our results to assess at what a level we can trust the GRB host galaxies that have been found so far. The UVOT on *Swift* can resolve a source to sub-pixels ($\sim 0.2''$). Hence, in our calculations we regard a GRB as a point source.

The approach that we adopt has the benefit of extending beyond the limit of current surveys and to broader types of problems. For example, with slight modification it can be applied to the calculation of the probability of Ly α forests in the spectra of quasars and GRBs which has important applications in probing the high- z Universe (Loeb, 2002).

3.1.1 The Galaxy Luminosity Function

The galaxy luminosity function (LF) is a fundamental characteristics of the galaxy population and is essential for studying statistical properties of galaxies and their evolution. It gives the abundance of galaxies as a function of their luminosity, defined by the comoving number density of all galaxies with luminosity between L and $L + dL$ at redshift z . The LF of a population of galaxies is usually described by the Schechter function (Schechter 1976)

$$\Phi(L)dL = \Phi^* \left(\frac{L}{L^*} \right)^\alpha \exp \left(-\frac{L}{L^*} \right) \frac{dL}{L^*}, \quad (3.1)$$

where L^* is a characteristic luminosity, the constant α is the faint-end slope, and Φ^* is the normalization. These three parameters are determined by fitting the LF to the data from a galaxy survey.

The LF is often expressed in terms of magnitudes rather than luminosities, which is more convenient to use in UV and optical observations. The absolute magnitude

M is related to the galaxy luminosity by $M - M^* = -2.5 \log(L/L^*)$, where M^* is a characteristic magnitude corresponding to the characteristic luminosity L^* . Then, the Schechter LF becomes

$$\begin{aligned} \Phi(M)dM &= (0.4 \ln 10) \Phi^* \\ &\times 10^{0.4(\alpha+1)(M^*-M)} \exp[-10^{0.4(M^*-M)}] dM. \end{aligned} \quad (3.2)$$

In a flat universe, the number of galaxies within a solid angle Ω with magnitude in the range $M_{\min} - M_{\max}$ and comoving distance D_{com} in the range $D_1 - D_2$ is calculated by integral:

$$N = \Omega \int_{D_1}^{D_2} dD_{\text{com}} D_{\text{com}}^2 \int_{M_{\min}}^{M_{\max}} dM \Phi(M). \quad (3.3)$$

The solid angle Ω is the solid angle covered by a survey, and $M_{\max} = M_{\max}(m, z)$ is the maximum absolute magnitude arising from the apparent magnitude limit m of the telescope. The comoving distance to a galaxy at redshift z is calculated by

$$D_{\text{com}} = \frac{c}{H_0} \int_0^z \frac{dz}{\sqrt{\Omega_m (1+z)^3 + \Omega_\Lambda}}, \quad (3.4)$$

where c is the speed of light, H_0 is the Hubble constant, Ω_m is the fraction of mass contained in baryonic and dark matter in the Universe, and Ω_Λ is the fraction of mass contained in the cosmological constant or dark energy.

Throughout the paper we adopt a cosmology with $H_0 = 70 \text{ km s}^{-1} \text{ Mpc}^{-1}$, $\Omega_m = 0.3$, and $\Omega_\Lambda = 0.7$.

3.1.2 Morphology and Redshift Dependent LF

The LF is one of the fundamental observational properties of galaxies, and the amount of work dedicated by different groups of people to derive an accurate LF is substantial. The LF has been measured from many galaxy surveys with differing sample selections and redshift coverage, and different outcomes are compared by de Lapparent et al. (2003). The results in the literature have shown that there is no universal galaxy LF. Instead, the galaxy LF evolves with redshift and galaxy morphology.

It has been found that, in general, the faint-end LF of early-type galaxies is steeper than that of late-type galaxies, and the characteristic luminosity of early-type galaxies is smaller than that of late-type galaxies (Madgwick et al. 2002; Nakamura et al. 2003).

The LF of local galaxies is now well constrained by two large spectroscopic surveys: the Two-Degree Field Redshift Survey (2dFGRS; e.g. Norberg et al. 2002), and the Sloan Digital Sky Survey (SDSS; e.g. Blanton et al. 2003). The Canada-France Redshift Survey (CFRS), which includes galaxies up to $z \sim 1$, showed that the LF evolves with the cosmic redshift and the evolution depends on the galaxy populations.

For example, the CFRS survey shows unambiguously that the population evolves and that this evolution is strongly differential with color and, less strongly, with luminosity (Lilly et al. 1995). The LF of red galaxies changes little over $0.05 < z < 1$, while the LF of blue galaxies shows substantial evolution at redshifts $z > 0.5$.

At higher redshift, the evolution of LF in blue bands over the redshift range $0.5 < z < 5.0$, and in red bands over the redshift range $0.5 < z < 3.5$, has been derived from the FORS Deep Field survey (Gabasch et al. 2004, 2006). The LF measurements for different galaxy types have been derived up to $z = 1.5$ from the VVDS survey (Zucca et al. 2006).

In this paper, we consider the LF for each type of galaxies separately.

3.1.3 The Radius-Luminosity Relation

To calculate the probability for a GRB to be coincident with a galaxy on the sky, we need to measure the projected radius of the galaxy on the sky. To do so, we associate with each galaxy a physical projected area, as a function of the redshift and of the luminosity of galaxies.

For an elliptical galaxy, we assume that the area covered by the galaxy on the sky is $S = \pi R^2$, where R is an averaged radius. For a spiral or an irregular galaxy, which is not spherical, we assume that the galaxy has a random distribution in orientation. For a spiral or an irregular galaxy with an inclination angle θ , the area on the sky is $S' = \pi R^2 \cos \theta$ ($0 < \theta < \pi/2$).

Generally, the size of a galaxy is correlated with its luminosity. Hence, The value of R for a galaxy with a given luminosity can be derived from a statistical relation between the observed radius and luminosity, at a given redshift. The relation can be fitted by a power law

$$R = \left(\frac{L}{\zeta_i} \right)^{\varphi_i}, \quad (3.5)$$

where R is in kpc and L is in erg s^{-1} , ζ_i and φ_i are constants that depend on the galaxy

morphological types and on the bandpass of the telescope.

Dahlen et al. (2007) have shown that the galaxy size evolves strongly with redshift. In particular they have claimed that there is a similar evolution in the size-luminosity relation in several wavelengths, over the range $0 < z < 6$. The evolution is consistent with the form $R_h \propto (1+z)^\beta$, where $\beta \sim -1$ and R_h is the half-light radius of the galaxy. The ratio R_{90}/R_{50} (radius containing 90% and 50% of the flux) is approximately constant for de Vaucouleurs and exponential profile galaxies (~ 3.3 and ~ 2.3 , respectively), so we can assume that $R_{90} \propto (1+z)^\beta$.

The solid angle occupied by a galaxy is then

$$\omega_{\text{gal}} = \frac{\langle S \rangle}{D_A^2}, \quad (3.6)$$

where D_A is the angular-diameter distance to the galaxy [related to the comoving distance by Etherington's reciprocity law $D_A = D_{\text{com}}/(1+z)$; Etherington 1933], $\langle S \rangle$ is the projected area of the galaxy averaged over inclination.

For spherical or elliptical galaxies we have $\langle S \rangle = \pi R_0^2 (1+z)^{2\beta}$, where R_0 is the radius of the galaxy. For disk spiral galaxies and irregular galaxies with a random distribution of inclination we have $\langle S \rangle = (1/2)\pi R_0^2 (1+z)^{2\beta}$.

3.2 Computation of the Probability

The probability for a GRB to be aligned to a galaxy is always small. Hence, the probability is simply given by the ratio of the solid angle spanned by galaxies to the total solid angle

$$P = \frac{\Omega_{\text{gal}}}{\Omega}, \quad (3.7)$$

where Ω is the solid angle of space covered by a survey, and Ω_{gal} is the total solid angle occupied by galaxies. Using relations (5.2) and (3.6), the total solid angle occupied by galaxies is ($\Omega = 4\pi$)

$$\Omega_{\text{gal}} = 4\pi \int_0^{z_{\text{max}}} dD_{\text{com}} D_{\text{com}}^2 \int_{M_{\text{min}}}^{M_{\text{max}}} dM \frac{\langle S \rangle}{D_A^2} \Phi(M), \quad (3.8)$$

where z_{max} is the maximum redshift that can be reached by a survey. Then, by Etherington's reciprocity law, we have

$$P = \int_0^{z_{\text{max}}} dD_{\text{com}} \int_{M_{\text{min}}}^{M_{\text{max}}} dM \langle S \rangle (1+z)^2 \Phi(M), \quad (3.9)$$

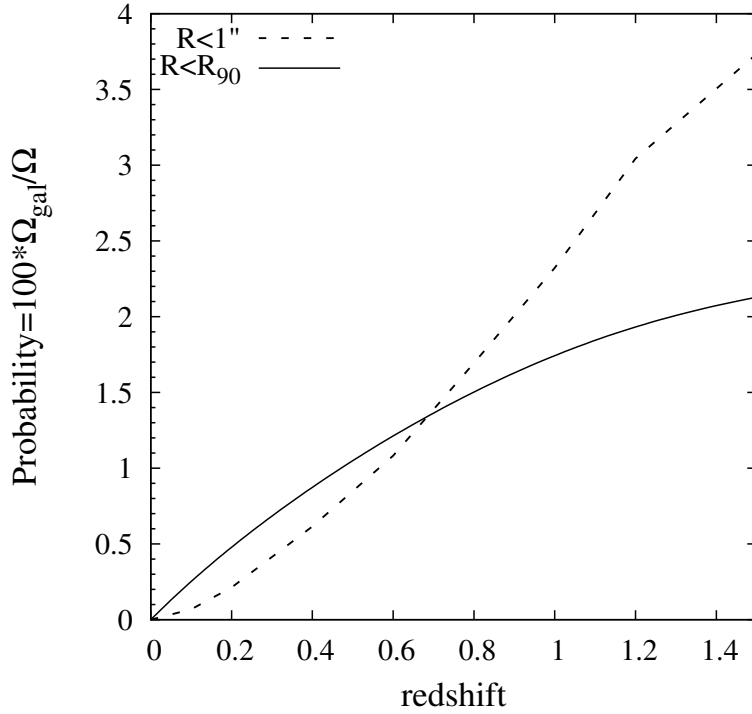


Figure 3.2 Probability for a GRB to be coincident with a galaxy on the sky, with $0 < z < 1.5$ and the B -band magnitude limit $m_b = 26.5$. The solid curve is calculated with equation (3.9), which assumes that a GRB is associated with a galaxy if the linear distance from the GRB to the galaxy center is less than R_{90} . The dashed curve is calculated with equation (3.11), which assumes that a GRB is associated with a galaxy if the angular distance from the GRB to the galaxy center is less than $1''$.

we will adopt $\beta = -1$ to compute $\langle S \rangle$.

Since the LF decays exponentially toward the bright end, the exact value of M_{\min} does not affect the final result. In our numerical calculation we take $M_{\min} = -30$. For a given luminosity distance D_{lum} , the value of M_{\max} is related to the magnitude limit of the telescope, m , by

$$M_{\max} = m - 5 \log \frac{D_{\text{lum}}}{10 \text{ pc}} - K, \quad (3.10)$$

where K is the K-correction depending on the filter.

The parameters in the LF are derived from the SDSS and the VVDS catalogs (Nakamura et al.2003; Zucca et al. 2006) and the radius-luminosity relation from the SDSS catalogs (York et al.2000). Then, the probability can be calculated by equation (3.9). The calculated results of P for the parameters in the B -band obtained from the VVDS survey (Zucca et al. 2006) are shown in Fig. 3.2 (solid line). In the calculations the K-corrections were provided by E. Zucca (see also Fukugita, Shimasaku, & Ichikawa

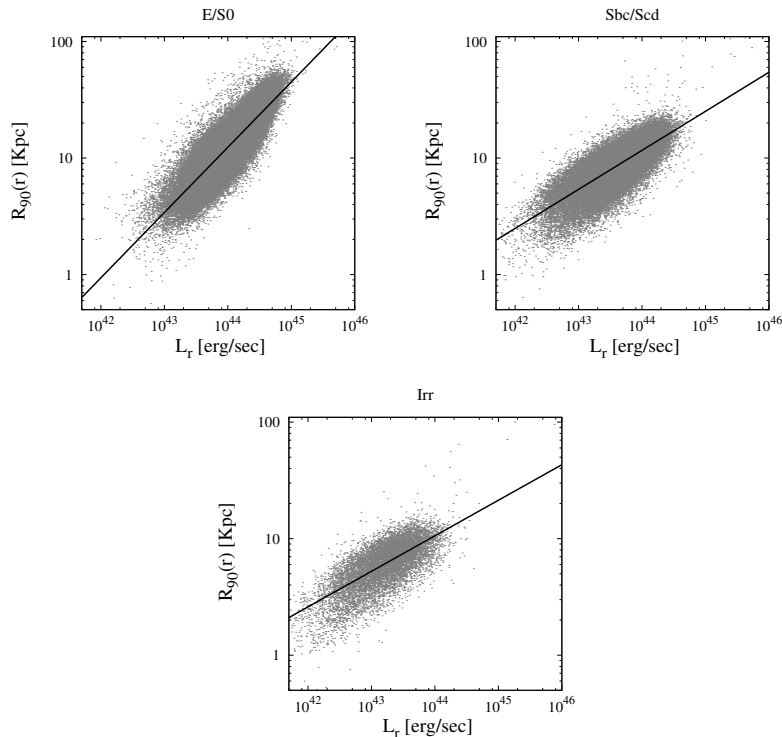


Figure 3.3 The sky-projected R_{90} versus the luminosity in the r^* -band for the SDSS galaxies with $15.6 < r^* < 19.6$ and $0 < z < 0.3$. Each panel corresponds to a galaxy type (elliptical/S0, spiral/Sbc-Scd, and Irregular galaxies). The solid line is the best-fit with equation (3.5) (divided by $\sqrt{2}$ for spiral and irregular galaxies for the average random projection effect). The values of the fitted parameters are listed in Table 3.1.

1995).

The SDSS Catalog

SDSS catalog (York et al. 2000)¹ contains the largest redshift sample of galaxies with both photometric and spectroscopic observations. It is a homogeneous data set that is suitable for statistical studies of galaxies. The SDSS sample for LF measurements (Nakamura et al. 2003) contains ~ 1500 bright galaxies, in the redshift range $0.01 < z < 0.12$ with $13.2 \leq r^* \leq 15.9$. The galaxies are classified into four groups by the $g - r$ color: $0 \leq T \leq 1.0$ (corresponding to Hubble type E-S0), $1.5 \leq T \leq 3$ (S0/a-Sb), $3.5 \leq T \leq 5.0$ (Sbc-Sd), and $5.5 \leq T \leq 6$ (Im) (Fukugita et al. 1995). The LF was calculated with three methods: ML (maximum likelihood), SWML (stepwise maximum likelihood), and the V_{\max} method.

To derive the radius-luminosity relation, we take from the SDSS catalog the Petrosian

¹<http://www.sdss.org/>

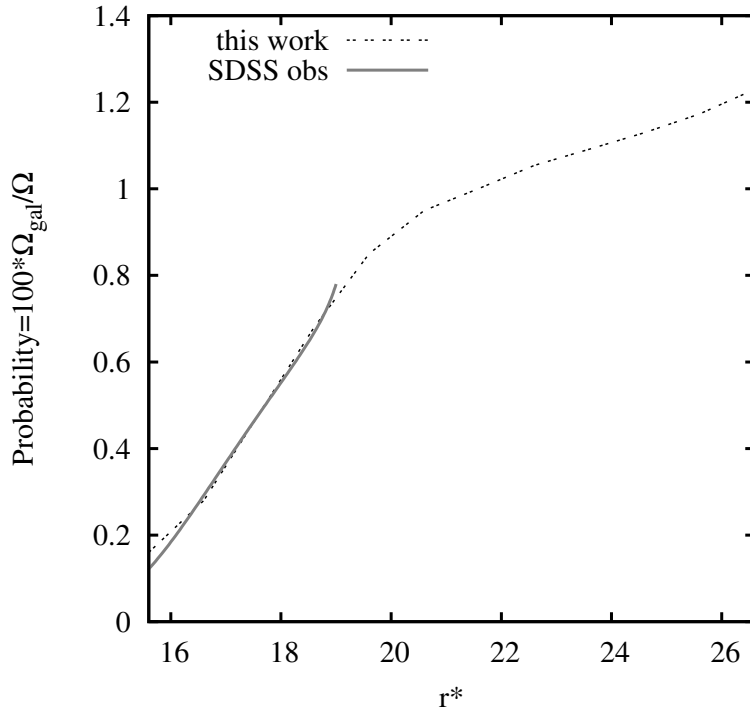


Figure 3.4 Probability for a GRB to be coincident with a galaxy on the sky, obtained from the SDSS galaxies with $0 < z < 0.3$. The solid line is the ratio of the total solid angle occupied by the SDSS galaxies to the total solid angle covered by the survey. The dashed line is calculated with equation(3.9).

radius R_{90} in the r^* band (which contains 90% of the Petrosian flux), the value of the apparent brightness r^* , and the galaxy redshift. Note that, SDSS has adopted a modified form of the Petrosian system (Petrosian 1976) to define the radius of a source (see Blanton et al. 2001 for details). For the exponential profile, R_{90} corresponds to the true 90% light radius, while for the de Vaucouleurs profile $R_{90} = 0.43R_{90\text{true}}$.

Then we convert the apparent magnitude r^* to an absolute magnitude M and luminosity L , adopting the K-correction supplied by Fukugita et al. (1995) for each galaxy type. The derived sky-projected radius and luminosity in the r^* -band for about 240000 galaxies with $r^* < 19.6$ in a sky region of 2500 deg^2 are shown in Fig. 3.3 for different galaxy types (elliptical, spiral, and irregular). Power-law fits to the R - L relation (eq. 3.5; divided by $\sqrt{2}$ for spiral and irregular galaxies for the average random projection effect) are summarized in Table 3.1.

We selected a subsample of galaxies with $15.6 < r^* < 19.6$ (to be consistent with the magnitude limit adopted in eq. 3.9), and computed the ratio of the sky area covered by them to the total area of the sky. The results are shown in Fig. 3.4. They agree well

Galaxy type	ζ_i	φ_i
E/S0	1.12e+42	0.561
Sbc/Scd	2.33e+40	0.335
Irr	1.40e+40	0.305

Table 3.1 Best-fit parameters in the radius-luminosity relation (3.5) in the r -band for SDSS galaxies, with R in kpc and L in erg s^{-1} .

Galaxy type	ζ_i	φ_i
E/S0	3.32e+41	0.413
Sbc/Scd	3.36e+40	0.322
Irr	8.46e+40	0.361

Table 3.2 Best-fit parameters in the radius-luminosity relation (3.5) in the B -band for VVDS galaxies, with R in kpc and L in erg s^{-1} .

with that calculated with equation (3.9) with $z < 0.3$ (the redshift covered by the SDSS galaxies).

The VVDS LF

The VIMOS VLT Deep Survey (VVDS) is a deep spectroscopic survey, containing galaxies up to redshift $z \sim 1.5$. The first epoch VVDS deep sample covers a sky area of about 2200 arcmin^2 , containing about 7700 galaxies with $17.5 \leq I_{AB} \leq 24$. Using this sample, Zucca et al. (2006) derived an evolving and morphology-dependent LF. The galaxies were divided into four types: E/S0, early spiral, late spiral, and irregular. The parameters in the derived luminosity functions are listed in table 3 of Zucca et al. (2006). The best-fit parameters for the radius-luminosity relation are listed in Table 3.2.

For a given galaxy survey, the projected area of resolved galaxies on the sky can be measured. Then equation (3.7) can be directly applied to calculate the probability for chance coincidence of a GRB with a galaxy on the sky. As an example, the fraction of the sky covered by galaxies in the Hubble Deep Fields (HDFs) is $\sim 5\%$ if the boundary of a galaxy is defined by twice the isophotal radius containing $\sim 90\%$ flux (Bernstein, Freedman, & Madore 2002).

3.3 Comparison with observed host galaxies

For those GRBs with known hosts, we find out the distribution of the distance, projected on the sky, between the GRB's position and the center of the associated host galaxy.

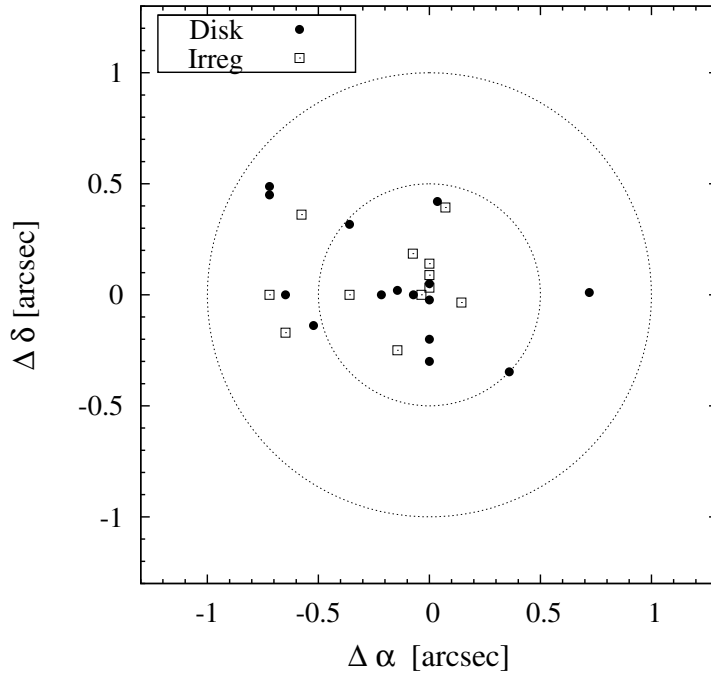


Figure 3.5 Displacement of GRB positions with respect to the center of their host galaxies for a sample of 27 long GRBs with well measured and resolved hosts (in the redshift range $0.089 \leq z \leq 3.42$).

From this distribution, we can check if the observed distance is within the galaxy radius defined in the equation (3.5). From ~ 50 GRBs with both redshift and host associate,² we select 27 long GRBs, including only GRBs with sure host galaxy types and R-band magnitudes. Figure 3.5 shows the displacement between RA/DEC of the GRB's position and the host galaxy counterpart in the sample (see table C1 of the Appendix). Most GRBs with reliable host measurements have a separation smaller than $1''$ from the center of their counterpart. Our comparison is in agreement with previous works (Bloom et al., 2002; Fruchter et al., 2006).

In Fig. 3.6, we compare the galaxy radius defined by equation (3.5) and the observed distance between GRBs from the center of their host galaxies. Since all of the observed GRBs fall in the defined galaxy radius, equation (3.5) provides a reasonable estimate for galaxy radii and a scale measuring the association of GRBs and their hosts. The probability calculated with the galaxy radius that we have defined would lead to a reasonable estimate on the probability for a GRB to be coincident with a galaxy on the sky.

²<http://www.grbhosts.org/>

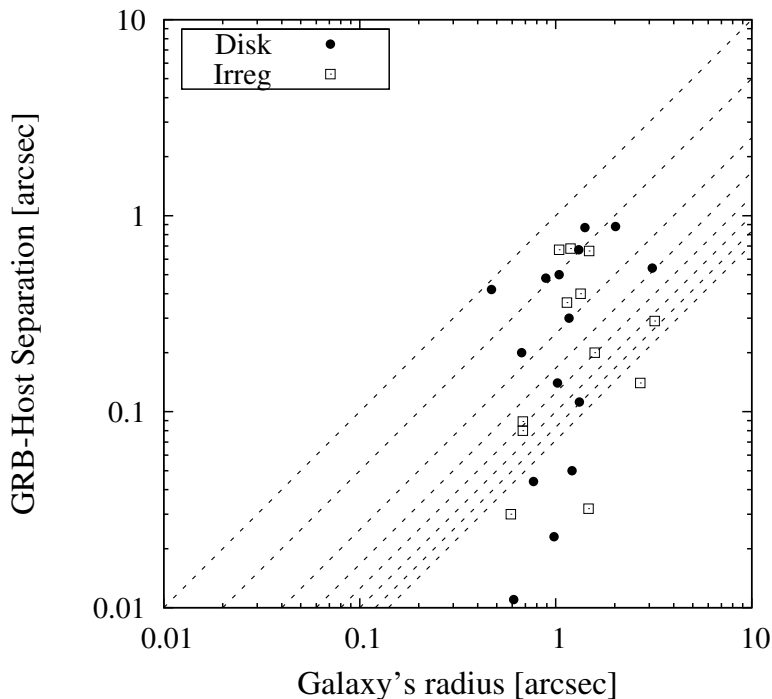


Figure 3.6 Radius of the host galaxies, computed with equation (3.5), versus the observed distance between GRBs for the same sample and their host galaxies. Dashed lines labels the relations of separation/galaxy radius = 1/14, 1/12, 1/10, 1/8, 1/6, 1/4, 1/2, 1 (blue-dashed line).

The Long GRB sample

In Table 1 we provide details on the long GRBs used in the Figs. 3.5 and 3.6. The sample contains 27 GRB hosts from the *GHostS* archive (<http://www.grbhosts.org>).

In practice people often identify association of a GRB with a galaxy by requiring that the projected distance from a GRB to the center of a galaxy on the sky is smaller than a critical angular distance, say $< 1''$. Then the probability for chance coincidence of a GRB and a galaxy on the sky is calculated by

$$P = \omega_c \int_0^{z_{\max}} D_{\text{com}}^2 dD_{\text{com}} \int_{M_{\min}}^{M_{\max}} dM \Phi(M), \quad (3.11)$$

where $\omega_c = \pi(1'')^2 = 7.384 \times 10^{-11}$ is the solid angle corresponding to a circle of radius $1''$. The probability calculated with this formula is shown in Fig. 3.2 with a dashed curve.

It appears that the probability calculated with an angular radius $1''$ is higher than that calculated with a linear radius R_{90} . This is caused by the fact that for a fixed angular radius the corresponding linear radius increases with distance while the luminous R_{90} decreases with redshift. Our results indicate that identifying the GRB-galaxy association

Table 3.3 Sample of 27 long GRBs with known redshift and host.

GRB name (1)	z (2)	d_L [Mpc] (3)	M_R (4)	R_{90} [arcsec] (5)	D [arcsec] (6)	α_H (J2000.0) (7)	δ_H (J2000.0) (8)	α_{GRB} (J2000.0) (9)	δ_{GRB} (J2000.0) (10)	Ref. (11)
Disk galaxies										
030323	3.372	29251	27.28	1.02	0.14	166.5391	-21.7704	166.5391	-21.77033	[1]
020819	0.41	2245	19.48	3.11	0.54	351.8310	+6.2655	351.831145	+6.26554	[2]
011211	2.141	16888	25.97	1.04	0.49	168.8250	-21.9489	168.8249	-21.94894	[3]
011121	0.362	1939	23.23	2.02	0.88	173.6240	-76.0282	173.6235	-76.0282	[4]
010921	0.451	2513	22.58	1.17	0.29	344.0000	+40.9312	344.000	+40.93128	[5]
010222	1.48	10735	25.61	0.77	0.044	223.0520	+43.0184	223.05202	+43.0184	[6]
000418	1.118	7594	24.15	0.98	0.023	186.3300	+20.1031	186.3300	+20.10311	[7]
000210	0.846	5386	24.22	0.89	0.48	29.8149	-40.6592	29.815	-40.6591	[8]
991208	0.706	4315	24.6	0.67	0.19	248.4730	+46.4558	248.4730	+46.455834	[9]
990712	0.434	2401	22.45	1.21	0.049	337.9710	-73.4079	337.97096	-73.40786	[10]
990705	0.842	5355	22.78	1.41	0.87	77.47670	-72.1317	77.4770	-72.1315	[11]
990123	1.6	11817	24.41	1.31	0.67	231.3760	+44.7664	231.3762	+44.7664	[12]
980703	0.966	6341	22.9	1.32	0.11	359.7780	+8.58530	359.77780	+8.585300	[13]
970508	0.835	5300	25.2	0.61	0.011	103.4560	+79.2721	103.45604	+79.27208	[14]
970228	0.695	4233	25.88	0.47	0.43	75.4444	+11.7816	75.4442	+11.78159	[15]
Irregular galaxies										
060614	0.125	587	22.52	1.14	0.36	320.8839	-53.0267	320.884	-53.0267	[16]
060218	0.0331	148	20.16	3.21	0.29	50.4153	+16.8671	50.41534	16.86717	[17]
050826	0.296	1535	21.67	1.34	0.40	87.7566	-2.6433	87.75658	-2.64327	[18]
041006	0.712	4360	25.15	0.59	0.03	13.7093	+1.2349	13.70931	+1.23490	[19]
030528	0.782	4890	22.0	1.48	0.66	256.0010	-22.6194	256.0012	-22.6194	[20]
030429	2.66	21986	26.3	1.04	0.67	183.2810	-20.9138	183.28118	-20.91381	[21]
030328	1.52	11110	24.06	1.19	0.68	182.7015	-9.3476	182.70166	-9.34750	[22]
020405	0.691	4204	21.59	1.58	0.19	209.5130	-31.3728	209.5130208	-31.37275	[23]
000926	2.036	15882	24.18	1.47	0.032	256.0400	+51.7862	256.0400	+51.78611	[24]
000911	1.06	7094	25.27	0.68	0.079	34.6432	+7.7410	34.64316	+7.74102	[25]
980613	1.097	7418	25.33	0.68	0.089	154.4910	+71.4571	154.4910	+71.457083	[26]
971214	3.42	29750	26.35	2.72	0.14	179.1100	+65.2001	179.1100	+65.20013	[27]

Note. — Col. (1) GRB name. Col. (2-3) Redshift and luminosity distance in Mpc. Col. (4) Observed host magnitude in the R -band AB system (Fruchter et al. 2006, and references therein). Col. (5) Radius in arcsec used in this work. Col. (6) Distance in arcsec between GRB and host. Col. (7-8) Positions of the host. Col.(9-10) Positions of the GRB. Col. (11) References: [1] Graziani et al. (2003); Vreeswijk et al. (2004); [2] Jakobsson et al. (2005); [3] Grav et al. (2001); Holland et al. (2002); [4] Subrahmanyan et al. (2001); Bloom et al. (2002); [5] Price et al. (2002); [6] Henden and Vrba (2001); Galama et al. (2003); [7] Mirabal et al. (2000); Bloom et al. (2003); [8] Gorosabel et al. (2003b); [9] Jensen et al. (1999); Christensen et al. (2004) ; [10] Sahu et al. (2000); Christensen et al. (2004); [11] Palazzi et al. (1999); Le Floch et al. (2002); [12] Bloom et al. (1999); [13] Taylor et al. (1998); Djorgovski et al. (1998); Christensen et al. (2004); [14] Frail et al. (1997); Bloom et al. (1998); Christensen et al. (2004); [15] Margon et al. (1997); Bloom et al. (2001); [16] Parsons et al. (2006); Gal-Yam et al. (2006); Gehrels et al. (2006); [17] Mirabal et al. (2006); [18] Mirabal et al. (2007); [19] Yamaoka et al. (2004); Wainwright et al. (2007); [20] Butler et al. (2004); Rau et al. (2004); [21] Jakobsson et al. (2004); [22] Peterson and Price (2003); Gorosabel et al. (2005); [23] Wainwright et al. (2007); [24] Price et al. (2001); Fynbo et al. (2001); [25] Price (2000); Masetti et al. (2005); [26] Hjorth et al. (2002); Halpern and Fesen (1998); [27] Odewahn et al. (1998).

with a linear distance scale is more reliable than with an angular scale from the galaxy center.

3.3.1 Discussion

We have calculated the probability for a GRB to be coincident with a galaxy on the sky, using the luminosity function and the radius-luminosity relation derived from the SDSS and VVDS surveys.

Since there is not a reliable luminosity function available to higher redshifts, the probability is calculated only up to a redshift $z \sim 1.5$ (Fig. 3.2). The results are in agreement with that of Cobb et al. (2006) and Cobb and Bailyn (2008) which were obtained with different approaches. The total probability at $z = 1.5$ is a few percent.

We have also calculated the probability of chance coincidence with a criterion that a GRB is considered to be associated with a galaxy if the distance from the GRB to the galaxy center is smaller than $1''$ (Fig. 3.2, dashed line). This probability is larger than that calculated with R_{90} for $z > 0.7$ (Fig. 3.2, solid line), caused by the fact that for a fixed angular separation the corresponding linear separation increases with z and R_{90} decreases with z .

Although the chance probability is small, it warns us that identifying a GRB host based only on the superposition of a GRB with a galaxy on the sky is dangerous. So far about 350 GRBs have been detected by *Swift*, our results imply that several chance coincidence of a GRB with a galaxy might have already happened. As a result, some GRB hosts that have been found might be superficial. However, for the case of GRB 060614, calculation of the chance superposition of it and a $z < 0.125$ galaxy with separation $< 0.5''$ leads to a probability $P = 0.02\%$, consistent with the result of Gal-Yam et al. (2006). This small probability indicates that the association of GRB 060614 and its host is secure.

Obviously, a secure identification of a GRB's host would be obtained by (1) the superposition of the GRB with a galaxy; and (2) the afterglow of the GRB and the host candidate give rise to the same measured redshift.

We have also calculated the probability directly from the data of SDSS, following the approach of Cobb et al. The results agree with our analytical results.

Chapter 4

Host Galaxies in Cosmological Simulations

We analyse the properties of host galaxies of LGRBs, using a galaxy catalogue constructed by combining high-resolution N-body simulations with a semi-analytic model of galaxy formation. In particular, we use the models discussed in Wang et al. (2008) for two cosmological models with parameters taken from the first-year and the third-year Wilkinson Microwave Anisotropy Probe (WMAP) (Spergel et al., 2003) measurements. To select candidate host galaxies of LGRBs, we extract from the available semi-analytic galaxy catalogues the information for the age and metallicity of newly formed stars and we adopt the collapsar model. We built three samples of host galaxies with different metallicity thresholds, and we compare the properties of the selected galaxies with observational data, in particular the data in Savaglio et al. (2008). Compared with previous theoretical studies, the simulations used in our study have the largest volume, and they also allow us to explore the cosmological dependence. Finally, the information available from the semi-analytic catalogues enable us to study the clustering and descendent properties of LGRB hosts.

4.1 The Simulated Galaxy Catalogues

In this study, we use the galaxy catalogues constructed by Wang et al. (2008) for two simulations with cosmological parameters from the first and third-year WMAP results. The two sets of cosmological parameters are listed in Table 4.1. As discussed in Wang et al. (2008), the most significant differences between WMAP1 and WMAP3 cosmological parameters are a lower value of σ_8 and a redder (smaller) primordial power

	WMAP1	WMAP3
Ω_m	0.25	0.226
Ω_Λ	0.75	0.774
Ω_b	0.045	0.04
σ_8	0.9	0.722
h	0.73	0.743
n	1	0.947

Table 4.1 Cosmological parameters of the two simulations used in Wang et al. (2008). Ω_m , Ω_Λ , Ω_b represent the density of matter, dark energy, and baryons respectively. σ_8 and n are the amplitude of the mass density fluctuations, and the slope of the initial power spectrum. The Hubble constant is parameterised as $H_0 = 100 h \text{ km s}^{-1} \text{ Mpc}^{-1}$.

spectrum index n in WMAP3, resulting in a significant delay for structure formation. Both simulations correspond to a box of $125 h^{-1} \text{ Mpc}$ comoving length and a particle mass 8.6×10^8 (WMAP1) and $7.8 \times 10^8 M_\odot$ (WMAP3). The softening length is $5 h^{-1} \text{ kpc}$ in both simulations (see Table 2 in Wang et al. 2008). Simulation data were stored in 64 outputs, that are approximately logarithmically spaced in time between $z = 20$ and $z = 1$, and linearly spaced in time for $z < 1$. Each simulation output was analysed with the post-processing software originally developed for the Millennium Simulation (Springel et al., 2005).

Merging history trees for self-bound structures extracted from the simulations were used as input for the Munich semi-analytic model of galaxy formation. Interested readers are referred to Croton et al. (2006), De Lucia and Blaizot (2007) and references therein for details on the physical processes explicitly modelled. Previous work has shown that the galaxy population predicted by this particular model provides a reasonably good match with the observed local galaxies properties and relations among stellar mass, gas mass, and metallicity (De Lucia et al., 2004), luminosity, colour, morphology distributions (Croton et al., 2006; De Lucia et al., 2006), and the observed two-point correlation functions (Springel et al., 2005; Wang et al., 2008). In addition, Kitzbichler and White (2007) have shown that the model also agrees reasonably well with the observed galaxy luminosity and mass function at higher redshift.

We remind the reader that the models discussed in Wang et al. (2008) adopt the same physics, but different combinations of model parameters are used for the simulations with WMAP1 and WMAP3 cosmology. The WMAP1 simulation uses the same parameters (and physical model) adopted in De Lucia and Blaizot (2007). For the WMAP3 simulation, the model adopts lower supernovae and AGN feedback efficiencies in

order to compensate for the delay in structure formation obtained with a lower σ_8 . This combination of model parameters corresponds to the WMAP3B model used in Wang et al. (2008). The alternative model WMAP3C used in that paper leads to very similar results and so will not be discussed further in this paper. In the following, we limit our analysis to galaxies with stellar mass larger than $2 \times 10^8 M_\odot$, which is above the resolution limit of the N-body simulations used.

We note that the most recent cosmological model from the five-year data of WMAP is between WMAP1 and WMAP3, so the results from the two simulations used here are expected to bracket results from a simulation with the 5-year WMAP cosmology.

4.2 Identification of LGRB host galaxies

In order to identify candidate GRB host galaxies, we adopt the collapsar model for LGRBs: all young stars with mass $> 30 M_\odot$ ending their life with a supernova should be able to create a BH remnant. If the collapsar has high angular momentum, the formation of the BH is accompanied by a GRB event (Yoon et al., 2006, 2008). As mentioned in Sec. ??, recent studies on the final evolutionary stages of massive stars have suggested that a Wolf-Rayet (WR) star can produce a LGRB if its mass loss rate is small, which is possible only if the metallicity of the star is very low. When metallicities are lower than $\sim 0.1 - 0.3 Z_\odot$, the specific angular momentum of the progenitor allows the loss of the hydrogen envelope while preserving the helium core (Woosley and Heger, 2006; Fryer et al., 1999). The loss of the envelope reduces the material that the jet needs to cross in order to escape, while the helium core should be massive enough to collapse and power a GRB.

In order to construct our host galaxy sample, we have extracted from the available semi-analytic catalogues the information about the age and metallicity of all stars. We have then created the following host samples:

1. HOST1, obtained by selecting galaxies containing stars with age $< t_c = 5 \times 10^7 \text{yr}$;
2. HOST2, including galaxies with stars of age $< t_c$ and metallicity $Z \leq 0.3 Z_\odot$;
3. HOST3, defined by selecting galaxies containing stars with age $< t_c$ and metallicity $Z \leq 0.1 Z_\odot$.

In order to count the number of GRB events in each galaxy, we make use of two

	$N[M_{\odot}^{-1}]$	$m_{*,\min}$	$m_{*,\max}$
SNe	7.421×10^{-3}	8	100
BH	1.035×10^{-3}	30	100

Table 4.2 Number of SNe and BHs per solar mass of stars formed, using a Salpeter IMF.

important pieces of information: (a) the rate of GRB with respect to the SNe explosions (without any cut in metallicity for the progenitors stars); (b) the rate of very massive stars (producing remnant BHs) as a function of redshift and metallicity with respect to the total number of SNe events. In this way we are able to count how many BHs with low metallicity progenitors will produce GRBs.

We assume a Salpeter Initial Mass Function (IMF) and compute the number of stars ending their lives as supernovae (SNe) or as black-holes (BHs) per unit mass of stars formed by:

$$N = \frac{\int_{m_{*,\min}}^{m_{*,\max}} \phi(m_*) dm_*}{\int_{0.1}^{m_{*,\max}} m_* \phi(m_*) dm_*}, \quad (4.1)$$

where $\phi(m_*)$ is the IMF, $m_{*,\min}$ is the minimum initial mass to form a supernova or a black hole, and $m_{*,\max}$ is the upper limit of the mass function. We take $m_{*,\min}$ to be $8 M_{\odot}$ for SNe and $30 M_{\odot}$ for BHs (Fryer et al., 1999), and $m_{*,\max} = 100 M_{\odot}$ (the lower limit of the IMF is taken to be $0.1 M_{\odot}$). Eq. 4.1, evaluated for progenitor stars of all metallicities, provides the numbers listed in Table 4.2. Without any restriction on the metallicity of the progenitor stars, the relative number of BHs and supernovae is ~ 14 per cent (140 BHs per 1000 SNe). When considering the metallicity threshold for BHs, the rate is reduced and varies with redshift (Langer and Norman, 2006; Wolf and Podsiadlowski, 2007). This is illustrated in Fig. 5.3 for the two different metallicity thresholds adopted in our study. At low redshift, there are from 0.1 to 6 low-metallicity BHs formed per 1000 SNe. The rate grows with increasing redshift, reaching values between ~ 10 ($Z < 0.1 Z_{\odot}$) and ~ 70 ($Z < 0.3 Z_{\odot}$) at redshift ~ 9 .

Integrating over the redshift, Fig. 5.3 allows us to calculate the average ratio between the number of black holes from different progenitors and the number of supernovae in the Universe. However, not every black hole will produce a LGRB. To normalise the LGRB abundance, we assume that the rate of GRB per SNe is on average (over all cosmic times)

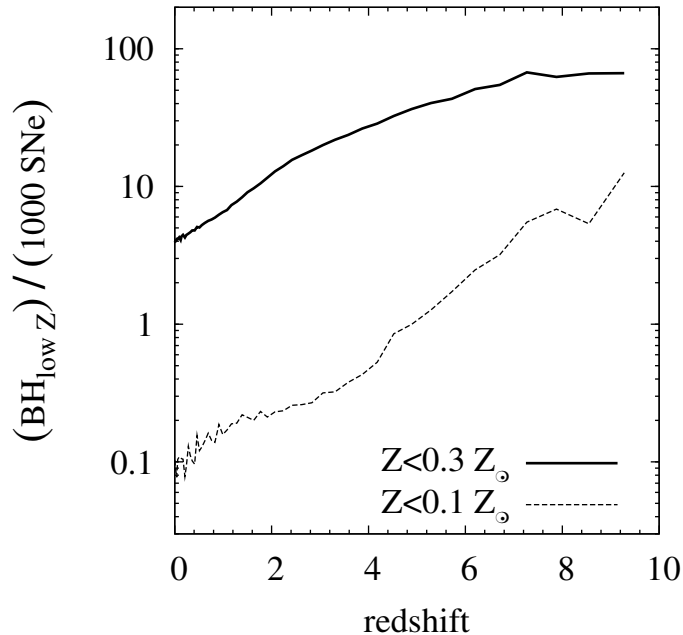


Figure 4.1 Number of low-Z BHs per 1000 SNe as a function of redshift, for progenitor stars with metallicity lower than $0.3 Z_{\odot}$ and $0.1 Z_{\odot}$. Results are shown for the model WMAP3B. Similar results are obtained in the WMAP1 case.

of about 1 GRB event every 1000 SNe (Porciani and Madau, 2001; Langer and Norman, 2006). The number of LGRBs relative to the black holes in the three samples (with or without the metallicity cutoff) is given by

$$R_{\text{GRB}} = \frac{\text{GRBs}}{\text{BHs}_{\text{lowZ}}} = \frac{\text{GRBs}}{1000\text{SNe}} \times \left\langle \frac{1000\text{SNe}}{\text{BHs}_{\text{lowZ}}} \right\rangle. \quad (4.2)$$

where the last term is obtained by integrating over redshift (or cosmic time). For the HOST1 sample, the last term is a constant ($1/140$), and thus $R_{\text{GRB}} \sim 0.007$; for the other two samples, we obtain $R_{\text{GRB}} \sim 0.056$ and ~ 1 .

For each galaxy in the simulation box, we can count how many BHs are produced from low metallicity progenitors and then obtain the corresponding number of LGRBs:

$$N_{\text{LGRBs}} = \text{BHs}_{\text{lowZ}} \times R_{\text{GRB}}.$$

It is important to note that our model provides only an upper limit to the number of LGRB events because the formation of BHs and low metallicity are only two of many requirements for the production of LGRBs. E.g., high spin of the progenitor star is another requirement that cannot be handled in our model. In the following, we consider each galaxy hosting at least one GRB event ($N_{\text{LGRBs}} \geq 1$) as a ‘host galaxy’.

There are relatively few galaxies with $N_{\text{LGRBs}} < 1$ and their inclusion does not change our results significantly.

We stress that we are not using the (average) galaxy metallicity to select our host galaxy samples, but the metallicity of each ‘pocket’ of stars formed at each time-step. Stars are assumed to form with the metallicity of the interstellar medium at the time of star formation, and the model adopts an instantaneous recycling approximation for metal enrichment. So, the gas-phase metallicity of host galaxies will generally be higher than the metallicity threshold we have adopted for our samples.

Note that the LGRB rate computed above is not directly comparable to the observed rate because that would require us to take into account many unknown factors like the jet angle, and to include any possible observational bias (see Lapi et al., 2008; Li, 2008b).

4.3 Results

In this section, we discuss the physical properties of LGRB hosts selected using the procedure described in Sec. 4.2. In particular, we compare the LGRB rate to the cosmic star formation rate (Sec. 4.3.1), and the properties of LGRBs hosts to the global properties of galaxies at the same cosmic epoch (Sec. 4.3.2). We also study the typical environment (Sec. 4.3.3) and evolutionary stage (Sec. 4.3.4) of LGRB host galaxies.

4.3.1 The cosmic star formation rate versus the LGRB rate

The collapsar model links LGRBs to the evolution of single massive stars whose lifetimes are negligible on cosmological scales. If no other condition is required for producing a LGRB event, then the rate of LGRBs should be an unbiased tracer of the global star formation in the Universe (e.g. Totani, 1997; Wijers et al., 1998; Mao and Mo, 1998; Porciani and Madau, 2001; Bromm and Loeb, 2002; Fynbo et al., 2006; Price et al., 2006; Savaglio, 2006; Totani et al., 2006; Prochaska et al., 2007; Li, 2008b, and references therein). Fynbo et al. (2008) have recently suggested that GRB and Damped Lyman-Alpha samples, in contrast with magnitude limited samples, provide an almost complete census of $z \sim 3$ star-forming galaxies. We note, however, that the sample used in this study are biased against high-metallicity and dusty systems.

However, both observations and theoretical studies indicate that the metallicity of the progenitor star plays an important role in setting the necessary conditions for a LGRB

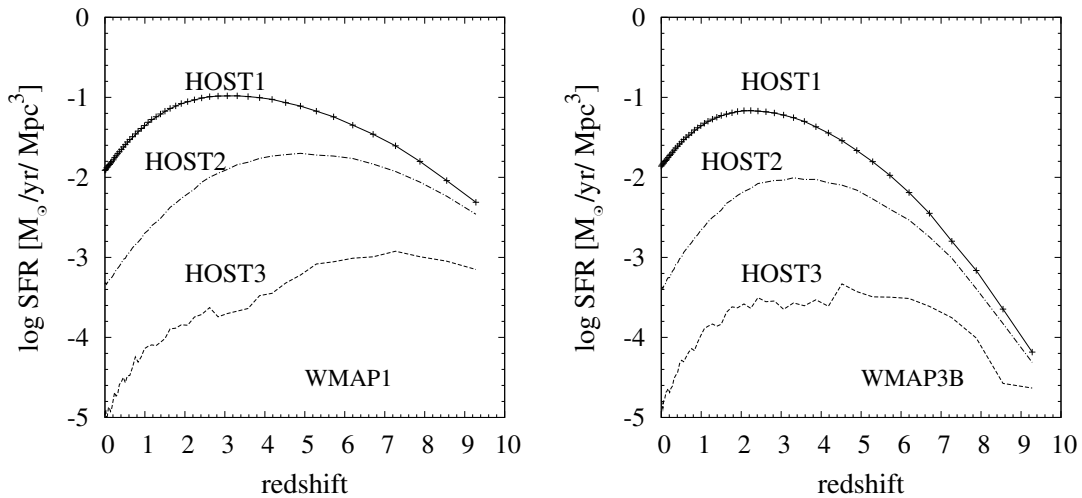


Figure 4.2 Log $SFR [M_{\odot} \text{yr}^{-1} \text{Mpc}^{-3}]$ as a function of redshift, computed for all galaxies in the simulation box (solid line). Left and right panels correspond to the WMAP1 and WMAP3 simulations respectively. The dot-dashed and dashed lines corresponds to the HOST2 and HOST3 samples. The sample with no threshold on metallicity (HOST1) traces exactly the global star formation rate measured considering all galaxies in the simulated boxes (solid line).

explosion. In this case, the rate of LGRBs is expected to be a biased tracer of the cosmic star formation rate. This is demonstrated explicitly in Fig. 5.1, which compares the cosmic star formation rate obtained using all galaxies in the simulation box to that obtained for the three LGRB host samples defined in the Sec. 4.2.

The sample with no threshold on metallicity (HOST1) traces exactly the global star formation rate (solid line in Fig. 5.1). This is not the case for the two samples with metallicity thresholds (HOST2 - dot-dashed line and HOST3 - dashed line). For the HOST2 and HOST3 samples, the LGRB rate peaks at higher redshift than the cosmic star formation rate, as a consequence of the global decrease of metallicity with increasing redshift. At higher redshift, the mean metallicity of the intergalactic medium is lower, which implies that a larger fraction of stars form below the metallicity thresholds adopted for HOST2 and HOST3. Therefore the deviation of the LGRB rate from the star formation rate decreases with increasing redshift. At $z \sim 9$, the HOST2 sample measures about 99 per cent of the global star formation density. The fraction decreases to about 30 per cent at $z \sim 5$ and to only about 10 per cent at present. For the HOST3 sample, the bias is even stronger because of the lower metallicity threshold: it traces only 30 per cent of the global star formation density at $z \sim 9$, and less than 10 per cent at $z < 5$. The results shown in Fig. 5.1 are in qualitative agreement with recent observational estimates (Kistler et al.,

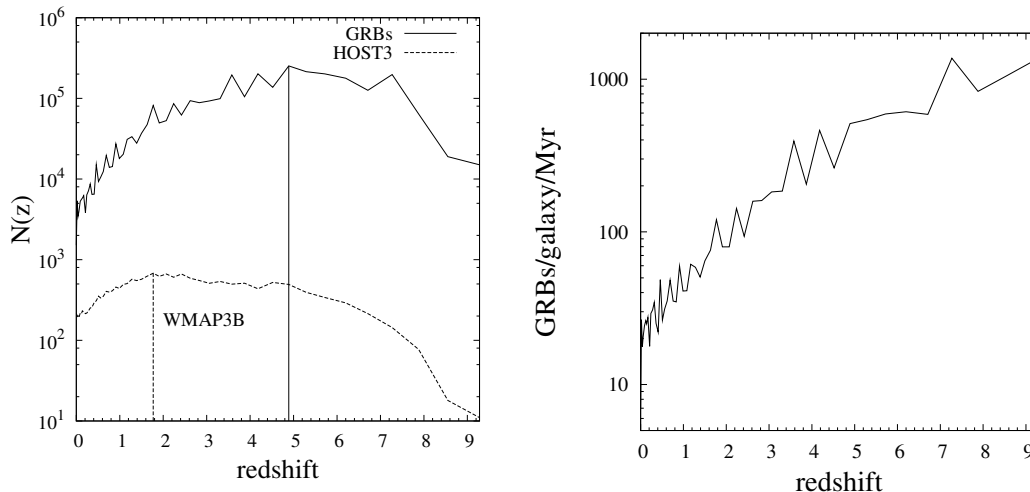


Figure 4.3 Left panel: redshift distribution of LGRB events (solid line) and of host galaxies (dashed line), for the sample HOST3 (with metallicity threshold $0.1 Z_{\odot}$). The vertical lines indicate the peaks of the distributions. Right panel: the rate of LGRBs per galaxy per Myr. Both panels correspond to results from the WMAP3 simulation.

2008), and with recent theoretical studies also based on the collapsar model (Yoon et al. 2006, Cen and Fang 2007, Nuza et al. 2007, Lapi et al. 2008).

Finally, Fig. 5.1 also shows that adopting a cosmological model compatible with third-year WMAP measurements (right panel), a delay is produced in the cosmic star formation rate, due to the delay in structure formation. Except for this delay, the predicted trends are the same for the WMAP1 and WMAP3 simulations. In the following, we will only show results obtained using the WMAP3 simulation as those obtained for the WMAP1 simulation are very similar. In addition, we will focus only on the two host samples with metallicity thresholds (HOST2 and HOST3).

We remind the reader that we consider as ‘hosts’ all galaxies which can host at least one LGRB event between two simulation output. Since galaxies at higher redshift have lower metallicities and form stars at higher rates, the rate of LGRBs per host galaxy increases rapidly with redshift. The left panel in Fig. 4.3 shows the redshift evolution of the number of LGRBs (solid line) and of host galaxies (HOST3 - dashed line). The two vertical lines indicate the peaks of the distributions: the number of LGRBs peaks at $z \sim 5$, while the number of host galaxies is maximum at $z \sim 2$. The right panel of Fig. 4.3 shows the rate of LGRBs per galaxy and per Myr computed for the WMAP3 simulation and for the HOST3 sample. The predicted rate of LGRBs decreases from ~ 1000 at $z \sim 9$ to about $10 \text{ Myr}^{-1} \text{ galaxy}^{-1}$ at $z \sim 0$, in agreement with calculations by Fryer et al.

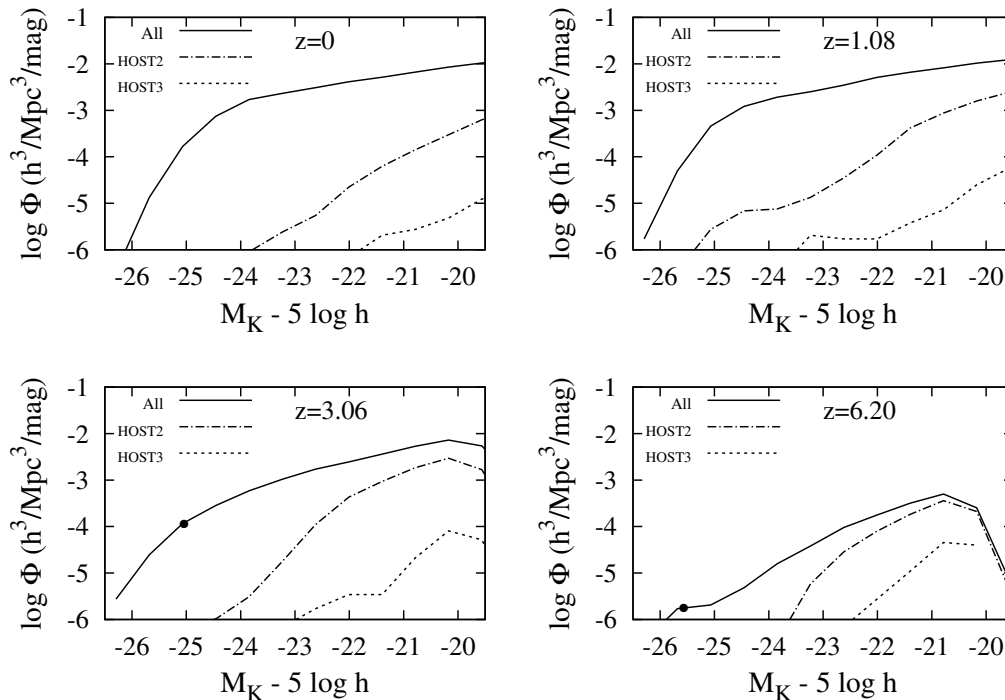


Figure 4.4 Luminosity function of the HOST2 (dot-dashed line) and the HOST3 (dashed line) samples, compared to the galaxy luminosity function measured using all galaxies in the simulation box (solid line). Different panels are for different redshifts: 0 (top left panel), 1.08 (top right panel), 3.06 (bottom left panel), and 6.20 (bottom right panel). In the last two panel the dark bullet shows the characteristic luminosity L_* .

(1999). Note that the LGRB rate computed above is not directly comparable to the observed rate because that would require us to take into account many unknown factors like the jet angle, and to include any possible observational bias (see Lapi et al., 2008; Li, 2008b).

4.3.2 Physical properties of LGRB host galaxies

A number of recent papers have studied the physical properties of LGRB host galaxies using deep observations covering a large wavelength range, both in imaging and in spectroscopy. These studies have revealed that LGRB host galaxies are typically faint and star forming galaxies, dominated by young and metal-poor stellar populations (Le Floch et al., 2003; Fruchter et al., 2006; Wainwright et al., 2007; Savaglio et al., 2008). In this section, we analyse the physical properties of our model host galaxies, and compare these with the properties of the average galaxy population, and with observational estimates.

Fig. 4.4 shows the K-band rest-frame luminosity function of host galaxies for the HOST2 (dot-dashed line) and the HOST3 (dashed line) samples, compared with the galaxy luminosity function measured considering all galaxies in the simulation box, at different redshift. At all redshifts, LGRB host galaxies have luminosities well below the characteristic luminosity L_* , in agreement with observational measurements. While the total luminosity function evolves strongly with the redshift (particularly beyond $z \sim 1$), the number densities and the range of luminosities of LGRB host galaxies vary more mildly, due to the fact that at higher redshift a larger fraction of the whole galaxy population can host LGRBs.

Recent observational studies have focused on the stellar mass distribution of GRB host galaxies. Castro Cerón et al. (2008) have found that the typical stellar mass of host galaxies is smaller than the stellar mass of field galaxies at the same redshift. For a sample of 30 LGRB hosts, they provide estimates of the stellar mass between 10^7 and $10^{11} M_\odot$, with a mean value of $M_* \sim 10^{9.7} M_\odot$. About 70 per cent of the host galaxies in their sample have stellar mass $M_* < 10^{10.1} M_\odot$. Similar results have been found by Savaglio et al. (2008). Using a sample of 46 GRB hosts -the largest sample so far- they estimate a median stellar mass of $10^{9.3} M_\odot$, and find that about 83 per cent of the studied systems have stellar mass between $10^{8.5}$ and $10^{10.3} M_\odot$.

In Fig. 4.5 we compare the galaxy mass distribution for model host galaxies from the HOST2 and HOST3 samples to the distribution obtained considering all galaxies in the simulated box. For this figure, all galaxies and hosts at all redshifts up to $z \sim 9$ have been used. Fig. 4.5 shows that LGRB host galaxies have typically low mass with a small fraction of them having stellar mass up to $\sim 10^{11} M_\odot$. About 90 per cent of the host galaxies have stellar mass $< 10^9 M_\odot$ and $< 10^{10} M_\odot$ for HOST3 and HOST2 respectively.

It is well known that the galaxy stellar mass is tightly correlated with the rest-frame K-band luminosity. Savaglio et al. (2008) have shown that this relation applies to GRB host galaxies as well, but they argue that GRB galaxies have on average higher luminosity than “field” galaxies with the same stellar mass, implying a lower M_*/L_K ratio, as expected for younger galaxies. We compare results from our model to observational measurements in Fig. 4.6. The dashed black line is the best-fit to the observational data by Savaglio et al. (2008): $\log M_* = -0.463 \times M_K - 0.102$. The red line in Fig. 4.6 shows the mean luminosity-

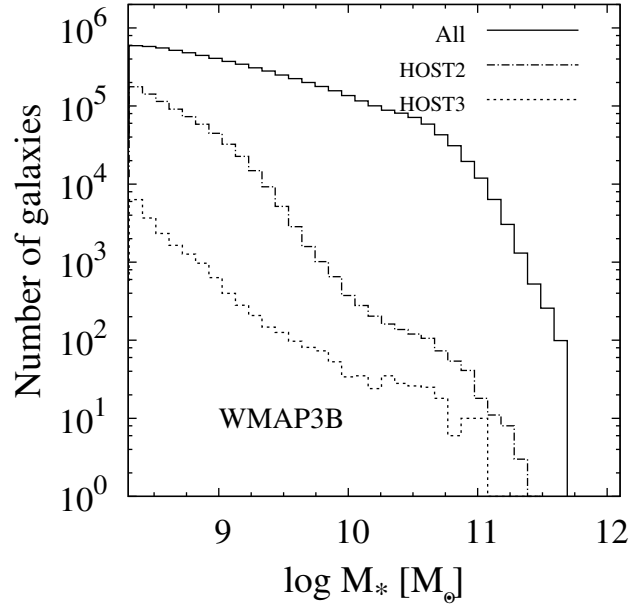


Figure 4.5 Galaxy mass function for the HOST2 (dot-dashed line) and HOST3 (dashed line) samples, compared to the galaxy mass function measured using all galaxies in the simulation box (solid line). All galaxies with $z \leq 9$ have been used in this figure.

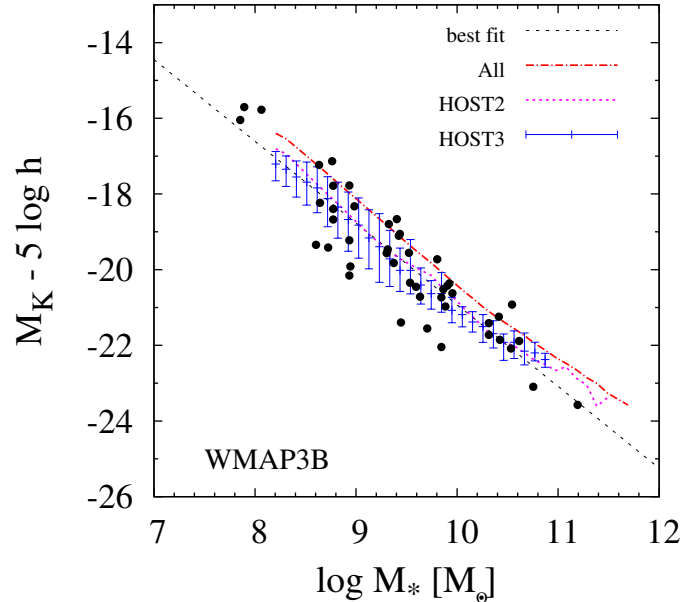


Figure 4.6 Mean K-band absolute magnitude as a function of stellar mass for all galaxies in the simulation (red line), for galaxies in the HOST2 sample (green), and for galaxies in the HOST3 sample (blue). Black symbols correspond to observational data from Savaglio et al. (2008), and the dotted black line is the fit provided by the same author ($\log M_* = -0.463 \times M_K - 0.102$).

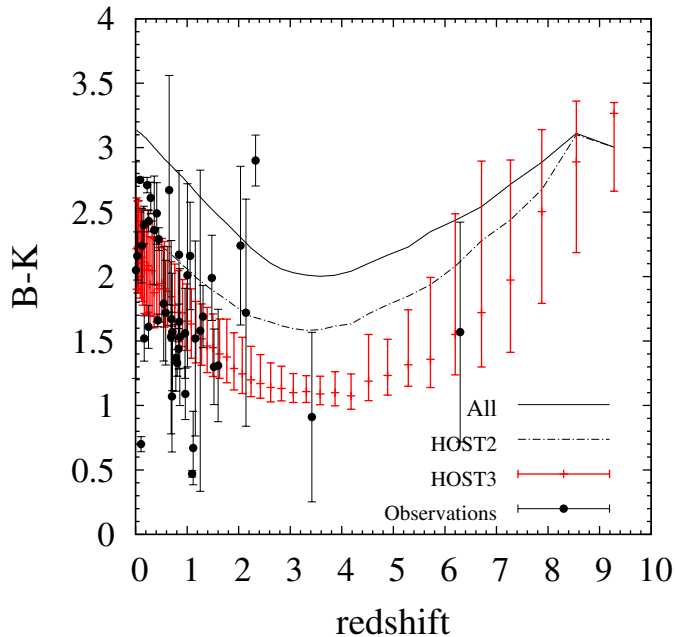


Figure 4.7 Median B-K colour as a function of redshift for observed GRB hosts (black crosses), all galaxies in the simulation (solid line), galaxies from the HOST2 sample (dot-dashed line), and galaxies from the HOST3 sample (red crosses).

mass relation obtained by using all galaxies in the simulation boxes up to $z \sim 9$. The pink line shows the mean value for host galaxies in the HOST2 sample, and the blue line corresponds to the mean value obtained for the HOST3 sample. For this sample, we also show the quartiles of the distribution. We note that Savaglio et al. (2008) adopt a Baldry & Glazebrook IMF for their stellar mass estimates, while the model used in this study adopts a Chabrier IMF to compute model magnitudes. In order to compare model results with observational estimates, we have decreased the observed stellar mass by a factor 1.3. Fig. 4.6 shows that the K-band absolute magnitude distribution of simulated GRB host galaxies is in good agreement with observations. It also shows that, on average, host galaxies have stellar masses which are lower, although with a large scatter, than “typical” galaxies with the same mass, in agreement with observational findings.

In Fig. 4.7, we compare the median colour of model LGRB host galaxies with observational measurements by Savaglio et al. (2008, shown as black symbols). Model results indicate that GRB galaxies are typically bluer than the average galaxy population at the same redshift. We note that the observed colours exhibit a quite large scatter, probably due to the unknown dust extinction.

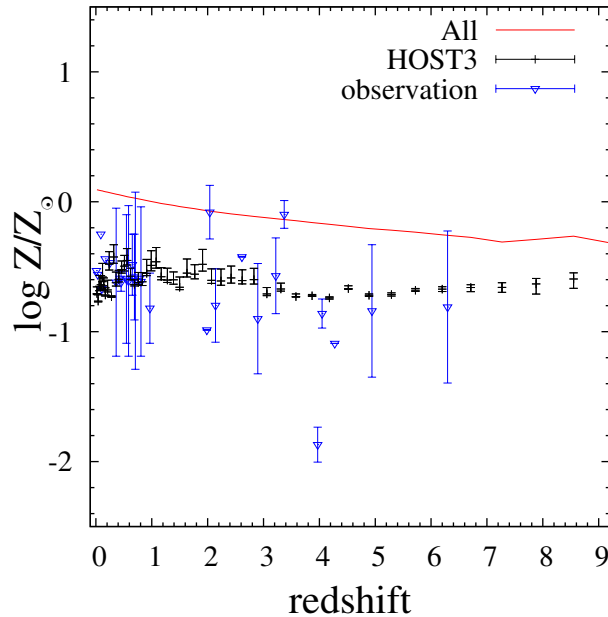


Figure 4.8 Median gas metallicity as a function of redshift for all galaxies in the simulation box (red line), and for galaxies from the HOST3 sample (dark crosses, error bars show the quartiles of the distributions). The blue triangles are observational measurements for GRB-DLAs host galaxies from Savaglio (2006) and for the GRB host galaxies studied in Savaglio et al. (2008).

Fig. 4.8 shows the median gas metallicity evolution for the HOST3 sample (black crosses) compared with the observational estimates for the GRB-DLAs studied in Savaglio et al. (2006, 2008 - blue triangles with error bars a few show the lower and upper-branch metallicity solution in Savaglio et al. 2008). The red line in Fig. 4.8 shows the median metallicity obtained using all galaxies in the simulation box. The figure shows that the metallicity of model galaxies (both “normal” and hosts) does not evolve significantly with redshift. The observational measurements exhibit a large scatter and have typically large uncertainties. Within these, model predictions are in relatively good agreement with observational data. It should be noted that the lack of evolution in the gas-phase metallicity of the HOST3 sample is essentially due to our selection method. In order to enter this sample, host galaxies must have young stars with metallicity lower than $Z \leq 0.1Z_{\odot}$. In the model used in this study, stars form with the metallicity of the gas-phase component, so the adopted selection requires host galaxies to have gas-phase metallicity close to the adopted threshold (it will be typically higher because the model adopts an instantaneous recycling approximation).

Another important and well studied relation is the luminosity-metallicity relation. This

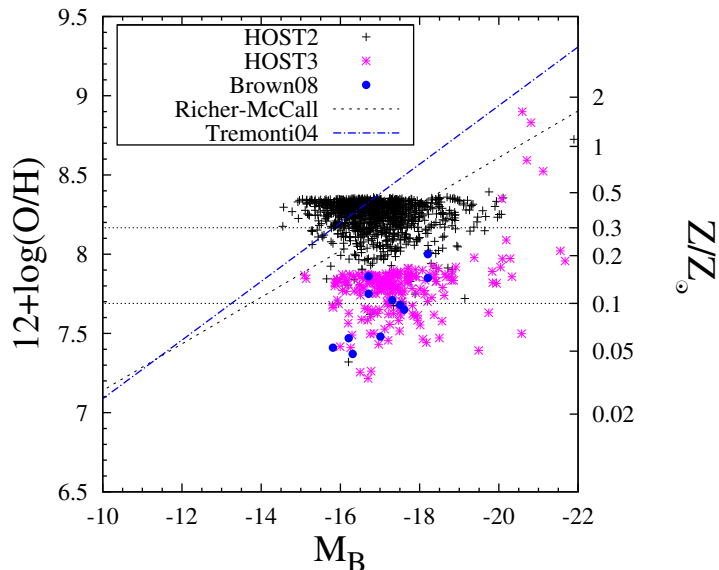


Figure 4.9 Gas metallicity as function of the B-band luminosity for model galaxies with $z < 0.1$ from the HOST3 (magenta asterisks) and HOST2 (black crosses) samples, compared with observational measurements by Brown et al. (2008, blue circles) for a sample of metal-poor galaxies. The blue-dashed and black-dotted lines show the metallicity-luminosity relation measured by Richer and McCall (1995) for a sample of dwarf galaxies, and by Tremonti et al. (2004) for SDSS star forming galaxies.

has been measured for a very large sample of star forming galaxies from the Sloan Digital Sky Survey (SDSS) by Tremonti et al. (2004), and for smaller samples of galaxies by other authors. In particular, Brown et al. (2008) have recently suggested a technique to identify extremely metal-poor galaxies which share very similar properties (age, metallicity, star formation rates) with hosts of LGRBs. The data from Brown et al. (2008) are plotted in Fig. 4.9 as blue circles, together with the observed relations by Tremonti et al. (2004), and by Richer and McCall (1995) for a sample of irregular galaxies. Model results for the HOST3 sample are plotted as magenta asterisks and lie in the same region occupied by the Brown et al. data. Dark crosses show the corresponding results for the HOST2 sample. As explained above, the adopted selection results in clear metallicity cuts in Fig. 4.9. Observational studies of gas-phase metallicity of GRB hosts could therefore provide important information on the metallicity of the progenitor stars, although inhomogeneous mixing of metals could complicate the interpretation. The few objects in the HOST3 samples with high metallicity are galaxies with very high star formation rate (which coupled with the instantaneous recycling approximation, results in quite high metallicities

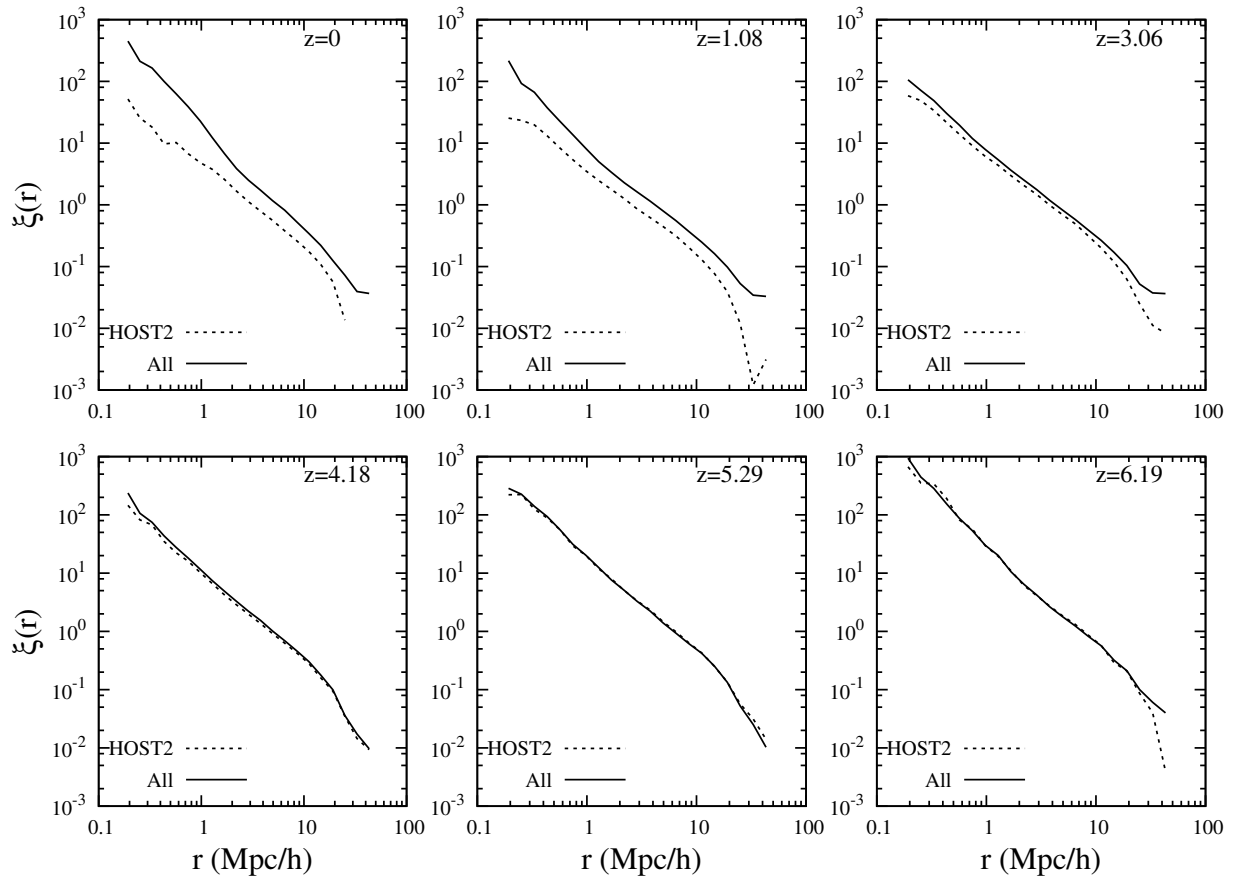


Figure 4.10 Two-point auto-correlation function for LGRB host galaxies from the HOST2 sample (dashed line) and for normal galaxies (solid line), at different redshifts, for WMAP3B cosmology.

of the inter-stellar medium).

4.3.3 The environment of LGRB host galaxies

The physical environment of LGRB host galaxies can provide important information on the origin of LGRBs. The analysis of GRB hosts environments is, however, quite difficult from the observational viewpoint, given the very low number of identified and well studied host galaxies. Only a few observational studies have attempted to address this question in the past few years. Gorosabel et al. (2003a) used photometric redshift information in a field of $6\text{arcmin} \times 6\text{arcmin}$ containing the host galaxy of GRB 000210, and found no obvious galaxy concentration around the host. Bornancini et al. (2004) analysed the cross-correlation function between host galaxies and surrounding field galaxies using VLT and public HST data, and concluded that host galaxies do not reside in high density environments.

The semi-analytic catalogues used in our study provide the positions of the LGRB host galaxies, as well as of all other galaxies in the simulation box. We have used this information to study the auto-correlation function of host galaxies, and the cross-correlation function between hosts and all galaxies in the simulation (which we will call “normal” galaxies).

In order to compute the two-point correlation function, we adopt the Landy and Szalay (1993) estimator:

$$\xi(r) = \frac{DD(r) - 2DR(r)}{RR(r)} + 1 \quad (4.3)$$

where $DD(r)$ is the number of galaxy-galaxy pairs at distance r , $RR(r)$ is the number of random-random pairs, and $DR(r)$ is the number of random-galaxy pairs.

Fig. 4.10 shows the auto-correlation function for LGRB host galaxies in the HOST2 sample (dashed line) and for normal galaxies (solid line). The number of galaxies in the HOST3 sample are too low to compute a reliable correlation function. Results are shown for the WMAP3B model, but they are similar for the WMAP1 simulation. At low redshift, the auto-correlation function of host galaxies is lower than the corresponding function for normal galaxies. The difference between the two functions decreases with increasing redshift and the two functions almost perfectly overlap at $z > 4$. As explained in Sec. 4.3.1, this is due to the decrease of metallicity at high redshift which implies that an increasing fraction of the global galaxy population can host a LGRB event according to our selection (see Sec. 4.2).

The two point auto-correlation functions for the HOST2 sample and for normal galaxies at $z = 0$ is repeated in Fig. 4.11, together with the cross-correlation function between host and normal galaxies (solid line). The cross-correlation function lies in between the two auto-correlation functions, suggesting that the probability of finding another host near a GRB host is lower than the corresponding probability of finding a normal galaxy.

Our results are in qualitative agreement with those found by Bornancini et al. (2004) and suggest that LGRB host galaxies tend to populate regions with density lower than average. This is not entirely surprising if one considers that host galaxies are typically low-mass star forming galaxies which preferentially live in low density environments (Kauffmann et al., 2004).

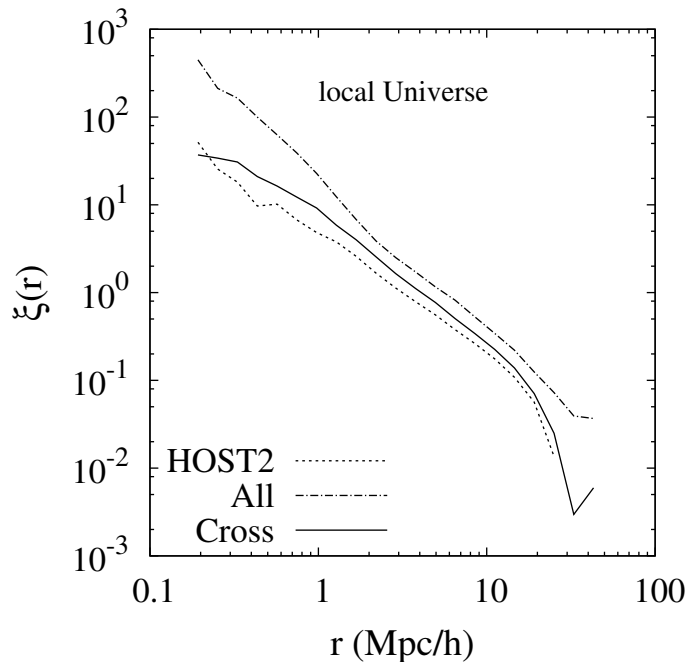


Figure 4.11 Two-point auto-correlation function for HOST2 galaxies (dashed line) and for normal galaxies (dot-dashed line) in the WMAP3B model. The solid line shows the cross-correlation function between host and normal galaxies.

4.3.4 Descendants of high- z LGRB host galaxies

From the theoretical point of view, it is interesting to ask which are the ‘descendants’ of high-redshift LGRB host galaxies. Do they preferentially end up in massive haloes? What are the typical morphology, colour, mass and metallicity of the descendants? While this is a very difficult (if not impossible) question to address observationally, it can be easily addressed with the available semi-analytic catalogues, which contain the full merger tree information for all galaxies in the simulation box.

In this section, we use this information to study the fate of LBRG host galaxies selected at $z \sim 4$ (hereafter *progenitors*) in the observed mass-metallicity and colour-magnitude planes, and the distribution of host halo virial mass of the descendant galaxies. For simplicity, we only show results for our HOST3 sample which contains a lower number of host galaxies than the HOST2 sample. Results are, however, similar for HOST2.

The top-left panel in Fig. 4.12 shows the mass-metallicity relation for our HOST3 sample at $z = 4.18$. The other panels show the location in the same plane of the descendant galaxies, down to $z = 0$. Galaxies are colour-coded as functions of their morphological types which are assigned by the ratio of the total bulge mass to the total

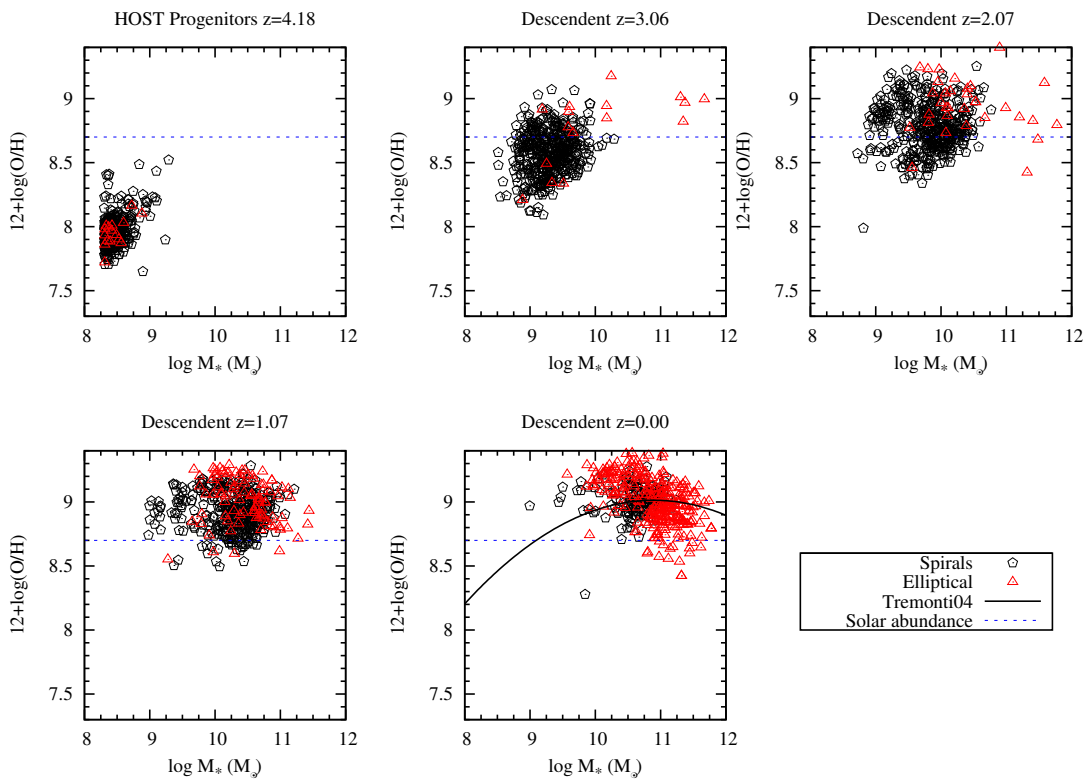


Figure 4.12 Mass-metallicity relation for HOST3 galaxies at redshift 4.18 (top left panel), and for their descendants at lower redshifts in the WMAP3B model. The colour coding indicates galaxies with different morphologies (red triangles for ellipticals and black diamonds for spirals). The solid black line in the bottom right panel shows the best fit relation found by Tremonti et al. (2004). The horizontal dashed line corresponds to the adopted solar abundance.

stellar mass, B/T . Objects with $B/T > 0.5$ are classified as ‘ellipticals’ and are shown as red triangles, black diamonds represent ‘spirals’ ($B/T < 0.5$).

Fig. 4.12 shows that the LGRB host galaxies at redshift ~ 4 are low-mass and low-metallicity galaxies (as discussed in the previous sections), and that the great majority of them do not have a significant bulge component. At later time, galaxies grow in mass and their gas-phase metallicity increases. Fig 4.12 shows that the increase of the gas-phase metallicity is very rapid: a relatively large fraction of descendants at $z \sim 3$ already have solar metallicity [$12+\log(\text{O}/\text{H}) \sim 8.7$, Allende Prieto et al. 2001] and most of the descendants at $z \sim 2$ have super-solar metallicity. This efficient enrichment of the interstellar medium is due to the fact that the semi-analytic model used in our study assumes a perfect mixing efficiency of the metals formed by new stars (De Lucia et al., 2004). The stellar mass of the descendants evolves more slowly, with very few objects jumping to masses larger than $10^{11} M_{\odot}$, probably as a consequence of major mergers. At $z = 0$, all descendants of LGRBs at $z \sim 4$ have relatively high gas-phase metallicities and cover all the mass range between a few times 10^9 and $10^{12} M_{\odot}$. Interestingly, a large fraction of these (about 66 per cent) have a dominant bulge component.

Fig. 4.13 shows the location in the colour-magnitude diagram of LGRB host galaxies at $z = 4.18$ (top left panel) and of all their descendants at later time. LGRB hosts selected at $z \sim 4$ have very blue colours ($R-K < 1$) and relatively faint magnitudes. The descendants of these galaxies become progressively redder (they all have $R-K > 2$ at $z = 0$) and cover a wider range of magnitudes at low redshift. A few objects become very luminous and very red already at $z \sim 3$ (these are the same objects which appear very massive and metal rich at the same redshift in Fig. 4.12).

Finally, in Fig. 4.14 we show the parent halo mass of all descendant of LGRB host galaxies at $z \sim 4$ versus the halo mass of the host. The blue dashed line in each panel shows the one-to-one relation and is plotted to guide eyes. As expected, descendant galaxies reside in larger and larger haloes as time goes on. At $z \sim 2$, the majority of the descendant galaxies still reside in haloes of mass $\sim 10^{11} M_{\odot}$ but a few of them are in relatively massive haloes ($\sim 10^{14} M_{\odot}$) and are satellite galaxies of a very massive cluster at $z = 0$. In the local Universe, the descendants of high- z LGRB hosts reside in haloes of different mass but most of them still reside in haloes with mass between 10^{12} and $10^{13} M_{\odot}$, in agreement with the results in Sec. 4.3.3.

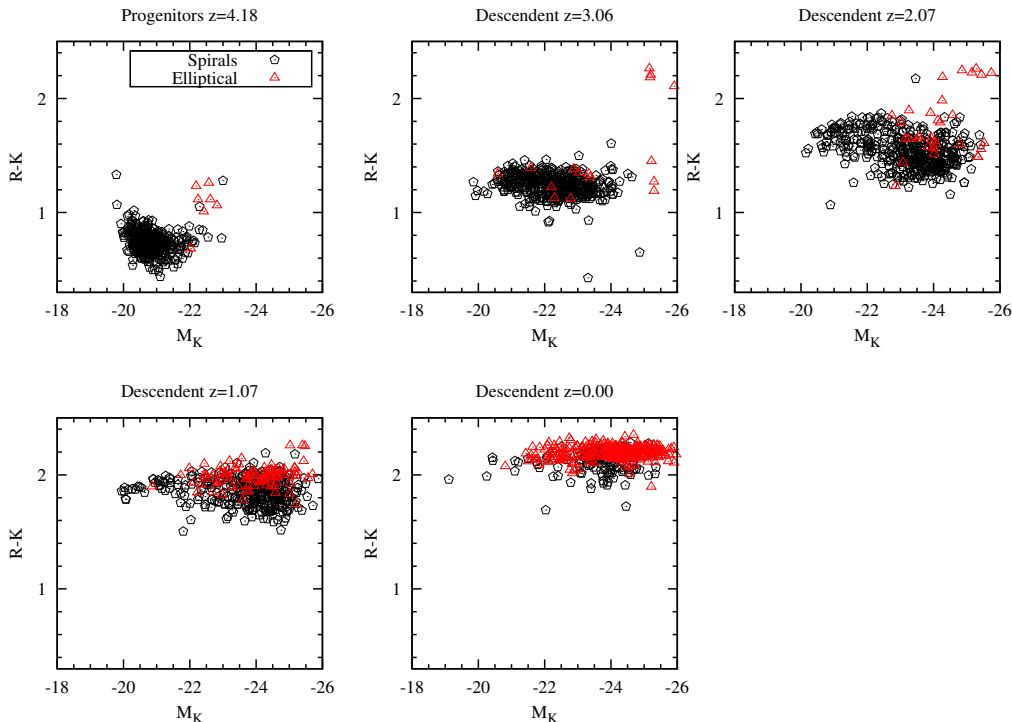


Figure 4.13 $R - K$ colour as a function of the K-band magnitude for HOST3 galaxies at $z \sim 4$ (top-left panel), and for their descendants at lower redshifts in the WMAP3B model. Red triangles are for elliptical galaxies while black diamonds are for spirals.

4.4 Discussion and Conclusions

In this work, we have studied the physical and environmental properties of galaxies hosting Long Gamma-Ray Bursts (LGRBs) in the context of a hierarchical model of galaxy formation. In order to select host galaxies, we have adopted the collapsar model and used information available from a semi-analytic model of galaxy formation coupled to high-resolution cosmological simulations (Wang et al. 2008).

By imposing different metallicity constraints on the progenitor stars, we have constructed three host galaxies samples: HOST1 is built without any cut on the metallicity of progenitor stars of GRBs, while the HOST2 and HOST3 samples are constructed by selecting galaxies with progenitor stars of metallicity lower than $0.3Z_{\odot}$ and $0.1Z_{\odot}$ respectively.

A number of recent studies have adopted a similar but not identical approach to study the host galaxies of LGRBs. Nuza et al. (2007) developed a Monte Carlo code to identify hosts of LGRBs within a cosmological hydrodynamical simulations. Their analysis was

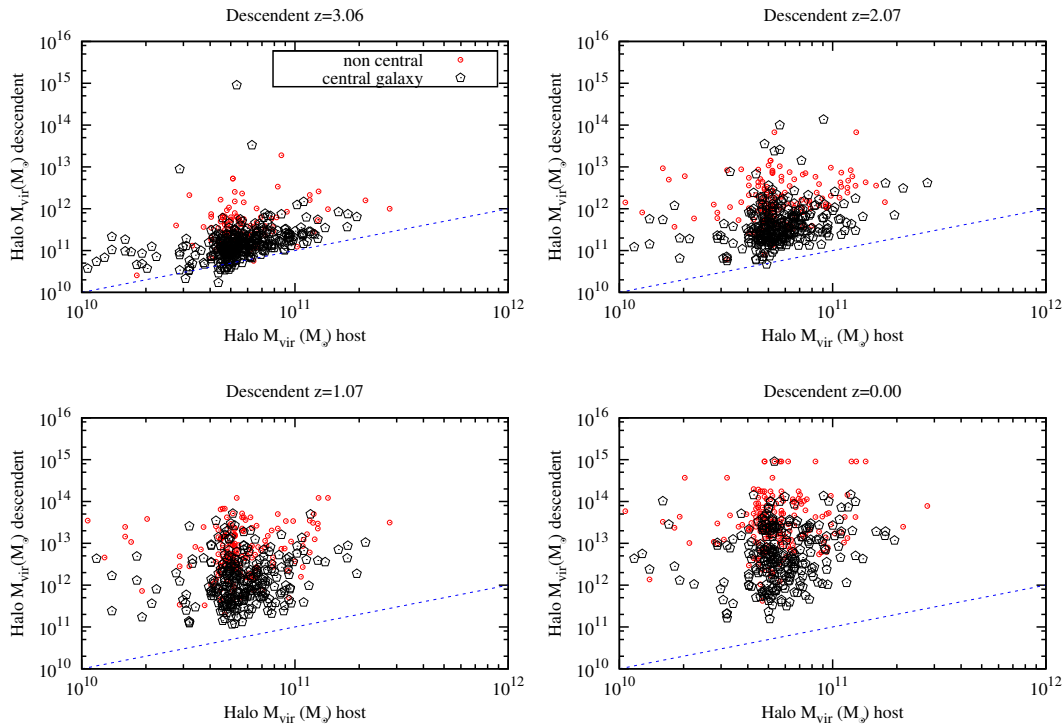


Figure 4.14 Parent halo mass of all descendants of HOST3 galaxies selected at $z = 4.18$, as a function of the halo mass of the host galaxies in the WMAP3B case. Red symbols are used for satellite galaxies and black symbols for central galaxies.

also based on the collapsar model and limited to $z \leq 3$. The simulation used in Nuza et al. was relatively small ($10h^{-1}\text{Mpc}$) and therefore did not allow a detailed investigation of the environmental properties of LGRB hosts. As confirmed by our study, they pointed out that if LGRBs are generated by the death of massive young stars of metallicity lower than a certain value, they do not provide a good tracer of the cosmic star formation history (see Sec. 4.3.1 and later).

Lapi et al. (2008) used the cosmological star formation rate below a critical metallicity to estimate the event rate of LGRBs. To this purpose, they employed the galaxy formation model presented in Granato et al. (2004). Lapi et al. find that their predicted number counts of LGRBs agrees well with the bright *SWIFT* data, without the need for an intrinsic luminosity evolution. They find that host galaxies are dominated by young stellar populations, are gas rich and metal-poor. The model adopted in Lapi et al. (2008) does not follow galactic disks nor does it consider mergers between galaxies or between haloes. In addition, the model does not provide spatial information of model galaxies.

In another recent study, Courty et al. (2007) used N-body/Eulerian hydrodynamic

simulations, and identified GRB host galaxies with those having SFR and SFR-to-luminosity similar to those of 10 observed GRB hosts in the redshift range $0.43 < z < 2.03$. They found that the host galaxies have low stellar masses and low mass-to-light ratios, are young and bluer than typical galaxies at the same cosmic epochs. Their identification of simulated galaxies with observed hosts is limited by uncertainties on the observational estimates of the SFR and luminosity of host galaxies. In addition, their simulated volume is relatively small ($32 h^{-1} \text{ Mpc}$) and the analysis is limited to relatively low redshifts.

Compared to previous works, our study uses a much larger simulated volume (a box of $125 h^{-1} \text{ Mpc}$ on a side - see Sec. 5.1) that allows us to study the environmental properties of model host galaxies. In addition, the use of two different cosmological models allows us to analyse the dependence of results on cosmology. The semi-analytic model employed in our work has been studied in a number of previous papers, and it has been shown to successfully reproduce a number of observational results for the global galaxy population in the local Universe and at higher redshift (see Sec. 5.1).

In agreement with previous work, and as expected due to the global increase of the ISM metallicity with decreasing redshift, we find that when assuming a metallicity threshold for progenitor stars of LGRBs, they do not represent a perfect tracer of the cosmic star formation history. The bias is stronger as the metallicity threshold assumed is lowered. At higher redshift, the cold-phase metallicity of model galaxies is lower, and galaxies form stars at higher rates. As a consequence, there is a higher rate of LGRBs per galaxy and the host galaxy population includes a larger fraction of the global galaxy population, with the two populations sharing very similar physical properties.

At lower redshift, the host galaxy population is dominated by galaxies with low-masses, relatively young ages, blue colours, and luminosity below L_* , in qualitative agreement with observational measurements. We note, however, that while ~ 90 per cent of the galaxies in our simulations have stellar masses lower than $\sim 10^{10} M_{\odot}$, only ~ 0.3 per cent of them are in the HOST3 sample and ~ 13 per cent in the HOST2 sample.

The metal content and metallicity evolution of host galaxies also appear to be in agreement with observational estimates. Since in the model adopted in this study stars form with the metallicity of the cold-phase component at the time of the star formation, host galaxies have average metallicity lower or close to the metallicity threshold adopted. Metallicity studies of LGRB host galaxies could therefore provide important constraints

on the adopted collapsar model. It is important to note, however, that inhomogeneous mixing of metals (which is not considered in the model adopted here) could significantly complicate this picture. The metal content of host galaxies does not significantly evolve with redshift, while the overall galaxy population exhibit some weak evolution.

Taking advantage of the spatial information provided by the semi-analytic model used in our work, we study the clustering properties of model host galaxies and compare them to the corresponding properties of the global galaxy population. Since a larger fraction of the whole galaxy population can host LGRBs at high redshift, the clustering properties of host galaxies do not differ significantly from the clustering properties of ‘normal’ galaxies. At lower redshift, the host galaxies are significantly less clustered than normal galaxies, as expected due to their physical properties. Interestingly, we find that the cross-correlation function between host and normal galaxies lies in between the the auto-correlation functions of host galaxies and normal galaxies, suggesting that the probability of finding another host galaxy nearby a GRB host is lower than the corresponding probability of finding a normal galaxy. This implies that LGRBs reside in regions with density lower than average. When larger samples of LGRB host galaxies will become available, it will be possible to test our clustering predictions.

Using the available semi-analytic catalogues, which contain the full merger tree information for all galaxies in the simulation box, we find that LGRB host galaxies at redshift ~ 4 (which have low stellar mass, low metallicity and no significant bulge component) evolve into relatively massive, red galaxies at redshift zero. While the descendants of high- z LGRBs reside in haloes of different mass in the local Universe, most of them still sit in haloes with mass between 10^{12} and $10^{13} M_{\odot}$.

Chapter 5

Redshift Distribution of Long Gamma-ray Burst

The detection of LGRBs at high redshift and the connection with Type Ic SNe, make them main challenges to understand the cosmology, they are probably the only objects that let us study the cosmos and the early evolution of stars possible near to PopIII sample. Therefore, understanding where the GRB are distributed in the universe and how they are connected with the star formation rate (SFR) is very intriguing. Since the launch of the *Swift* satellite (Gehrels and et al, 2004) , the number of GRBs with measured redshift has been greatly increased. Nonetheless to date there are only ~ 140 *Swift* GRBs with known redshifts. This sample is still too poor to constrain their luminosity function (hereafter LF).

Previous studies (Porciani and Madau, 2001; Guetta et al., 2005; Natarajan et al., 2005; Daigne et al., 2006; Salvaterra and Chincarini, 2007, and others) addressed the problem of determining the redshift distribution of GRBs differently. Their method is based on constraining the GRBs distribution by assuming an average energy spectrum for all the bursts and that they trace the evolving SFR, either with a constant or evolving LF. The redshift distribution, together with the LF, can provide important insights not only into the physics of the individual objects themselves, but also into the evolution of matter in the Universe.

One of the first pioneering work was Porciani & Madau (2001). The rate of GRB is mapping fitting observational data, using the assumption that SFR is proportional to the GRB rate (Hopkins and Beacom, 2006). Finally the rate it is convolved with a selection function dependent on the instrument used. They find that the rate of burst is

of about 1-2 GRBs for every one million Type II SNe. Notable recent attempts include: Guetta, Piran & Waxman (2005) explore a variety of different star-formation rate histories and GRB luminosity function; Natarajan et al. (2005) additionally incorporate a simple prescription for a low-metallicity preference for GRBs. Daigne et al. 2006 used Monte Carlo simulations to predict GRB evolution, assuming that GRBs follow the SFR, the LF is a power-law (independent from redshift) and the peak energy is determined by two possible relations. They find that: the slope of the LF is between 1.5 – 1.7, the Amati relation should be intrinsic and, the GRB rate density at $z = 7$ is about 6-7 times larger than at $z = 2$. They deduced also that the properties of GRBs and GRB-progenitors are redshift dependent, since the redshift distribution of *Swift* burst strongly favors their SFR3 model (see Daigne et al 2006), that it is an unrealistic model.

Salvaterra follows this approach in two different works (Salvaterra & Chincarini 2007, Salvaterra et al. 2008), assuming that GRB luminosity evolves with redshift and that GRBs form preferentially in low-metallicity environments. They use this constraint to set a robust upper limit on the bright-end of GRB LF, finding that the number of bright GRB detected by *Swift* implies that this cannot be very steep ($\delta < 2.6$ for progenitors with $Z < 0.3Z_{\odot}$). Moreover they found that assuming a threshold of $F > 0.4 \text{ ph/cm}^2/\text{s}$, at least $\sim 5 - 10\%$ of all detected GRB should lie at redshift $z > 5$.

In this work, we do not use a GRB comoving rate proportional to the star formation in the Universe, but only we assume that global in the Universe the rate of GRB per SNe is on average (over all cosmic times) of about 1 GRB event every 1000 SNe (Langer and Norman, 2006). We derive the LF and formation rate of GRBs using hydrodynamical-simulation (Wang et al. 2008). We fit the observed logN-logP (Kommers et al., 2000) derived from data taken by the Burst And Transient Source Experiment on board the *CGRO* satellite (BATSE, Fishman et al. 1989) in order to constrain the free parameters of the LF. We adopt this method for three GRBs' progenitors subsamples with different cuts in metallicity, following the collapsar model, and assuming a constant and evolving LF.

By comparing the cumulative distribution of peak photon fluxes, Dai (2009) recently proved that the *Swift* and BATSE samples track the same parent population of bursts. For this reason, following Porciani and Madau, we rely on the GRB observed by BATSE

as both samples should have comparable LF.

5.1 Simulated LGRB rate

In this study, we use the galaxy catalog constructed by Wang et al. (2008) for a simulations with cosmological parameters from the third-year WMAP results. The same catalog was used in Campisi et al. (2009), but we refer to Wang et al. (2008) for a discussion of the model. The simulation corresponds to a box of $125 h^{-1}\text{Mpc}$ comoving length and a particle mass of $7.8 \times 10^8 M_{\odot}$. The softening length is $5 h^{-1} \text{kpc}$. Simulation data were stored in 64 outputs, that are approximately logarithmically spaced in time between $z = 20$ and $z = 1$, and linearly spaced in time for $z < 1$. Each simulation output was analyzed with the post-processing software originally developed for the Millennium Simulation (Springel et al., 2005).

In order to extract from the catalog the rate of GRB events, we adopt the collapsar model for LGRBs: all young stars with mass $> 20 M_{\odot}$ (Larsson et al., 2007) ending their life with a supernova should be able to create a BH remnant¹. If the collapsar has high angular momentum, the formation of the BH can be accompanied by a GRB event (Yoon et al., 2006, 2008). Recent studies on the final evolutionary stages of massive stars suggested that a Wolf-Rayet (WR) star can produce a LGRB if its mass loss rate is small. This is possible only if the metallicity of the star is very low. When metallicities are lower than $\sim 0.1 - 0.3 Z_{\odot}$, the specific angular momentum of the progenitor allows the loss of the hydrogen envelope while preserving the helium core (Woosley and Heger, 2006; Fryer et al., 1999). The loss of the envelope reduces the material that the jet needs to cross in order to escape, while the helium core should be massive enough to collapse and power a GRB.

In order to count the number of GRB events in each snapshot, we select from our catalog objects with redshift between $0 < z < 9.2$, using a procedure similar to that described in section 3 of Campisi et al. 2009, we count all the possible GRB events in the simulated catalog in 3 different subsamples:

-*GRB1*, obtained by selecting stars with age $< t_c = 5 \times 10^7 \text{yr}$ and $M > 20 M_{\odot}$;

¹We also test the case with $M > 30 M_{\odot}$. We obtain that the rate of GRB in every box is very close to the rate whit $M > 20 M_{\odot}$, since using a Salpeter IMF the difference between the two cases is only 0.939×10^{-3} .

-*GRB2*, including stars of age $< t_c$, $M > 20 M_\odot$ and metallicity $Z \leq 0.3Z_\odot$;

-*GRB3*, defined by selecting stars with age $< t_c$, $M > 20 M_\odot$ and metallicity $Z \leq 0.1 Z_\odot$;

We compute the number of stars ending their lives as LGRBs, assuming a Salpeter Initial Mass Function (IMF) and that the rate of GRB per SNe is on average (over all cosmic times) of about 1 GRB event every 1000 SNe (Porciani and Madau, 2001; Langer and Norman, 2006)².

5.1.1 Star Formation History

The collapsar model links LGRBs to the evolution of massive stars whose lifetimes are negligible on cosmological scales. If no other condition is required for producing a LGRB event, then the rate of LGRBs should be an unbiased tracer of the global star formation in the Universe (e.g. Totani, 1997; Wijers et al., 1998; Mao and Mo, 1998; Porciani and Madau, 2001; Bromm and Loeb, 2002; Fynbo et al., 2006; Price et al., 2006; Savaglio, 2006; Totani et al., 2006; Prochaska et al., 2007; Li, 2008b, and references therein). However, both observations and theoretical studies indicate that the metallicity of the progenitor star plays an important role in setting the necessary conditions for a LGRB explosion. In this case, the rate of LGRBs is expected to be a biased tracer of the cosmic star formation rate.

In Fig. 5.1 we show the SFH for the simulated and for observed samples. We compare the cosmic star formation rate obtained using all galaxies in the simulation box to that obtained for the three samples defined in the Sec. 5.1 and to the observed SFR in the Universe. Since normally the SFR calibrations used for deriving the SFH estimates (Hopkins and Beacom, 2006) are defined assuming the Salpeter (1955) Initial Mass Function, to ensure consistent assumptions throughout, we convert SFH estimates in our simulation³ to the Salpeter IMF using a simple scale factor. This scale factor is established by using the Starburst99 code, which models a population-synthesis.

In Fig. 5.1, the sample with no threshold on metallicity (GRB1) traces the global star formation rate (dotted line in Fig. 5.1), this sample also identify all galaxies in the simulation. This is not the case for the two samples with metallicity thresholds (GRB2 - dot-dashed line and GRB3 - dashed line). In the GRB2 and GRB3 samples, the LGRB

²We test however in section 5.3 a different rate (1 GRB every 10.000 SNe), in order to check how the results change with different assumption.

³The simulation adopts the Chabrier IMF

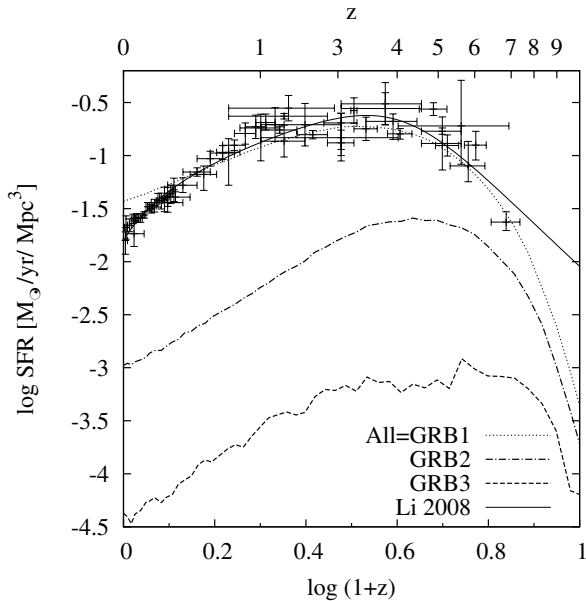


Figure 5.1 Star Formation Rate History: $\log SFR [M_{\odot} \text{ yr}^{-1} \text{ Mpc}^{-3}]$ as a function of redshift. Dotted line are the results from GRB1 which also identify all galaxies in the simulation, dot-dashed line is GRB2 and GRB3 is the dashed line. Symbols with error bars are a compilation of observational data (Hawkins 2006), the solid line is a best fit of observational data taken from Li 2008b.

rate peaks at higher redshift than the cosmic star formation rate, as a consequence of the global decrease of metallicity with increasing redshift. Data and the best fit (solid line) are taken from Hapkins (2006) and Li (2008b). The SFH of simulation is in agreement with data within their errors bars. As described in Campisi et al. 2009, the peaks of the SFH for the GRBs subsamples are shifted at higher redshift, due to the selection methods since the objects at higher redshift have lower metallicity.

The important goal of Fig. 5.1 is to shed some light on the following issue: do LGRBs trace the SFR? Our results head to the conclusion that LGRBs are not good tracers, albeit they might be biased tracers of SFR.

But all previous works on the study of redshift distribution on LGRB (see sect.1) adopted the assumption, i.e. that the GRB rate is proportional to the SFR, sometimes convolved with a function constraining a metallicity cut-off (e.g Salvaterra and Chincarini (2007); Daigne et al. (2006)). We show that selecting in our simulation burst with different progenitor's metallicity, the GRB rate follows a different evolution with respect to the SFH. Here, the results of the work which used a strong correlation between the SFR and the LGRB rate could be wrong and should be used with caution.

The results shown in Fig. 5.1 are in qualitative agreement with recent observational estimates (Kistler et al., 2008), and with recent theoretical studies also based on the collapsar model (Yoon et al. 2006 and others).

5.2 Observed distribution of LGRBs

To predict the observed distribution of the redshift of LGRBs, we should take into account that only brightest and pointing toward us burst will be observed, so we need to include two important effects:

- I) the collimation and beaming effects;
- II) the fraction of GRBs seen by the detector (or luminosity function of GRBs).

The number of observed LGRBs is given by:

$$N_{obs} \sim N_{real} f_b \int_{L_{Lim}}^{\infty} \Phi(L) dL; \quad (5.1)$$

where N_{real} is the total rate of LGRBs in the simulation, f_b is the fraction of LGRBs pointing toward us and the integral give the fraction of LGRBs with luminosity bigger than the corresponding limit flux of the detector.

5.2.1 Beaming effect

There is a general consensus that GRBs are jetted sources (Waxman et al., 1998; Rhoads, 1997). This implies fundamental corrections to the energy budget and the GRB rates. A canonical GRB does not light up the full celestial sphere but rather a fraction, the so called beaming fraction (Sari et al., 1998):

$$f_b = (1 - \cos \theta) \sim \theta^2/2$$

where θ is the opening angle of the jet. Thus, the overall GRB rate clearly depends on the fact that GRBs are beamed and the rates have to be corrected by a factor f_b . Thus the true rate integrated over a time interval is $N_{real} = (f_b)^{-1} N_{obs}$. This has been computed traditionally in terms of the beaming correction factor, which is defined as the ratio of the total number of bursts to the observed ones. To estimate the overall GRB rate we use the average beaming correction f_b . The average value of θ is $\sim 6 \text{ deg}$ (Ghirlanda et al., 2007), giving $\langle f_b \rangle \sim 0.0055$. We will use this average beaming factor throughout our work.

5.2.2 LGRB luminosity function

The luminosity function (LF) of LGRBs is still poorly tested as the data are too sparse for an empirical determination of the burst luminosity function. The standard approach to constrain the GRB LF from observations (Porciani e Madau 2001, Daigne et al. 2006, Salvaterra et al. 2007, and others) is first to assume a model for the LF, for the GRB rate, and for the energy spectrum. Secondly the model parameters are constrained by the observed data. To this aim it is customary to fit the GRBs observed by BATSE using the differential peak flux distribution, $\log N - \log P$ diagram (Schmidt 1999). In particular we fit the observed rate of burst with observed peak fluxes F between (F_1, F_2) , described by the equation:

$$\begin{aligned} \frac{dN}{dt}(F_1 < F < F_2) &= \int_0^\infty dz \frac{dV(z)}{dz} \frac{\Delta\Omega}{4\pi} \frac{R_{\text{GRB}}(z)}{1+z} \\ &\times \int_{L(F_1, z)}^{L(F_2, z)} dL' \phi(L') \epsilon(F), \end{aligned} \quad (5.2)$$

where $(dV(z)/dz)$ is the comoving volume element⁴, $\Delta\Omega$ is the solid angle covered on the sky by the survey, the factor $(1+z)^{-1}$ accounts the cosmological time dilation, $R_{\text{GRB}}(z)$ is the comoving GRB rate density, $\phi(L')$ is the GRB luminosity function, and $\epsilon(F)$ is the detector efficiency as a function of photon flux.

We fit equation (5.2) using the rate of GRB described in section 5.1, and we assume the following models for the LF and for the energy spectrum.

Luminosity function

To model the number of GRBs at different flux limits, we assume that the luminosity function has the form:

$$\Phi(L) = K \left(\frac{L}{L_*} \right)^\xi \exp\left(-\frac{L_*}{L} \right) \quad (5.3)$$

where L is the isotropic equivalent intrinsic burst luminosity, ξ is the asymptotic slope at the faint end, L_* is the characteristic cutoff luminosity, and K is the normalization constant so that the integral over the luminosity function equals unity. We take $K = [L_0 \Gamma(-\xi - a)]^{-1}$ (for $\xi < -1$) (Porciani & Madau 2001). For the cutoff luminosity we consider different scenarios, since L^* could to increase with redshift follow the equation $L_* = L(z) = L_0(1+z)^\delta$.

⁴ $dV(z)/dz = 4\pi c d_L^2(z)/[H(z)(1+z)^2]$

Energy spectrum

We assume the empirical form for the GRB spectrum proposed by Band et al. 1993:

$$S(E) \propto \begin{cases} \left(\frac{E}{100 \text{ keV}}\right)^\alpha \exp\left[\frac{E(\beta - \alpha)}{E_b}\right] & E < E_b, \\ \left(\frac{E_b}{100 \text{ keV}}\right)^{\alpha - \beta} \exp(\beta - \alpha) \left(\frac{E}{100 \text{ keV}}\right)^\beta & E \geq E_b. \end{cases} \quad (5.4)$$

We adopt the best fit energy spectral indices (i.e., $\alpha \sim -1$ and $\beta \sim -2.25$) reported in Preece et al. (2000), and the spectral break energy distribution at $E_b = 511$ keV (Porciani & Madau 2001). These were found fitting parameters from 5500 different spectra, and this is the most extensive GRB sample with spectral characterization to date.

The photon flux F [$ph/cm^2/s$] observed at the Earth in the energy band $E_{min} < E < E_{max}$, emitted by an isotropically radiating source at redshift z can be written by:

$$F = \frac{(1+z) \int_{(1+z)E_{min}}^{(1+z)E_{max}} S(E) dE}{4\pi D_L^2}, \quad (5.5)$$

where D_L is the luminosity distance and $S(E)$ is the rest frame energy spectrum. We consider $E_{min}=50$ keV and $E_{max}=300$ keV for BATSE, while for the Burst Alert Telescope (BAT, Barthelmy et al. (2005)) we use $E_{min}=15$ keV and $E_{max}=150$ keV. It is customary to define the isotropic equivalent burst luminosity in the rest frame photon energy 30–2000 keV by:

$$L = \int_{30 \text{ keV}}^{2000 \text{ keV}} E S(E) dE, \quad (5.6)$$

Thus, combining equations (4-5-6) we get $L(F, z)$ to use in the integration limit of eq. (2).

5.2.3 Best fit: results

In our model we have different parameters to fit: the characteristic cutoff luminosity L_* , the slope ξ of the LF and a third parameter δ which is the evolution of L_* with redshift, and we fixed it to values between 0-3.5 (Salvaterra et al., 2009b). We follow the approach of Porciani & Madau (2001), using the observed differential number counts of BATSE in the range 50-300 keV from Tab. 2 in Kommers et al. (2000). The observed sample

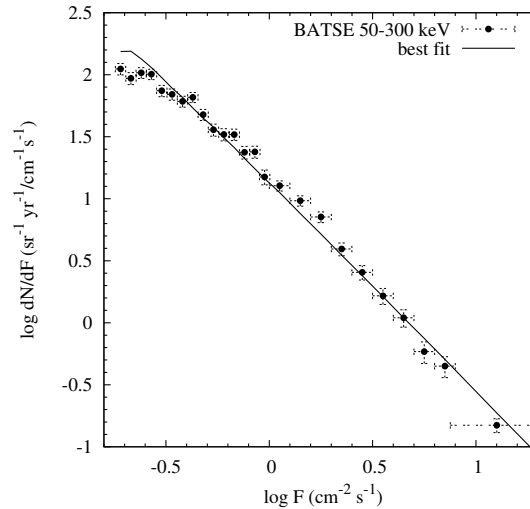


Figure 5.2 Comparison between BATSE and best fit model for the $\log N - \log P$ distribution. The dots are the observed BATSE LGRBs in the 50-300 keV band (Kommers et al. 2000), and the dark line is the predicted distribution with the best fit parameters (we show only for one subsamples, similar fits are obtained for the others cases).

include 1998 GRBs with peak flux in the range $0.18 - 20.0 [ph/cm^2/s]$, and detector efficiency described by $\epsilon(F) = 0.5[1 + \text{erf}(-4.801 + 29868 F)]$ (Kommers et al., 2000). Dai (2009) showed that the choice of the BATSE sample with respect to the *Swift* one is equivalent since the two samples represent the same population of bursts. Moreover, Dai shows that the distribution of the *Swift* sample matches that of the BATSE sample (when approaching the detection limits) so in the follow we can use the same trigger efficiency for *Swift* triggers.

The fits to the data are done by minimizing the difference of the *logarithm* between model and observational data. This is like a simple χ^2 minimization, but the points are not independent. We tried to fit the data directly, finding that the best fit value gave too much weight to the central regions. We fitted in *logarithm* values so that the overall shape of the contours has an increased influence on the fit. In all considered cases we always find a clear minimum.

The best-fit model is shown in Fig.5.2 and the parameters for all the subsamples are listed in Table 1. In Fig.5.2 we show only a comparison between the observed distribution of LGRBs and the predicted distribution obtained using the GRB2's subsample, similar lines are obtained with the others subsamples and models. The observed distribution is taken from Kommers et al. (2000), for BATSE detector (energy range 50-300 keV). The

Sample GRB1		
δ	$L_0/(10^{50} \text{ erg s}^{-1})$	$-\xi$
0	5.132 ± 0.791	1.838 ± 0.061
1.5	0.665 ± 0.079	1.726 ± 0.039
2.0	0.347 ± 0.039	1.709 ± 0.036
2.5	0.181 ± 0.019	1.699 ± 0.034
3.0	0.095 ± 0.013	1.694 ± 0.069
3.5	0.049 ± 0.015	1.692 ± 0.176
Sample GRB2		
δ	$L_0/(10^{50} \text{ erg s}^{-1})$	$-\xi$
0	6.973 ± 2.066	1.763 ± 0.430
1.5	0.742 ± 0.088	1.702 ± 0.035
2.0	0.355 ± 0.041	1.694 ± 0.033
2.5	0.171 ± 0.019	1.688 ± 0.032
3.0	0.081 ± 0.009	1.686 ± 0.032
3.5	0.038 ± 0.007	1.686 ± 0.066
Sample GRB3		
δ	$L_0/(10^{50} \text{ erg s}^{-1})$	$-\xi$
0	77.875 ± 19.243	2.135 ± 0.184
1.5	4.574 ± 0.410	1.820 ± 0.047
2.0	1.970 ± 0.157	1.787 ± 0.042
2.5	0.865 ± 0.064	1.768 ± 0.039
3.0	0.386 ± 0.028	1.760 ± 0.038
3.5	0.173 ± 0.022	1.760 ± 0.041

Table 5.1 Best-fit parameters for different GRBs' subsamples (see section 2) and different luminosity evolution with $L_* = L(z) = L_0(1+z)^\delta$. Errors are computed using bootstrap technique.

data are converted into rates per unit time per unit solid angle following Kommers's work. The horizontal and vertical error bars on data represent the size of the energy bin and Poisson uncertainties, respectively.

Table 1 shows the best fit parameters for all subsamples. The errors we quoted are the rms (root mean square) spread in errors from fitting bootstrap catalogue in the same way. The given error bars confirm that the characteristic luminosity cutoff remains better determined when there is an evolution of the LF with redshift. We note that for *all subsamples* and with very different value of δ , the slope ξ of the LF is well constrained in a range of values between $1.686 < -\xi < 1.838$ (except one case). These values are in agreement with the results in the literature on the slope of the LF, (e.g. in Daigne et al. 2006, where $1.52 < \xi < 1.7$). Conversely, the characteristic luminosities span a large range of values ($0.038 < L_0 < 77.875$) $\times 10^{50}[\text{erg/s}]$, adopting higher values when we consider the GRB3 subsample, in particular when the LF is constant with the redshift.

	δ					
	0.	1.5	2.0	2.5	3.0	3.5
GRB1	1.71	1.89	1.98	2.08	2.19	2.33
GRB2	2.43	2.66	2.77	2.90	3.04	3.19
GRB3	3.12	3.18	3.22	3.27	3.34	3.44
<i>Swift</i> $\langle z \rangle \sim 2.28$						

Table 5.2 Mean redshift for every subsample of GRB with different LF evolution, compared with the mean *Swift* redshift.

5.3 LGRB redshift distribution: results

About 458 GRBs have been detected by the *Swift* satellite since its launch in 2004 November until August 2009. Among these ~ 150 have spectroscopic or photometric redshift determination. The number of GRBs with redshift is tightly linked with observing conditions, as explained in Jakobsson et al. (2006) (hereafter J06). J06 suggested that in order to study the redshift distribution of GRBs we should use a subset of all GRBs well placed for optical observations. This can be achieved by following 6 criteria, necessary to “clean” the sample: 1) the burst should have an X-ray position made public within 12 hours; 2) the Galactic foreground should be low, i.e. $A_V < 0.5$; 3) the burst should be $> 55^\circ$ from the Sun; 4) the burst should be not at a polar declination, $|dec| < 70^\circ$; 5) the burst has to be localised with the XRT; and 6) no nearby bright star. Imposing these restrictions does not bias the sample towards optically bright afterglows; instead each GRB in the sample has favourable observing conditions, i.e. useful follow-up observations are likely to be secured.

Our best-fitting parameters for the LF of GRBs (shown in table 1) are used to predict the redshift distribution for the *Swift* case. We use equation 5.2 to compute the model prediction of the number of GRB with $L > L(L_{lim}, z)$, considering values of F corresponding to $F_{lim} = 0.2 [ph/cm^2/s]$ (in order to compare with Daigne et al. 2006). In Fig. 5.3 we compare our model predictions with the number of burst detected by the *Swift* satellite, following the prescriptions of the analysis performed by J06 and by using the updated catalog⁵ until GRB 090812. We assume that the observed sample of GRBs with redshift determination is representative of all bursts, within the error area (Jakobsson et al., 2009). Fig. 5.3 shows the cumulative redshift distribution of observed

⁵<http://www.raunvis.hi.is/~pja/GRBsample.html>

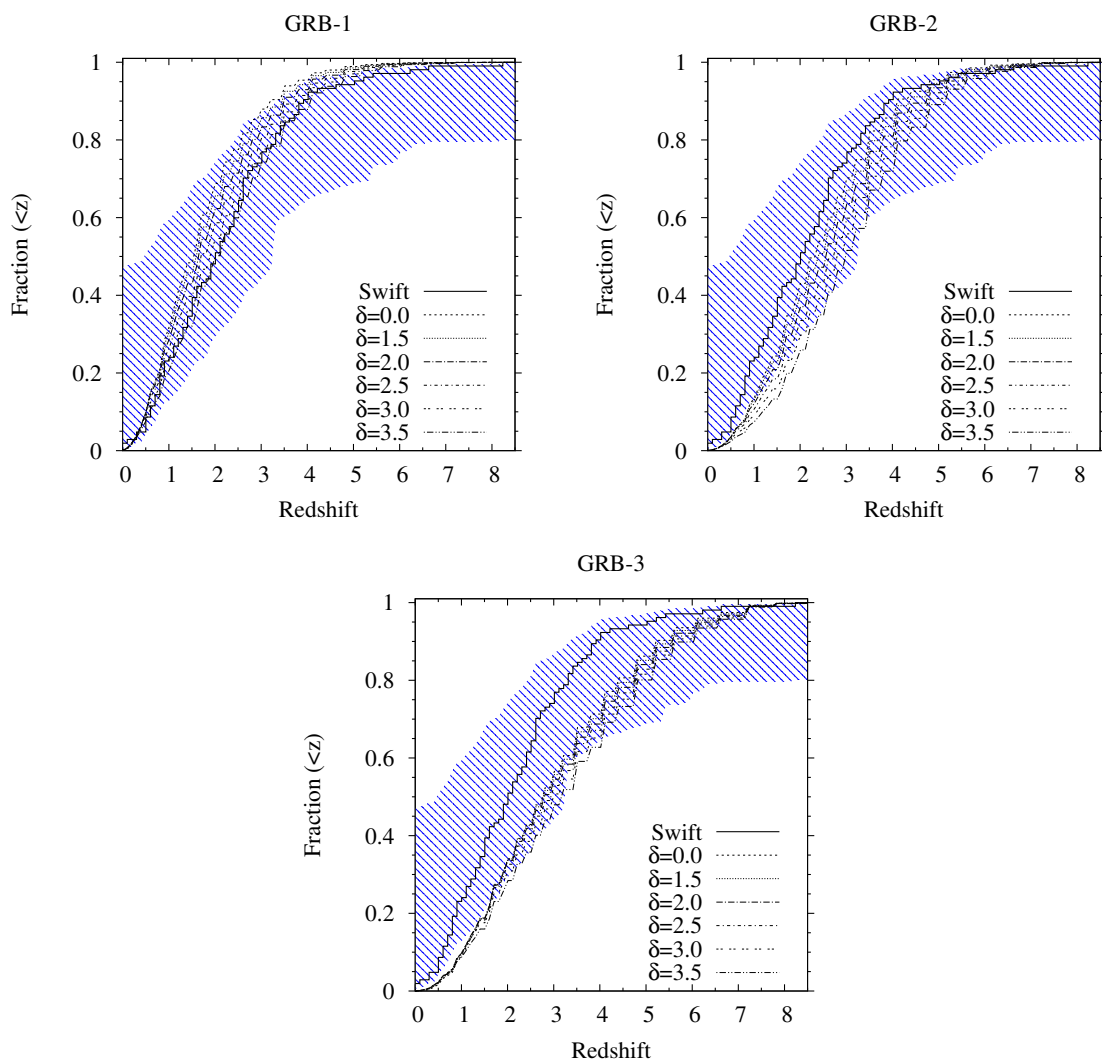


Figure 5.3 Redshift distribution for LGRB. Thick step is the observed distribution of *Swift* burst with sure measured redshift (J06). The yellow area takes in consideration the error region for the steps, following the procedure of Jakobsson et al. 2009. The upper envelope is produced placing GRBs without redshift and those with redshift upper limits at $z = 0$. The lower envelope placing the GRBs without firm redshift at the maximum redshift they can have (giving their bluest photometric detection). The model for the expectation of the redshift distribution from our simulation are the dashed lines. For progenitor stars without cut in metallicity (GRB1) and with metallicity lower than $0.3 Z_{\odot}$ (GRB2) and $0.1 Z_{\odot}$ (GRB3). Results are shown for the model with luminosity evolution between 0-3.5.

and simulated GRBs for the 3 different subsamples.

In the model, the expected redshift distribution depends on the assumption made on GRB progenitors but also by the evolution of the LF with redshift. The distribution in the case of the GRB1 sample is not so far from the observed one. In particular seems that GRB1 subsample with high evolution for the LF ($\delta > 2.5$) reproduce the data. The observed *Swift* distribution lies also close to the distribution of the GRB2 sample without evolution in L_* , more at high redshift. This imply that the properties of the GRBs do not change with the redshift, since in our simulation the progenitor's characteristic does not evolve.

Figure 5.3 shows also that the GRB3 subsample is not a good reproduction of observed data, in particular at low redshift ($z < 1.5$) where the lines are outside the error area.

For completeness in Tab. 2 we also show the comparison between the average value of the redshift for the updated GRBs' sample of J06 and the simulated one. We predict that the value of the $\langle z \rangle$ evolves with the threshold in metallicity, in agreement with the SFR evolution for the three subsamples. In fact, while the GRB1 prediction gives an average redshift between 1.71 – 2.33 (for different values of δ), GRB2 and GRB3 have higher values up to $\langle z \rangle \sim 3.44$ for the extreme case where $\delta = 3.5$ and $Z < 0.1Z_\odot$. However the observed LGRB have an average redshift of $\langle z \rangle \sim 2.27$, which is more lower than the one predicted from the GRB3 model. From 5.3 and Tab.2, we are able to rule out the GRB3 subsample and we conclude that either GRB1 with evolving LF and GRB2 with a non-evolving LF are possible model within error bars.

GRB rate

In order to compute the rate of GRB in our simulation, in section 3 we assume to have 1 GRB every 1000 SNe globally in the Universe, in agreement with Porciani and Madau (2001); Langer and Norman (2006). Nevertheless we explore also how change the results assuming a different rate for GRBs. This is what we want test in this appendix. We repeat all the work, using a rate of 1 GRB every 10000 SNe. We fit the BATSE sample, obtaining of course different values for the luminosity function, and we will use this value to compute the redshift distribution. To compare with Fig. 5.3, we show in Fig. 5.4 the redshift distribution for GRB1 and GRB2 subsample, for GRB3 subsample the rate of GRB is too low to find a best fit for the LF of the BATSE data.

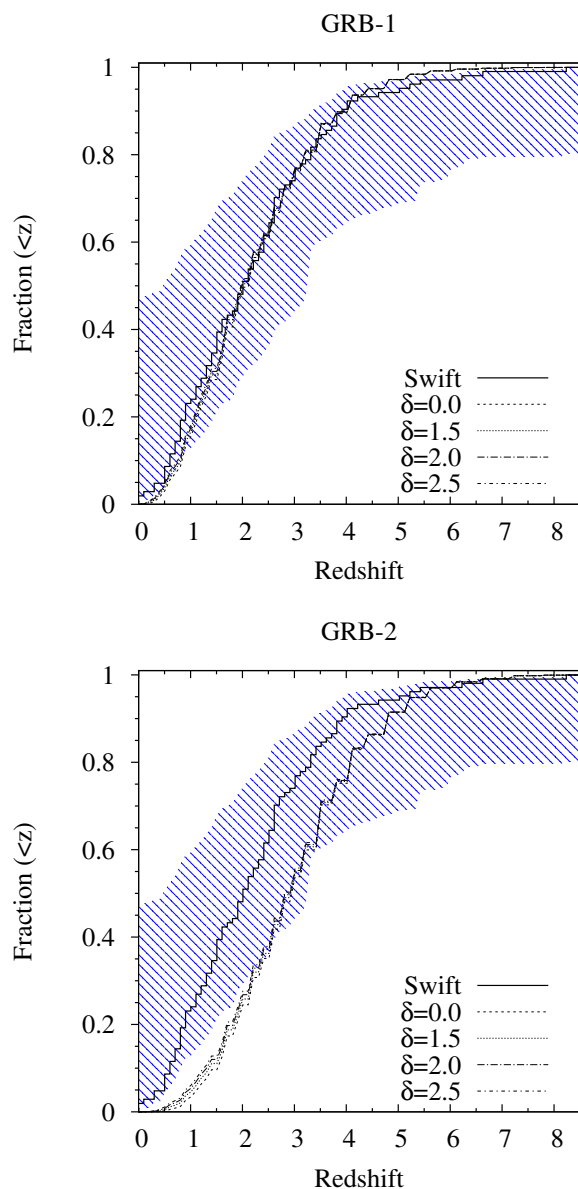


Figure 5.4 Redshift distribution for LGRB. Thick step is the observed distribution of *Swift* burst with sure measured redshift (J06). The yellow area takes in consideration the error region for the steps, following the procedure of Jakobsson et al. 2009. The upper envelope is produced placing GRBs without redshift and those with redshift upper limits at $z=0$, instead the lower envelope placing the GRBs without firm redshift at the maximum redshift they can have (giving their bluest photometric detection). The model for the expectation of the redshift distribution from our simulation are the dashed lines. For progenitor stars without cut in metallicity (GRB1) and with metallicity lower than $0.3 Z_{\odot}$ (GRB2). Results are shown for the model with luminosity evolution between 0-2.5.

The dependence of the LF with the redshift is not remarkable, since (as in GRB3 in Fig.5.3) the rate of GRB is smaller than previous case. In fig. 5.4 is evident that the best model to reproduce the data is the GRB1 subsample (with and without LF evolution). We expect this results because the assumption to have 1 GRB every 10000 SNe calls for a big number of SNe where there are also more low metallicity objects, and for this reason the redshift distribution of GRB1 and GRB2 is shifted at high redshift respect Fig.5.3. We conclude that, since models and observations suggest that a metallicity dependency is required, a rate smaller than that using in our work could be unrealistic.

5.3.1 Bright and Faint LGRBs

Also if there would be an evolution of GRB LF with time (high-z GRB are typically brighter than low z ones), from Fig.5.3. seems to need a very strong evolution to reconcile GRB1 with observed data ($\delta > 2.5$). This evolution should imply that the properties of GRBs change more with the redshift. Since we assume in the simulation that the collapsar model is valid at all redshift, we should gather that the properties of GRB change with redshift and the progenitors characteristics do not change with redshift. This scenario seem to be enough unrealistic.

In order to step over the detection problem, following the same approach of Daigne et al. (2006), we defined two subsamples of *Swift* bursts by selecting those with peak flux $F_{lim} > 1.0 [ph/cm^2/s]$ (*Bright*) and those with $F_{lim} \leq 1.0 [ph/cm^2/s]$ (*Faint*).

In Fig.5.5 we show the cumulative redshift distribution of observed and expected burst. We decided to show only the GRB2 subsample, without evolution in LF, since it seems to be the more realistic model from Fig.5.3.

It is evident that *Bright* and *Faint* objects have different redshift distribution, both for expected and observed one. We note that the *Bright* observed sample almost overlaps the simulated distribution of bursts, overcoming the problem of Fig.5.3. Conversely, there are more *Faint* bursts at low redshift than predicted in the simulation. Both *Bright* and *Faint* have similar behavior a redshift $z > 6$. However we argue from Fig.5.3 that GRB2 subsample with a non-evolving LF is the best possible model to reproduce *Swift* data.

We quantify the probability to find burst a redshift $z > 5$ and $z > 6$ in Tab. 3 for both subsamples. We expected from model to have about 1.% of GRBs with redshift $z > 6$. For both cases we find results lower than Daigne et al. (2006), which found that

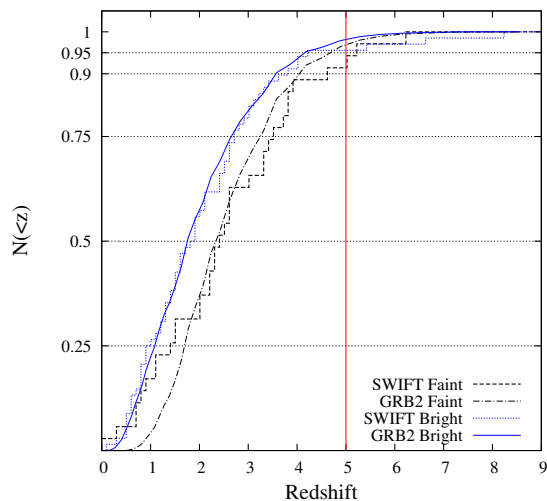


Figure 5.5 Redshift distribution for *Swift* observed and expected burst for *Faint* burst with peak flux $F \leq 1 \text{ ph/cm}^2/\text{s}$ and *Bright* LGRB with $F > 1 \text{ ph/cm}^2/\text{s}$. The lines are the simulations and the steps are the *Swift* data.

Rate	<i>Faint</i>		<i>Bright</i>	
%	$z > 5$	$z > 6$	$z > 5$	$z > 6$
GRB2	~ 3.8	~ 1.0	~ 2.0	~ 0.9
Obs	~ 11.4	~ 2.8	~ 4.4	~ 2.9

Table 5.3 Fraction of GRBs with redshift $z > 5$ for GRB2 subsample without evolution for the LF, and observation data from J06, for burst with peak flux $F \leq 1 \text{ ph/cm}^2/\text{s}$ and with $F > 1 \text{ ph/cm}^2/\text{s}$.

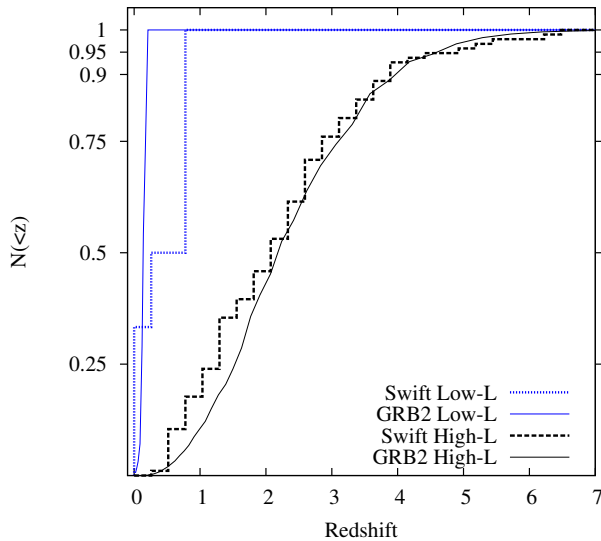


Figure 5.6 Cumulative redshift distribution for *Swift* observed (steps) low luminosity bursts with $L \leq 10^{49} \text{ erg/s}$ and high luminosity with $L > 10^{49} \text{ erg/s}$ (blue and dark steps respectively), compared with simulated distribution (lines).

at $z > 6$ the fraction of *Bright* burst should be $\sim 2 - 6\%$. The difference between our estimation and Daigne's one is that their SFR3 (preferred by redshift distribution of observational data) is probably unrealistic as written in the conclusion of Daigne's paper, suggesting that their results provide strong evidence that the properties of GRBs are redshift dependent. Instead in our case we take into consideration of the GRB luminosity function by considering a model where the characteristic luminosity does not change with redshift, holding unchanged the progenitors' properties of GRBs.

We claim that if the distribution of the observed sample will not change with the increase of the number of observed LGRB, the LF should not have an evolving cutoff among our modelled values. Moreover the correlation between *Swift* bursts and GRB2 sample implies that LGRB should be produced by a very massive star with metallicity $Z < 0.3Z_{\odot}$.

5.3.2 Low and High Luminosity LGRBs

In the recent past it was carried out the possibility to have 2 population of LGRB: one with low luminosity and one with high luminosity (e.g. Guetta and Della Valle (2007); Virgili et al. (2009); Liang and Zhang (2006); Chapman et al. (2007)). E.g.: Guetta et al. suggest the existence of 2 physically distinct classes of GRBs in which low luminosity

GRB are more frequent events than high luminosity GRB in the local Universe (redshift $z < 0.1$); they cannot exclude, however, the possibility of a single population of GRB. Virgili et al. propose that low luminosity GRBs could be a separate GRB population from high luminosity ones, with different rate and luminosity function.

In order to test if there is a real difference between low and high luminosity GRBs, at first stage we can compare the redshift distribution between observed data and simulated ones. We use the same sample of observed GRB of previous case with 103 GRB, for which we can compute the bolometric (i.e. 30-2000 keV rest frame) luminosity. We divided the sample in two subclasses of objects: 6 Low luminosity (Low-L) bursts with $L \leq 10^{49} \text{ erg/s}$ and 97 High luminosity (High-L) bursts with $L > 10^{49} \text{ erg/s}$. Then we assume the same cut in luminosity for GRBs in the simulation.

We show the cumulative redshift distribution of these 2 subsamples in Fig. 5.6 for simulated and observed objects. The Low-L and High-L distributions are clearly very different. In particular at redshift lower $z < 1$, where more Low-L are observed than High-L bursts, in agreement with past work. But what surprise in Fig. 5.6 is that both subsamples are also reproduced by our simulated distributions. We assume the collapsar model for low-L and High-L, so we assume the same progenitors for all bursts in the simulation and also we use the same luminosity function described in previous sections.

The results of our simulation strong suggest that since we assume only one LGRB population that reproduce very well the observed redshift distribution, the different rate of Low-L and High-L in the local Universe can be explained by a single population as it is shown in Fig 5.

5.4 Discussion and conclusions

In this work, we have studied the luminosity function (LF), the comoving rate and the detection rate of Long Gamma-Ray Burst (LGRBs) in the context of a hierarchical model of galaxy formation.

Assuming the collapsar model and imposing different metallicity constraints we find that:

- GRBs with low metallicity progenitors ($Z < 0.1 - 0.3Z_{\odot}$) do not represent a perfect

tracer of the cosmic star formation history. The deviation of the LGRB rate from the star formation rate decreases with increasing redshift (as a consequence of the global decrease of metallicity with increasing redshift) and the bias is stronger as the metallicity threshold assumed is lowered.

- The LF of LGRBs is well described by a power-law with exponential cut-off, with well determined slope between $1.686 < \xi < 1.838$. Conversely, the characteristic luminosity spans a large range of values ($0.038 < L_0 < 77.875 \times 10^{50}[\text{erg/s}]$), increasing at lower metallicity threshold.
- It is possible to reproduce, within error bars, the redshift distribution of a subset⁶ of *Swift* data with $F > 0.2 \text{ ph/cm}^2/\text{s}$, using: (I) a model without cut in metallicity with a very strong evolving LF, or (II) a model with metallicity threshold $Z < 0.3Z_\odot$ and a non-evolving LF. Selecting only Brights LGRBs ($F > 1 \text{ ph/cm}^2/\text{s}$) and suspecting that a scenario where the properties of GRB change so strong with redshift seem to be enough unrealistic, we rule out the (I) model.
- We predict to have $\sim 1\%$ Bright bursts with high redshift ($z > 6$).
- We test the hypothesis to have at low redshift two different populations, comparing the expected and observed redshift distribution. Assuming the same model for progenitors (collapsar model) and the same luminosity function, low and high luminosity GRBs are well reproduced by the simulated distribution.

Our work constrains the LF function of LGRBs, using a rate of GRB not proportional to SFR, and assuming different metallicity for the progenitors, giving us the possibility to assert that the most probable model for LGRB's progenitor have $Z < 0.3Z_\odot$ and without evolution in the LF.

⁶Only GRBs well placed for optical observations, Jakobsson et al. (2006)

Chapter 6

Conclusions

In the last decades, cosmology passed from being mostly a theoretical science to be one of the most accurate physical sciences in the phenomenological sense. Ever since the establishment of their cosmological nature, GRBs promised to become new probes of cosmology and galaxy evolution. Nowadays, studies of cosmic GRBs and of their host galaxies are starting to provide interesting or even unique new insights in observational cosmology. The study of GRBs and of their afterglows is a rapidly expanding field. Detections of GRB at $z > 8$ may provide an unprecedented way to probe the primordial star formation, massive IMF, early IGM, and chemical enrichment at the end of the cosmic reionization era. There are now plausible or certain host galaxies found for roughly all of the bursts with optical, radio, or X-ray afterglows localized with arcsec precision, and over 70 redshifts measured for GRB hosts and/or afterglows, ranging from 0.0085 to 8.3, with the median $z \sim 2.7$. Moreover, GRBs and their afterglows should be detectable at the largest redshifts (Lamb & Reichart 2000).

As the numbers of GRB redshifts and detected hosts and afterglows grow, it becomes possible to use GRBs in new, systematic studies in cosmology. Moreover, GRBs, after standardizing their energetics through adequate relations, are probing to be reliable distance indicators detectable up to very high redshifts and free from dust extinction.

The aim of present work was: (i) probing the host galaxies of GRBs with cosmological simulation; (ii) studying the luminosity function and GRB at high redshift.

Chapter 3 and 4 presented a deep analysis of the physical and environmental properties of galaxies hosting Long Gamma-Ray Bursts (LGRBs) in the context of a hierarchical model of galaxy formation. In order to select host galaxies, we have adopted the collapsar model and used information available from a semi-analytic model of galaxy formation

coupled to high-resolution cosmological simulations (Wang et al. 2008). By imposing different metallicity constraints on the progenitor stars, we have constructed three host galaxies samples: HOST1 is built without any cut on the metallicity of progenitor stars of GRBs, while the HOST2 and HOST3 samples are constructed by selecting galaxies with progenitor stars of metallicity lower than $0.3Z_{\odot}$ and $0.1Z_{\odot}$ respectively.

As expected, the host sample with no metallicity restriction on the progenitor stars provides a perfect tracer of the cosmic star formation history. When LGRBs are required to be generated by low-metallicity stars, they trace a decreasing fraction of the cosmic star formation rate at lower redshift, as a consequence of the global increase in metallicity. We study the properties of host galaxies up to high redshift (~ 9), finding that they typically have low-metallicity ($Z < 0.5Z_{\odot}$) and that they are small ($M < 10^9 M_{\odot}$), bluer and younger than the average galaxy population, in agreement with observational data. They are also less clustered than typical L_* galaxies in the Universe, and their descendants are massive, red and reside in groups of galaxies with halo mass between $10^{13} M_{\odot}$ to $10^{14} M_{\odot}$.

Chapter 5 presented a deep analysis of the observed and expected rate of high redshift and local GRBs. The rate of these events is highly uncertain, due to the scatter affecting the possible GRB beaming corrections and to the small number of bursts with confirmed redshift with respect to the total number of detected GRBs. We study the luminosity function (LF), the comoving rate and the detection rate at high redshift of LGRBs, using the same catalogues adopted for the study on the hosts galaxies. We assume that LGRBs originate from the death of massive young stars with different metallicity threshold. When LGRBs are required to be generated by low-metallicity stars ($Z < 0.1 \div 0.3 Z_{\odot}$), they trace a decreasing fraction of the cosmic star formation rate at lower redshift. This points to the conclusion that LGRBs are not good tracers of the star formation rate in the universe. Using the $\log N - \log P$ diagram for BATSE bursts, we estimate the LF (with and without evolution with redshift) and the formation rate of LGRBs, finding strong constraints for the slope of the power-law. We check the resulting redshift distribution, for *Swift*-BAT detector, with an unbiased sample of GRB selected by Jakobsson et al. (2006) updated to 2009 August. We find that models where LGRBs are produced by star with $Z < 0.3Z_{\odot}$ and no-evolution of the LF are in agreement with the data. We predict to have about ~ 1 bright burst every 100 LGRB at redshift $z > 6$. Finally, dividing the GRB *Swift* sample according to their luminosity, we conclude that two populations of

bursts with ridge $L \leq (>) 10^{49} \text{erg/s}$ are observable, but they are also reproducible by our simulation, assuming the same model for progenitors (collapsar model) and same LF for low and high luminosity bursts.

Chapter 7

Abstract of publications during the PhD project

Probability for chance coincidence of a gamma-ray burst with a galaxy on the sky

Author: M. A. Campisi and L.-X. Li

The nearby long GRB 060614 was not accompanied by a supernova, challenging the collapsar model for long-duration GRBs and the traditional classification scheme for GRBs. However, Cobb et al. have argued that the association of GRB 060614 and its host galaxy could be chance coincidence. In this work we calculate the probability for a GRB to be randomly coincident with a galaxy on the sky, using a galaxy luminosity function obtained from current galaxy surveys. We find that, with a magnitude limit that current telescopes can reach and an evolving galaxy luminosity function obtained from VVDS, the probability for chance coincidence of a GRB with a galaxy of redshift < 1.5 is about several percent. These results agree with previous estimates based on observed galaxies. For the case of GRB 060614, the probability for it to be coincident with a $z < 0.125$ galaxy by angular separation $< 0.5''$ is $\approx 0.02\%$, indicating that the association of GRB 060614 and its host galaxy is secure. If the telescope magnitude limit is significantly improved in future, the probability for GRB-galaxy association will be considerably large, making it very problematic to identify a GRB host based only on the superposition of a GRB and a galaxy on the sky.

Properties of Long Gamma-Ray Burst Host Galaxies in Cosmological Simulations

Author: M.A. Campisi, G. De Lucia, L-X. Li, S. Mao and X. Kang

We use galaxy catalogues constructed by combining high-resolution N-body simulations with semi-analytic models of galaxy formation to study the properties of Long Gamma-Ray Burst (LGRB) host galaxies. We assume that LGRBs originate from the death of massive young stars and analyse how results are affected by different metallicity constraints on the progenitor stars. As expected, the host sample with no metallicity restriction on the progenitor stars provides a perfect tracer of the cosmic star formation history. When LGRBs are required to be generated by low-metallicity stars, they trace a decreasing fraction of the cosmic star formation rate at lower redshift, as a consequence of the global increase in metallicity. We study the properties of host galaxies up to high redshift (~ 9), finding that they typically have low-metallicity ($Z < 0.5Z_{\odot}$) and that they are small ($M < 10^9 M_{\odot}$), bluer and younger than the average galaxy population, in agreement with observational data. They are also less clustered than typical L_* galaxies in the Universe, and their descendents are massive, red and reside in groups of galaxies with halo mass between $10^{13} M_{\odot}$ to $10^{14} M_{\odot}$.

Redshift distribution and luminosity function of long gamma-ray bursts from cosmological simulations

Author: M. A. Campisi, L.-X. Li and P. Jakobsson

We study the luminosity function (LF), the comoving rate and the detection rate of Long Gamma-Ray Burst (LGRBs) to high redshift, using galaxy catalogues constructed by combining high-resolution N-body simulations with semi-analytic models of galaxy formation. We assume the collapsar model and different metallicity thresholds, reach to the conclusion that LGRBs are not good tracers of the star formation history in the universe. Then using the $\log N - \log P$ diagram for BATSE bursts, we determine the LF (with and without evolution with redshift) and the formation rate of LGRBs, obtaining constraints for the slope of the power-law. We check the resulting redshift distribution with *Swift* data updated to 2009 August, finding that models where LGRBs are produced by star with $Z < 0.3Z_{\odot}$ and without evolution of the LF are in agreement with the data. We also predict that there are about $\sim 1\%$ of GRBs at redshift $z > 6$. Finally, dividing *Swift* GRB data into two population by luminosity ($L \leq 10^{49} \text{ erg/s}$ and $L > 10^{49} \text{ erg/s}$), we find that the two populations are reproduced by the our simulation, assuming the same model for progenitors (collapsar model) and same LF.

Bibliography

- Allende Prieto, C., Lambert, D. L., and Asplund, M. (2001). The Forbidden Abundance of Oxygen in the Sun. *ApJL*, 556:L63–L66.
- Amati, L., Frontera, F., Tavani, M., in't Zand, J. J. M., Antonelli, A., Costa, E., Feroci, M., Guidorzi, C., Heise, J., Masetti, N., Montanari, E., Nicastro, L., Palazzi, E., Pian, E., Piro, L., and Soffitta, P. (2002). Intrinsic spectra and energetics of BeppoSAX Gamma-Ray Bursts with known redshifts. *A&A*, 390:81–89.
- Band, D., Matteson, J., Ford, L., Schaefer, B., Palmer, D., Teegarden, B., Cline, T., Briggs, M., Paciesas, W., Pendleton, G., Fishman, G., Kouveliotou, C., Meegan, C., Wilson, R., and Lestrade, P. (1993). BATSE observations of gamma-ray burst spectra. I - Spectral diversity. *ApJ*, 413:281–292.
- Barthelmy, S. D., Barbier, L. M., Cummings, J. R., Fenimore, E. E., Gehrels, N., Hullinger, D., Krimm, H. A., Markwardt, C. B., Palmer, D. M., Parsons, A., Sato, G., Suzuki, M., Takahashi, T., Tashiro, M., and Tueller, J. (2005). The Burst Alert Telescope (BAT) on the SWIFT Midex Mission. *Space Science Reviews*, 120:143–164.
- Berger, E., in Holt, S., Gehrels, N., and Nousek, J. (2006). Gamma-Ray Bursts in the Swift Era. *Am. Inst. Phys.*, page 33.
- Bloom, J. S., Berger, E., Kulkarni, S. R., Djorgovski, S. G., and Frail, D. A. (2003). The Redshift Determination of GRB 990506 and GRB 000418 with the Echelle Spectrograph Imager on Keck. *AJ*, 125:999–1005.
- Bloom, J. S., Djorgovski, S. G., and Kulkarni, S. R. (2001). The Redshift and the Ordinary Host Galaxy of GRB 970228. *ApJ*, 554:678–683.
- Bloom, J. S., Djorgovski, S. G., Kulkarni, S. R., and Frail, D. A. (1998). The Host Galaxy of GRB 970508. *ApJL*, 507:L25–L28.
- Bloom, J. S., Kulkarni, S. R., and Djorgovski, S. G. (2002). The Observed Offset Distribution of Gamma-Ray Bursts from Their Host Galaxies: A Robust Clue to the Nature of the Progenitors. *AJ*, 123:1111–1148.
- Bloom, J. S., Odewahn, S. C., Djorgovski, S. G., Kulkarni, S. R., Harrison, F. A., Koresko, C., Neugebauer, G., Armus, L., Frail, D. A., Gal, R. R., Sari, R., Squires, G., Illingworth, G., Kelson, D., Chaffee, F. H., Goodrich, R., Feroci, M., Costa, E., Piro, L., Frontera, F., Mao, S., Akerlof, C., and McKay, T. A. (1999). The Host Galaxy of GRB 990123. *ApJL*, 518:L1–L4.
- Boella, G., Butler, R. C., Perola, G. C., Piro, L., Scarsi, L., and Bleeker, J. A. M. (1997). BeppoSAX, the wide band mission for X-ray astronomy. *A&A Supp.*, 122:299–307.
- Bornancini, C. G., Martínez, H. J., Lambas, D. G., Le Floc'h, E., Mirabel, I. F., and Minniti, D. (2004). The Galaxy Density Environment of Gamma-Ray Burst Host Galaxies. *ApJ*, 614:84–90.
- Bromm, V. and Loeb, A. (2002). The Expected Redshift Distribution of Gamma-Ray Bursts. *ApJ*, 575:111–116.
- Brown, W. R., Kewley, L. J., and Geller, M. J. (2008). MMT Extremely Metal-Poor Galaxy Survey. I. An Efficient Technique for Identifying Metal-Poor Galaxies. *AJ*, 135:92–98.
- Burrows, D. N. and Racusin, J. (2006). Swift X-ray afterglows: Where are the X-ray jet breaks? *Nuovo Cimento B Serie*, 121:1273–1287.

- Burrows, D. N., Romano, P., Falcone, A., Kobayashi, S., Zhang, B., Moretti, A., O'Brien, P. T., Goad, M. R., Campana, S., Page, K. L., Angelini, L., Barthelmy, S., Beardmore, A. P., Capalbi, M., Chincarini, G., Cummings, J., Cusumano, G., Fox, D., Giommi, P., Hill, J. E., Kennea, J. A., Krimm, H., Mangano, V., Marshall, F., Mészáros, P., Morris, D. C., Nousek, J. A., Osborne, J. P., Pagani, C., Perri, M., Tagliaferri, G., Wells, A. A., Woosley, S., and Gehrels, N. (2005). Bright X-ray Flares in Gamma-Ray Burst Afterglows. *Science*, 309:1833–1835.
- Butler, N., Dullighan, A., Ford, P., Ricker, G., Vanderspek, R., Hurley, K., Jernigan, J., Lamb, D., and Graziani, C. (2004). Optical and X-ray Observations of the Afterglow to XRF 030723. In Fenimore, E. and Galassi, M., editors, *Gamma-Ray Bursts: 30 Years of Discovery*, volume 727 of *American Institute of Physics Conference Series*, pages 111–114.
- Campana, S., Mangano, V., Blustin, A. J., Brown, P., Burrows, D. N., Chincarini, G., Cummings, J. R., Cusumano, G., Della Valle, M., Malesani, D., Mészáros, P., Nousek, J. A., Page, M., Sakamoto, T., Waxman, E., Zhang, B., Dai, Z. G., Gehrels, N., Immler, S., Marshall, F. E., Mason, K. O., Moretti, A., O'Brien, P. T., Osborne, J. P., Page, K. L., Romano, P., Roming, P. W. A., Tagliaferri, G., Cominsky, L. R., Giommi, P., Godet, O., Kennea, J. A., Krimm, H., Angelini, L., Barthelmy, S. D., Boyd, P. T., Palmer, D. M., Wells, A. A., and White, N. E. (2006). The association of GRB 060218 with a supernova and the evolution of the shock wave. *Nature*, 442:1008–1010.
- Campisi, M. A., De Lucia, G., Li, L., Mao, S., and Kang, X. (2009). Properties of Long Gamma-Ray Burst Host Galaxies in Cosmological Simulation. *ArXiv:astro-ph/0908.2427*.
- Campisi, M. A. and Li, L.-X. (2008). Probability for chance coincidence of a gamma-ray burst with a galaxy on the sky. *MNRAS*, 391:935–941.
- Castro Cerón, J. M., Michałowski, M. J., Hjorth, J., Malesani, D., Gorosabel, J., Watson, D., and Fynbo, J. P. U. (2008). On the distribution of stellar masses in gamma-ray burst host galaxies. *ArXiv e-prints*, 803.
- Cen, R. and Fang, T. (2007). Gamma-Ray Bursts May Be Biased Tracers of Star Formation. *ArXiv:0710.4370*.
- Chapman, R., Tanvir, N. R., Priddey, R. S., and Levan, A. J. (2007). How common are long gamma-ray bursts in the local Universe? *MNRAS*, 382:L21–L25.
- Christensen, L., Hjorth, J., and Gorosabel, J. (2004). UV star-formation rates of GRB host galaxies. *A&A*, 425:913–926.
- Cobb, B. E. and Baily, C. D. (2008). Connecting Gamma-Ray Bursts and Galaxies: The Probability of Chance Coincidence. *ApJ*, 677:1157–1167.
- Cobb, B. E., Baily, C. D., van Dokkum, P. G., and Natarajan, P. (2006). Could GRB 060614 and Its Presumed Host Galaxy Be a Chance Superposition? *ApJL*, 651:L85–L88.
- Conselice, C. J., Vreeswijk, P. M., Fruchter, A. S., Levan, A., Kouveliotou, C., Fynbo, J. P. U., Gorosabel, J., Tanvir, N. R., and Thorsett, S. E. (2005). Gamma-Ray Burst-Selected High-Redshift Galaxies: Comparison to Field Galaxy Populations to $z \sim 3$. *ApJ*, 633:29–40.
- Costa, E., Frontera, F., Heise, J., Feroci, M., in't Zand, J., Fiore, F., Cinti, M. N., Dal Fiume, D., Nicastro, L., Orlandini, M., Palazzi, E., Rapisarda, M., Zavattini, G., Jager, R., Parmar, A., Owens, A., Molendi, S., Cusumano, G., Maccarone, M. C., Giarrusso, S., Coletta, A., Antonelli, L. A., Giommi, P., Muller, J. M., Piro, L., and Butler, R. C. (1997). Discovery of an X-ray afterglow associated with the γ -ray burst of 28 February 1997. *Nature*, 387:783–785.
- Courty, S., Björnsson, G., and Gudmundsson, E. H. (2007). Numerical counterparts of GRB host galaxies. *MNRAS*, 376:1375–1384.
- Croton, D. J., Springel, V., White, S. D. M., De Lucia, G., Frenk, C. S., Gao, L., Jenkins, A., Kauffmann, G., Navarro, J. F., and Yoshida, N. (2006). The many lives of active galactic nuclei: cooling flows, black holes and the luminosities and colours of galaxies. *MNRAS*, 365:11–28.
- Dai, X. (2009). Intensity Distribution and Luminosity Function of the Swift Gamma-Ray Bursts. *ApJL*, 697:L68–L71.

- Dai, Z. G., Liang, E. W., and Xu, D. (2004). Constraining Ω_M and Dark Energy with Gamma-Ray Bursts. *ApJL*, 612:L101–L104.
- Daigne, F., Rossi, E. M., and Mochkovitch, R. (2006). The redshift distribution of Swift gamma-ray bursts: evidence for evolution. *MNRAS*, 372:1034–1042.
- De Lucia, G. and Blaizot, J. (2007). The hierarchical formation of the brightest cluster galaxies. *MNRAS*, 375:2–14.
- De Lucia, G., Kauffmann, G., and White, S. D. M. (2004). Chemical enrichment of the intracluster and intergalactic medium in a hierarchical galaxy formation model. *MNRAS*, 349:1101–1116.
- De Lucia, G., Springel, V., White, S. D. M., Croton, D., and Kauffmann, G. (2006). The formation history of elliptical galaxies. *MNRAS*, 366:499–509.
- Della Valle, M., Chincarini, G., Panagia, N., Tagliaferri, G., Malesani, D., Testa, V., Fugazza, D., Campana, S., Covino, S., Mangano, V., Antonelli, L. A., D’Avanzo, P., Hurley, K., Mirabel, I. F., Pellizza, L. J., Piranomonte, S., and Stella, L. (2006). An enigmatic long-lasting γ -ray burst not accompanied by a bright supernova. *Nature*, 444:1050–1052.
- Djorgovski, S. G., Kulkarni, S. R., Bloom, J. S., Goodrich, R., Frail, D. A., Piro, L., and Palazzi, E. (1998). Spectroscopy of the Host Galaxy of the Gamma-Ray Burst 980703. *ApJL*, 508:L17–L20.
- Evans, P. A., Beardmore, A. P., Page, K. L., Osborne, J. P., O’Brien, P. T., Willingale, R., Starling, R. L. C., Burrows, D. N., Godet, O., Vetere, L., Racusin, J., Goad, M. R., Wiersema, K., Angelini, L., Capalbi, M., Chincarini, G., Gehrels, N., Kennea, J. A., Margutti, R., Morris, D. C., Mountford, C. J., Pagani, C., Perri, M., Romano, P., and Tanvir, N. (2009). Methods and results of an automatic analysis of a complete sample of Swift-XRT observations of GRBs. *MNRAS*, 397:1177–1201.
- Fan, Y.-Z. and Piran, T. (2008). High-energy γ -ray emission from gamma-ray bursts – before GLAST. *Frontiers of Physics in China*, 3:306–330.
- Fenimore, E. E. (1999). The Average Temporal and Spectral Evolution of Gamma-Ray Bursts. *ApJ*, 518:375–379.
- Fenimore, E. E., Epstein, R. I., Ho, C., Klebesadel, R. W., Lacey, C., Laros, J. G., Meier, M., Strohmayer, T., Pendleton, G., Fishman, G., Kouveliotou, C., and Meegan, C. (1993). The intrinsic luminosity of γ -ray bursts and their host galaxies. *Nature*, 366:40–42.
- Fernandez-Soto et al. (2009). GRB 090423: refined TNG analysis. *GRB Coordinates Network*, 9222:1–+.
- Firmani, C., Ghisellini, G., Avila-Reese, V., and Ghirlanda, G. (2006). Discovery of a tight correlation among the prompt emission properties of long gamma-ray bursts. *MNRAS*, 370:185–197.
- Fishman, G. J. and Meegan, C. A. (1995). Gamma-Ray Bursts. *ARA&A*, 33:415–458.
- Frail, D. A., Kulkarni, S. R., Nicastro, L., Feroci, M., and Taylor, G. B. (1997). The radio afterglow from the γ -ray burst of 8 May 1997. *Nature*, 389:261–263.
- Frail, D. A., Kulkarni, S. R., Sari, R., Djorgovski, S. G., Bloom, J. S., Galama, T. J., Reichart, D. E., Berger, E., Harrison, F. A., Price, P. A., Yost, S. A., Diercks, A., Goodrich, R. W., and Chaffee, F. (2001). Beaming in Gamma-Ray Bursts: Evidence for a Standard Energy Reservoir. *ApJL*, 562:L55–L58.
- Fruchter, A. S., Levan, A. J., and Strolger, e. a. (2006). Long γ -ray bursts and core-collapse supernovae have different environments. *Nature*, 441:463–468.
- Fryer, C. L., Woosley, S. E., and Hartmann, D. H. (1999). Formation Rates of Black Hole Accretion Disk Gamma-Ray Bursts. *ApJ*, 526:152–177.
- Fynbo, J. P. U., Prochaska, J. X., Sommer-Larsen, J., Dessauges-Zavadsky, M., and Møller, P. (2008). Reconciling the Metallicity Distributions of Gamma-Ray Burst, Damped Ly α , and Lyman Break Galaxies at $z \sim 3$. *ApJ*, 683:321–328.
- Fynbo, J. P. U., Watson, D., Thöne, C. C., Sollerman, J., Bloom, J. S., Davis, T. M., Hjorth, J., Jakobsson, P., Jørgensen, U. G., Graham, J. F., Fruchter, A. S., Bersier, D., Kewley, L., Cassan, A., Castro Cerón, J. M., and Foley, e. a. (2006). No supernovae associated with two long-duration γ -ray bursts. *Nature*, 444:1047–1049.

- Fynbo, J. U., Gorosabel, J., Dall, T. H., Hjorth, J., Pedersen, H., Andersen, M. I., Møller, P., Holland, S., Smail, I., Kobayashi, N., Rol, E., Vreeswijk, P., Burud, I., Jensen, B. L., Thomsen, B., Henden, A., Vrba, F., Canzian, B., Castro Cerón, J. M., Castro-Tirado, A. J., Cline, T., Goto, M., Greiner, J., Hanski, M. T., Hurley, K., Lund, N., Pursimo, T., Ostensen, R., Solheim, J., Tanvir, N., and Terada, H. (2001). The optical afterglow and host galaxy of GRB 000926. *A&A*, 373:796–804.
- Gal-Yam, A., Fox, D. B., Price, P. A., Ofek, E. O., Davis, M. R., Leonard, D. C., Soderberg, A. M., Schmidt, B. P., Lewis, K. M., Peterson, B. A., Kulkarni, S. R., Berger, E., Cenko, S. B., Sari, R., Sharon, K., Frail, D., Moon, D.-S., Brown, P. J., Cucchiara, A., Harrison, F., Piran, T., Persson, S. E., McCarthy, P. J., Penprase, B. E., Chevalier, R. A., and MacFadyen, A. I. (2006). A novel explosive process is required for the γ -ray burst GRB 060614. *Nature*, 444:1053–1055.
- Galama, T. J., Reichart, D., Brown, T. M., Kimble, R. A., Price, P. A., Berger, E., Frail, D. A., Kulkarni, S. R., Yost, S. A., Gal-Yam, A., Bloom, J. S., Harrison, F. A., Sari, R., Fox, D., and Djorgovski, S. G. (2003). Hubble Space Telescope and Ground-based Optical and Ultraviolet Observations of GRB 010222. *ApJ*, 587:135–142.
- Galama, T. J., Vreeswijk, P. M., van Paradijs, J., Kouveliotou, C., Augusteijn, T., Bönhardt, H., Brewer, J. P., Doublier, V., Gonzalez, J.-F., Leibundgut, B., Lidman, C., Hainaut, O. R., Patat, F., Heise, J., in't Zand, J., and Hurley, e. a. (1998). An unusual supernova in the error box of the γ -ray burst of 25 April 1998. *Nature*, 395:670–672.
- Gehrels, N. and Cannizzo, J. K. (2007). Combining Swift and GLAST to Explore GRBs. In Ritz, S., Michelson, P., and Meegan, C. A., editors, *The First GLAST Symposium*, volume 921 of *American Institute of Physics Conference Series*, pages 95–99.
- Gehrels, N., Cannizzo, J. K., and Norris, J. P. (2007). Gamma-ray bursts in the Swift era. *New Journal of Physics*, 9:37–+.
- Gehrels, N. and et al (2004). The Swift Gamma-Ray Burst Mission. *ApJ*, 611:1005–1020.
- Gehrels, N., Norris, J. P., Barthelmy, S. D., Granot, J., Kaneko, Y., Kouveliotou, C., Markwardt, C. B., Mészáros, P., Nakar, E., Nousek, J. A., O'Brien, P. T., Page, M., Palmer, D. M., Parsons, A. M., Roming, P. W. A., Sakamoto, T., Sarazin, C. L., Schady, P., Stamatikos, M., and Woosley, S. E. (2006). A new γ -ray burst classification scheme from GRB060614. *Nature*, 444:1044–1046.
- Gehrels, N., Sarazin, C. L., O'Brien, P. T., Zhang, B., Barbier, L., Barthelmy, S. D., Blustin, A., Burrows, D. N., Cannizzo, J., Cummings, J. R., Goad, M., Holland, S. T., Hurkett, C. P., Kennea, J. A., Levan, A., Markwardt, C. B., Mason, K. O., Meszaros, P., Page, M., Palmer, D. M., Rol, E., Sakamoto, T., Willingale, R., Angelini, L., Beardmore, A., Boyd, P. T., Breeveld, A., Campana, S., Chester, M. M., Chincarini, G., Cominsky, L. R., Cusumano, G., de Pasquale, M., Fenimore, E. E., Giommi, P., Gronwall, C., Grupe, D., Hill, J. E., Hinshaw, D., Hjorth, J., Hullinger, D., Hurley, K. C., Klose, S., Kobayashi, S., Kouveliotou, C., Krimm, H. A., Mangano, V., Marshall, F. E., McGowan, K., Moretti, A., Mushotzky, R. F., Nakazawa, K., Norris, J. P., Nousek, J. A., Osborne, J. P., Page, K., Parsons, A. M., Patel, S., Perri, M., Poole, T., Romano, P., Roming, P. W. A., Rosen, S., Sato, G., Schady, P., Smale, A. P., Sollerman, J., Starling, R., Still, M., Suzuki, M., Tagliaferri, G., Takahashi, T., Tashiro, M., Tueller, J., Wells, A. A., White, N. E., and Wijers, R. A. M. J. (2005). A short γ -ray burst apparently associated with an elliptical galaxy at redshift $z = 0.225$. *Nature*, 437:851–854.
- Ghirlanda, G., Ghisellini, G., and Lazzati, D. (2004a). The Collimation-corrected Gamma-Ray Burst Energies Correlate with the Peak Energy of Their νF_ν Spectrum. *ApJ*, 616:331–338.
- Ghirlanda, G., Ghisellini, G., Lazzati, D., and Firmani, C. (2004b). Gamma-Ray Bursts: New Rulers to Measure the Universe. *ApJL*, 613:L13–L16.
- Ghirlanda, G., Magliocchetti, M., Ghisellini, G., and Guzzo, L. (2006). On the correlation of short gamma-ray bursts and clusters of galaxies. *MNRAS*, 368:L20–L24.
- Ghirlanda, G., Nava, L., Ghisellini, G., and Firmani, C. (2007). Confirming the γ -ray burst spectral-energy correlations in the era of multiple time breaks. *A&A*, 466:127–136.
- Ghisellini, G. and Celotti, A. (1999). Quasi-thermal comptonization and GRBs. *A&A Supp.*, 138:527–528.

- Giuliani, A., Mereghetti, S., Fornari, F., Del Monte, E., Feroci, M., Marisaldi, M., Esposito, P., Perotti, F., Tavani, M., Argan, A., Barbiellini, G., Boffelli, F., Bulgarelli, A., Caraveo, P., Cattaneo, P. W., Chen, A. W., Costa, E., D'Ammando, F., di Cocco, G., Donnarumma, I., Evangelista, Y., Fiorini, M., Fuschino, F., Galli, M., Gianotti, F., Labanti, C., Lapshov, I., Lazzarotto, F., Lipari, P., Longo, F., Morselli, A., Pacciani, L., Pellizzoni, A., Piano, G., Picozza, P., Prest, M., Pucella, G., Rapisarda, M., Rappoldi, A., Soffitta, P., Trifoglio, M., Trois, A., Vallazza, E., Vercellone, S., Zanello, D., Salotti, L., Cutini, S., Pittori, C., Preger, B., Santolamazza, P., Verrecchia, F., Gehrels, N., Page, K., Burrows, D., Rossi, A., Hurley, K., Mitrofanov, I., and Boynton, W. (2008). AGILE detection of delayed gamma-ray emission from GRB 080514B. *A&A*, 491:L25–L28.
- Gorosabel, J., Christensen, L., Hjorth, J., Fynbo, J. U., Pedersen, H., Jensen, B. L., Andersen, M. I., Lund, N., and et al. (2003a). A multi-colour study of the dark GRB 000210 host galaxy and its environment. *A&A*, 400:127–136.
- Gorosabel, J., Christensen, L., Hjorth, J., Fynbo, J. U., Pedersen, H., Jensen, B. L., Andersen, M. I., Lund, N., Jaunsen, A. O., Castro Cerón, J. M., Castro-Tirado, A. J., Fruchter, A., Greiner, J., Pian, E., Vreeswijk, P. M., Burud, I., Frontera, F., Kaper, L., Klose, S., Kouveliotou, C., Masetti, N., Palazzi, E., Rhoads, J., Rol, E., Salamanca, I., Tanvir, N., Wijers, R. A. M. J., and van den Heuvel, E. (2003b). A multi-colour study of the dark GRB 000210 host galaxy and its environment. *A&A*, 400:127–136.
- Gorosabel, J., Jelínek, M., de Ugarte Postigo, A., Guziy, S., and Castro-Tirado, A. J. (2005). The GRB 030328 host: Another case of a blue starburst galaxy. *Nuovo Cimento C Geophysics Space Physics C*, 28:677–+.
- Grav, T., Hansen, M. W., Pedersen, H., Hjorth, J., Michelsen, R., Jensen, B. L., Andersen, M. I., Gorosabel, J., and Fynbo, J. U. (2001). GRB 011211 optical observations: likely afterglow. *GRB Coordinates Network*, 1191:1–+.
- Graziani, C., Shirasaki, Y., Matsuoka, M., Tamagawa, T., Torii, K., Sakamoto, T., Suzuki, M., Yoshida, A., Fenimore, E., Galassi, M., Tavenner, T., Donaghy, T., Nakagawa, Y., Takahashi, D., Satoh, R., Urata, Y., Ricker, G., Atteia, J.-L., Kawai, N., Lamb, D., Woosley, S., Vanderspek, R., Villasenor, J., Crew, G., Doty, J., Monnelly, G., Butler, N., Cline, T., Jernigan, J. G., Levine, A., Martel, F., Morgan, E., Prigozhin, G., Azzibrouck, G., Braga, J., Manchanda, R., Pizzichini, G., Boer, M., Olive, J.-F., Dezalay, J.-P., Barraud, C., and Hurley, K. (2003). GRB030323 (=H2640): a faint, long GRB localized by the HETE WXM and SXC. *GRB Coordinates Network*, 1956:1–+.
- Guetta, D. and Della Valle, M. (2007). On the Rates of Gamma-Ray Bursts and Type Ib/c Supernovae. *ApJL*, 657:L73–L76.
- Guetta, D., Piran, T., and Waxman, E. (2005). The Luminosity and Angular Distributions of Long-Duration Gamma-Ray Bursts. *ApJ*, 619:412–419.
- Halpern, J. P. and Fesen, R. (1998). GRB980613 optical observations. *GRB Coordinates Network*, 134:1–+.
- Henden, A. and Vrba, F. (2001). GRB010222, optical observations. *GRB Coordinates Network*, 967:1–+.
- Hjorth, J., Sollerman, J., Møller, P., Fynbo, J. P. U., Woosley, S. E., Kouveliotou, C., Tanvir, N. R., Greiner, J., Andersen, M. I., Castro-Tirado, A. J., Castro Cerón, J. M., Fruchter, A. S., Gorosabel, J., Jakobsson, P., Kaper, L., Klose, S., Masetti, N., Pedersen, H., Pedersen, K., Pian, E., Palazzi, E., Rhoads, J. E., Rol, E., van den Heuvel, E. P. J., Vreeswijk, P. M., Watson, D., and Wijers, R. A. M. J. (2003). A very energetic supernova associated with the γ -ray burst of 29 March 2003. *Nature*, 423:847–850.
- Hjorth, J., Thomsen, B., Nielsen, S. R., Andersen, M. I., Holland, S. T., Fynbo, J. U., Pedersen, H., Jaunsen, A. O., Halpern, J. P., Fesen, R., Gorosabel, J., Castro-Tirado, A., McMahon, R. G., Hoenig, M. D., Björnsson, G., Amati, L., Tanvir, N. R., and Natarajan, P. (2002). The Afterglow and Complex Environment of the Optically Dim Burst GRB 980613. *ApJ*, 576:113–119.
- Holland, S. T., Soszyński, I., Gladders, M. D., Barrientos, L. F., Berlind, P., Bersier, D., Garnavich, P. M., Jha, S., and Stanek, K. Z. (2002). The Optical Afterglow of the Gamma-Ray Burst GRB 011211. *AJ*, 124:639–645.
- Hopkins, A. M. and Beacom, J. F. (2006). On the Normalization of the Cosmic Star Formation History. *ApJ*, 651:142–154.
- Huang, Y. F., Gou, L. J., Dai, Z. G., and Lu, T. (2000). Overall Evolution of Jetted Gamma-Ray Burst Ejecta. *ApJ*, 543:90–96.

- Hurley, K., Boggs, S. E., Smith, D. M., Duncan, R. C., Lin, R., Zoglauer, A., Krucker, S., Hurford, G., Hudson, H., Wigger, C., Hajdas, W., Thompson, C., Mitrofanov, I., Sanin, A., Boynton, W., Fellows, C., von Kienlin, A., Lichti, G., Rau, A., and Cline, T. (2005). An exceptionally bright flare from SGR 1806-20 and the origins of short-duration γ -ray bursts. *Nature*, 434:1098–1103.
- Hurley, K., Dingus, B. L., Mukherjee, R., Sreekumar, P., Kouveliotou, C., Meegan, C., Fishman, G. J., Band, D., Ford, L., Bertsch, D., Cline, T., Fichtel, C., Hartman, R., Hunter, S., Thompson, D. J., Kanbach, G., Mayer-Hasselwander, H., von Montigny, C., Sommer, M., Lin, Y., Nolan, P., Michelson, P., Kniffen, D., Mattox, J., Schneid, E., Boer, M., and Niel, M. (1994). Detection of a γ -ray burst of very long duration and very high energy. *Nature*, 372:652–654.
- Jacobsson, P., Frail, D. A., Fox, D. B., Moon, D.-S., Price, P. A., Kulkarni, S. R., Fynbo, J. P. U., Hjorth, J., Berger, E., McNaught, R. H., and Dahle, H. (2005). The Radio Afterglow and Host Galaxy of the Dark GRB 020819. *ApJ*, 629:45–51.
- Jacobsson, P., Hjorth, J., Fynbo, J. P. U., Weidinger, M., Gorosabel, J., Ledoux, C., Watson, D., Björnsson, G., Gudmundsson, E. H., Wijers, R. A. M. J., Möller, P., Pedersen, K., Sollerman, J., Henden, A. A., Jensen, B. L., Gilmore, A., Kilmartin, P., Levan, A., Castro Cerón, J. M., Castro-Tirado, A. J., Fruchter, A., Kouveliotou, C., Masetti, N., and Tanvir, N. (2004). The line-of-sight towards GRB 030429 at $z = 2.66$: Probing the matter at stellar, galactic and intergalactic scales. *A&A*, 427:785–794.
- Jacobsson, P., Levan, A., Fynbo, J. P. U., Priddey, R., Hjorth, J., Tanvir, N., Watson, D., Jensen, B. L., Sollerman, J., Natarajan, P., Gorosabel, J., Castro Cerón, J. M., Pedersen, K., Pursimo, T., Árnadóttir, A. S., Castro-Tirado, A. J., Davis, C. J., Deeg, H. J., Fiuza, D. A., Mykolaitis, S., and Sousa, S. G. (2006). A mean redshift of 2.8 for Swift gamma-ray bursts. *A&A*, 447:897–903.
- Jacobsson, P., Malesani, D., Fynbo, J. P. U., Hjorth, J., and Milvang-Jensen, B. (2009). GRB Redshifts and Host Galaxies: An Unbiased Sample. In Meegan, C., Kouveliotou, C., and Gehrels, N., editors, *American Institute of Physics Conference Series*, volume 1133 of *American Institute of Physics Conference Series*, pages 455–463.
- Jensen, B. L., Hjorth, J., Pedersen, H., Kristen, H. E., Tomassi, L., Pian, E., and Hurley, K. (1999). GRB 991208 optical decay. *GRB Coordinates Network*, 454:1–+.
- Kauffmann, G., White, S. D. M., Heckman, T. M., Ménard, B., Brinchmann, J., Charlot, S., Tremonti, C., and Brinkmann, J. (2004). The environmental dependence of the relations between stellar mass, structure, star formation and nuclear activity in galaxies. *MNRAS*, 353:713–731.
- Kistler, M. D., Yüksel, H., Beacom, J. F., and Stanek, K. Z. (2008). An Unexpectedly Swift Rise in the Gamma-Ray Burst Rate. *ApJL*, 673:L119–L122.
- Kitzbichler, M. G. and White, S. D. M. (2007). The high-redshift galaxy population in hierarchical galaxy formation models. *MNRAS*, 376:2–12.
- Kocevski, D. and Butler, N. (2008). Gamma-Ray Burst Energetics in the Swift Era. *ApJ*, 680:531–538.
- Kommers, J. M., Lewin, W. H. G., Kouveliotou, C., van Paradijs, J., Pendleton, G. N., Meegan, C. A., and Fishman, G. J. (2000). The Intensity Distribution of Faint Gamma-Ray Bursts Detected with BATSE. *ApJ*, 533:696–709.
- Kouveliotou, C., Meegan, C. A., Fishman, G. J., Bhat, N. P., Briggs, M. S., Koshut, T. M., Paciesas, W. S., and Pendleton, G. N. (1993). Identification of two classes of gamma-ray bursts. *ApJL*, 413:L101–L104.
- Landy, S. D. and Szalay, A. S. (1993). Bias and variance of angular correlation functions. *ApJ*, 412:64–71.
- Langer, N. and Norman, C. A. (2006). On the Collapsar Model of Long Gamma-Ray Bursts: Constraints from Cosmic Metallicity Evolution. *ApJL*, 638:L63–L66.
- Lapi, A., Kawakatu, N., Bosnjak, Z., Celotti, A., Bressan, A., Granato, G. L., and Danese, L. (2008). Long gamma-ray bursts and their host galaxies at high redshift. *MNRAS*, 386:608–618.
- Larsson, J., Levan, A. J., Davies, M. B., and Fruchter, A. S. (2007). A new constraint for gamma-ray burst progenitor mass. *MNRAS*, 376:1285–1290.
- Lazzati, D., Ghirlanda, G., and Ghisellini, G. (2005). Soft gamma-ray repeater giant flares in the BATSE short gamma-ray burst catalogue: constraints from spectroscopy. *MNRAS*, 362:L8–L12.

- Lazzati, D., Ghisellini, G., and Celotti, A. (1999). Constraints on the bulk Lorentz factor in the internal shock scenario for gamma-ray bursts. *MNRAS*, 309:L13–L17.
- Lazzati, D., Ghisellini, G., Celotti, A., and Rees, M. J. (2000). Compton-dragged Gamma-Ray Bursts Associated with Supernovae. *ApJL*, 529:L17–L20.
- Le Floc’h, E., Duc, P.-A., Mirabel, I. F., Sanders, D. B., Bosch, G., Diaz, R. J., Donzelli, C. J., Rodrigues, I., Courvoisier, T. J.-L., Greiner, J., Mereghetti, S., Melnick, J., Maza, J., and Minniti, D. (2003). Are the hosts of gamma-ray bursts sub-luminous and blue galaxies? *A&A*, 400:499–510.
- Le Floc’h, E., Duc, P.-A., Mirabel, I. F., Sanders, D. B., Bosch, G., Rodrigues, I., Courvoisier, T. J.-L., Mereghetti, S., and Melnick, J. (2002). Very Large Telescope and Hubble Space Telescope Observations of the Host Galaxy of GRB 990705. *ApJL*, 581:L81–L84.
- Levan, A. J., Jakobsson, P., Hurkett, C., Tanvir, N. R., Gorosabel, J., Vreeswijk, P., Rol, E., Chapman, R., Gehrels, N., O’Brien, P. T., Osborne, J. P., Priddey, R. S., Kouveliotou, C., Starling, R., vanden Berk, D., and Wiersema, K. (2007). A case of mistaken identity? GRB060912A and the nature of the long-short GRB divide. *MNRAS*, 378:1439–1446.
- Levesque, E. M. and Kewley, L. J. (2007). The Host Galaxy of GRB 060505: Host ISM Properties. *ApJL*, 667:L121–L124.
- Li, L.-X. (2006). Correlation between the peak spectral energy of gamma-ray bursts and the peak luminosity of the underlying supernovae: implication for the nature of the gamma-ray burst-supernova connection. *MNRAS*, 372:1357–1365.
- Li, L.-X. (2007a). Redshift degeneracy in the $E_{iso} - E_{peak}$ relation of gamma-ray bursts. *MNRAS*, 374:L20–L23.
- Li, L.-X. (2007b). Variation of the Amati relation with cosmological redshift: a selection effect or an evolution effect? *MNRAS*, 379:L55–L59.
- Li, L.-X. (2008a). Are Gamma-Ray Bursts a Standard Energy Reservoir? *Acta Astronomica*, 58:103–112.
- Li, L.-X. (2008b). Star formation history up to $z = 7.4$: implications for gamma-ray bursts and cosmic metallicity evolution. *MNRAS*, 388:1487.
- Li, L.-X. and Paczyński, B. (1998). Transient Events from Neutron Star Mergers. *ApJL*, 507:L59–L62.
- Liang, E. and Zhang, B. (2006). Identification of Two Categories of Optically Bright Gamma-Ray Bursts. *ApJL*, 638:L67–L70.
- Liang, E.-W., Racusin, J. L., Zhang, B., Zhang, B.-B., and Burrows, D. N. (2008). A Comprehensive Analysis of Swift XRT Data. III. Jet Break Candidates in X-Ray and Optical Afterglow Light Curves. *ApJ*, 675:528–552.
- Loeb, A. (2002). Novel Ways to Probe the Universe with Gamma-Ray Bursts and Quasars. In Gilfanov, M., Sunyaev, R., and Churazov, E., editors, *Lighthouses of the Universe: The Most Luminous Celestial Objects and Their Use for Cosmology*, pages 137–+.
- Lu, T., Huang, Y. F., Dai, Z. G., and Wei, D. M. (2004). Gamma-ray bursts. In Cheng, K. S. and Romero, G. E., editors, *Cosmic Gamma-Ray Sources*, volume 304 of *Astrophysics and Space Science Library*, pages 225–+.
- Lyutikov, M. (2006). The electromagnetic model of gamma-ray bursts. *New Journal of Physics*, 8:119–+.
- MacFadyen, A. I. and Woosley, S. E. (1999). Collapsars: Gamma-Ray Bursts and Explosions in “Failed Supernovae”. *ApJ*, 524:262–289.
- MacFadyen, A. I., Woosley, S. E., and Heger, A. (2001). Supernovae, Jets, and Collapsars. *ApJ*, 550:410–425.
- Mangano, V., Holland, S. T., Malesani, D., Troja, E., Chincarini, G., Zhang, B., La Parola, V., Brown, P. J., Burrows, D. N., Campana, S., Capalbi, M., Cusumano, G., Della Valle, M., Gehrels, N., Giommi, P., Grupe, D., Guidorzi, C., Mineo, T., Moretti, A., Osborne, J. P., Pandey, S. B., Perri, M., Romano, P., Roming, P. W. A., and Tagliaferri, G. (2007). Swift observations of GRB 060614: an anomalous burst with a well behaved afterglow. *A&A*, 470:105–118.
- Mao, S. and Mo, H. J. (1998). The nature of the host galaxies for gamma-ray bursts. *A&A*, 339:L1–L4.

- Margon, B., Deutsch, E. W., Lamb, D. Q., Castander, F. J., and Metzger, M. (1997). GRB 970228. *iauc*, 6618:2–+.
- Masetti, N., Palazzi, E., Pian, E., Hunt, L., Fynbo, J. P. U., Gorosabel, J., Klose, S., Benetti, S., Falomo, R., Zeh, A., Amati, L., Andersen, M. I., Castro-Tirado, A. J., Castro Cerón, J. M., Danziger, J., Frontera, F., Fruchter, A. S., Greiner, J., Hjorth, J., Jensen, B. L., Kaper, L., Kouveliotou, C., Levan, A., Magazzù, A., Møller, P., Nicastro, L., Pedersen, H., Tanvir, N. R., Vreeswijk, P. M., Wijers, R. A. M. J., and van den Heuvel, E. P. J. (2005). Late-epoch optical and near-infrared observations of the GRB 000911 afterglow and its host galaxy. *A&A*, 438:841–853.
- Meegan, C. A., Fishman, G. J., Wilson, R. B., Horack, J. M., Brock, M. N., Pacieras, W. S., Pendleton, G. N., and Kouveliotou, C. (1992). Spatial distribution of gamma-ray bursts observed by BATSE. *Nature*, 355:143–145.
- Meegan, C. A., Pendleton, G. N., Briggs, M. S., Kouveliotou, C., Koshut, T. M., Lestrade, J. P., Pacieras, W. S., McCollough, M. L., Brainerd, J. J., Horack, J. M., Hakkila, J., Henze, W., Preece, R. D., Mallozzi, R. S., and Fishman, G. J. (1996). The Third BATSE Gamma-Ray Burst Catalog. *ApJS*, 106:65–+.
- Mereghetti, S., Götz, D., Borkowski, J., Walter, R., and Pedersen, H. (2003). The INTEGRAL Burst Alert System. *A&A*, 411:L291–L297.
- Mészáros, P. (2002). Theories of Gamma-Ray Bursts. *ARA&A*, 40:137–169.
- Mészáros, P. (2006). Gamma-ray bursts. *Reports on Progress in Physics*, 69:2259–2321.
- Meszáros, P. and Rees, M. J. (1993). Relativistic fireballs and their impact on external matter - Models for cosmological gamma-ray bursts. *ApJ*, 405:278–284.
- Mészáros, P. and Rees, M. J. (1999). GRB 990123: reverse and internal shock flashes and late afterglow behaviour. *MNRAS*, 306:L39–L43.
- Mirabal, N., Halpern, J. P., An, D., Thorstensen, J. R., and Terndrup, D. M. (2006). GRB 060218/SN 2006aj: A Gamma-Ray Burst and Prompt Supernova at $z = 0.0335$. *ApJL*, 643:L99–L102.
- Mirabal, N., Halpern, J. P., and O’Brien, P. T. (2007). GRB 050826: A Subluminous Event at $z=0.296$ Finds Its Place in the Luminosity Distribution of Gamma-Ray Burst Afterglows. *ApJL*, 661:L127–L130.
- Mirabal, N., Halpern, J. P., and Wagner, R. M. (2000). GRB 000418, optical observation. *GRB Coordinates Network*, 650:1–+.
- Nardini, M., Ghisellini, G., Ghirlanda, G., Tavecchio, F., Firmani, C., and Lazzati, D. (2006). Clustering of the optical-afterglow luminosities of long gamma-ray bursts. *A&A*, 451:821–833.
- Natarajan, P., Albanna, B., Hjorth, J., Ramirez-Ruiz, E., Tanvir, N., and Wijers, R. (2005). The redshift distribution of gamma-ray bursts revisited. *MNRAS*, 364:L8–L12.
- Norris, J. P., Marani, G. F., and Bonnell, J. T. (2000). Connection between Energy-dependent Lags and Peak Luminosity in Gamma-Ray Bursts. *ApJ*, 534:248–257.
- Nuza, S. E., Tissera, P. B., Pellizza, L. J., Lambas, D. G., Scannapieco, C., and de Rossi, M. E. (2007). The host galaxies of long-duration gamma-ray bursts in a cosmological hierarchical scenario. *MNRAS*, 375:665–672.
- Odehahn, S. C., Djorgovski, S. G., Kulkarni, S. R., Dickinson, M., Frail, D. A., Ramaprakash, A. N., Bloom, J. S., Adelberger, K. L., Halpern, J., Helfand, D. J., Bahcall, J., Goodrich, R., Frontera, F., Feroci, M., Piro, L., and Costa, E. (1998). The Host Galaxy of the Gamma-Ray Burst 971214. *ApJL*, 509:L5–L8.
- Ofek, E. O., Cenko, S. B., Gal-Yam, A., Fox, D. B., Nakar, E., Rau, A., Frail, D. A., Kulkarni, S. R., Price, P. A., Schmidt, B. P., Soderberg, A. M., Peterson, B., Berger, E., Sharon, K., Shemmer, O., Penprase, B. E., Chevalier, R. A., Brown, P. J., Burrows, D. N., Gehrels, N., Harrison, F., Holland, S. T., Mangano, V., McCarthy, P. J., Moon, D.-S., Nousek, J. A., Persson, S. E., Piran, T., and Sari, R. (2007). GRB 060505: A Possible Short-Duration Gamma-Ray Burst in a Star-forming Region at a Redshift of 0.09. *ApJ*, 662:1129–1135.
- O’Shaughnessy, R., Belczynski, K., and Kalogera, V. (2008). Short Gamma-Ray Bursts and Binary Mergers in Spiral and Elliptical Galaxies: Redshift Distribution and Hosts. *ApJ*, 675:566–585.

- Paciesas, W. S., Meegan, C. A., Pendleton, G. N., Briggs, M. S., Kouveliotou, C., Koshut, T. M., Lestrade, J. P., McCollough, M. L., Brainerd, J. J., Hakkila, J., Henze, W., Preece, R. D., Connaughton, V., Kippen, R. M., Mallozzi, R. S., Fishman, G. J., Richardson, G. A., and Sahi, M. (2000). The Fourth BATSE Burst Revised Catalog (Paciesas+ 1999). *VizieR Online Data Catalog*, 9020:0+.
- Palazzi, E., Masetti, N., and Pian, E. (1999). Updated astrometry for the IR counterpart of GRB990705. *GRB Coordinates Network*, 382:1+.
- Parsons, A. M., Cummings, J. R., Gehrels, N., Goad, M. R., Gronwall, C., Holland, S. T., Kennea, J. A., La Parola, V., Mangano, V., Marshall, F. E., McLean, K. M., Pagani, C., Palmer, D. M., Romano, P., and Stamatikos, M. (2006). GRB 060614: Swift detection of a burst with a bright optical and X-ray counterpart. *GRB Coordinates Network*, 5252:1+.
- Peterson, B. A. and Price, P. A. (2003). GRB 030328: optical afterglow candidate. *GRB Coordinates Network*, 1974:1+.
- Piran, T. (1999). Gamma-ray bursts and the fireball model. *Phys. Rep.*, 314:575–667.
- Piran, T. (2005). The physics of gamma-ray bursts. *Reviews of Modern Physics*, 76:1143–1210.
- Porciani, C. and Madau, P. (2001). On the Association of Gamma-Ray Bursts with Massive Stars: Implications for Number Counts and Lensing Statistics. *ApJ*, 548:522–531.
- Price, P. (2000). GRB000911: corrected coordinates. *GRB Coordinates Network*, 799:1+.
- Price, P. A., Cowie, L. L., Minezaki, T., Schmidt, B. P., Songaila, A., and Yoshii, Y. (2006). Cosmological Implications of the Very High Redshift GRB 050904. *ApJ*, 645:851–855.
- Price, P. A., Harrison, F. A., Galama, T. J., Reichart, D. E., Axelrod, T. S., Berger, E., Bloom, J. S., Busche, J., Cline, T., Diercks, A., Djorgovski, S. G., Frail, D. A., Gal-Yam, A., Halpern, J., Holtzman, J. A., Hunt, M., Hurley, K., Jacoby, B., Kimble, R., Kulkarni, S. R., Mirabal, N., Morrison, G., Ofek, E., Pevunova, O., Sari, R., Schmidt, B. P., Turnshek, D., and Yost, S. (2001). Multicolor Observations of the GRB 000926 Afterglow. *ApJL*, 549:L7–L10.
- Price, P. A., Kulkarni, S. R., Berger, E., Djorgovski, S. G., Frail, D. A., Mahabal, A., Fox, D. W., Harrison, F. A., Bloom, J. S., Yost, S. A., Reichart, D. E., Henden, A. A., Ricker, G. R., van der Spek, R., Hurley, K., Atteia, J.-L., Kawai, N., Fenimore, E., and Graziani, C. (2002). GRB 010921: Discovery of the First High Energy Transient Explorer Afterglow. *ApJL*, 571:L121–L125.
- Price, P. A., Songaila, A., Cowie, L. L., Bell Burnell, J., Berger, E., Cucchiara, A., Fox, D. B., Hook, I., Kulkarni, S. R., Penprase, B., Roth, K. C., and Schmidt, B. (2007). Properties of a Gamma-Ray Burst Host Galaxy at $z \sim 5$. *ApJL*, 663:L57–L60.
- Prochaska, J. X., Bloom, J. S., Chen, H.-W., Hurley, K. C., Melbourne, J., Dressler, A., Graham, J. R., Osip, D. J., and Vacca, W. D. (2004). The Host Galaxy of GRB 031203: Implications of Its Low Metallicity, Low Redshift, and Starburst Nature. *ApJ*, 611:200–207.
- Prochaska, J. X., Chen, H.-W., Dessauges-Zavadsky, M., and Bloom, J. S. (2007). Probing the Interstellar Medium near Star-forming Regions with Gamma-Ray Burst Afterglow Spectroscopy: Gas, Metals, and Dust. *ApJ*, 666:267–280.
- Racusin, J. L., Liang, E. W., Burrows, D. N., Falcone, A., Sakamoto, T., Zhang, B. B., Zhang, B., Evans, P., and Osborne, J. (2009). Jet Breaks and Energetics of Swift Gamma-Ray Burst X-Ray Afterglows. *ApJ*, 698:43–74.
- Rau, A., Greiner, J., Klose, S., Salvato, M., Castro Cerón, J. M., Hartmann, D. H., Fruchter, A., Levan, A., Tanvir, N. R., Gorosabel, J., Hjorth, J., Zeh, A., Küpcü Yoldaş, A., Beaulieu, J. P., Donatowicz, J., Vinter, C., Castro-Tirado, A. J., Fynbo, J. P. U., Kann, D. A., Kouveliotou, C., Masetti, N., Møller, P., Palazzi, E., Pian, E., Rhoads, J., Wijers, R. A. M. J., and van den Heuvel, E. P. J. (2004). Discovery of the near-IR afterglow and of the host of GRB 030528. *A&A*, 427:815–823.
- Rees, M. J. and Meszaros, P. (1992). Relativistic fireballs - Energy conversion and time-scales. *MNRAS*, 258:41P–43P.
- Rees, M. J. and Meszaros, P. (1994). Unsteady outflow models for cosmological gamma-ray bursts. *ApJL*, 430:L93–L96.

- Reichart, D. E. and Stephens, A. W. (2000). The Fading of Supernova Remnant Cassiopeia A from 38 MHz to 16.5 GHz from 1949 to 1999 with New Observations at 1405 MHz. *ApJ*, 537:904–908.
- Rhoads, J. E. (1997). How to Tell a Jet from a Balloon: A Proposed Test for Beaming in Gamma-Ray Bursts. *ApJL*, 487:L1+.
- Richer, M. G. and McCall, M. L. (1995). Oxygen abundances in diffuse ellipticals and the metallicity-luminosity relations for dwarf galaxies. *ApJ*, 445:642–659.
- Roming, P. W. A., Kennedy, T. E., Mason, K. O., Nousek, J. A., Ahr, L., Bingham, R. E., Broos, P. S., Carter, M. J., Hancock, B. K., Huckle, H. E., Hunsberger, S. D., Kawakami, H., Killough, R., Koch, T. S., McLelland, M. K., Smith, K., Smith, P. J., Soto, J. C., Boyd, P. T., Breeveld, A. A., Holland, S. T., Ivanushkina, M., Pryzby, M. S., Still, M. D., and Stock, J. (2005). The Swift Ultra-Violet/Optical Telescope. *Space Science Reviews*, 120:95–142.
- Sahu, K. C., Vreeswijk, P., Bakos, G., Menzies, J. W., Bragaglia, A., Frontera, F., Piro, L., Albrow, M. D., Bond, I. A., Bower, R., Caldwell, J. A. R., Castro-Tirado, A. J., Courbin, F., Dominik, M., Fynbo, J. U., Galama, T., Glazebrook, K., Greenhill, J., Gorosabel, J., Hearnshaw, J., Hill, K., Hjorth, J., Kane, S., Kilmartin, P. M., Kouveliotou, C., Martin, R., Masetti, N., Maxted, P., Minniti, D., Møller, P., Muraki, Y., Nakamura, T., Noda, S., Ohnishi, K., Palazzi, E., van Paradijs, J., Pian, E., Pollard, K. R., Rattenbury, N. J., Reid, M., Rol, E., Saito, T., Sackett, P. D., Saizar, P., Tinney, C., Vermaak, P., Watson, R., Williams, A., Yock, P., and Dar, A. (2000). Discovery of the Optical Counterpart and Early Optical Observations of GRB 990712. *ApJ*, 540:74–80.
- Sakamoto, T., Lamb, D. Q., Kawai, N., Yoshida, A., Graziani, C., Fenimore, E. E., Donaghy, T. Q., Matsuoka, M., Suzuki, M., Ricker, G., Atteia, J.-L., Shirasaki, Y., Tamagawa, T., Torii, K., Galassi, M., Doty, J., Vanderspek, R., Crew, G. B., Villaseñor, J., Butler, N., Prigozhin, G., Jernigan, J. G., Barraud, C., Boer, M., Dezalay, J.-P., Olive, J.-F., Hurley, K., Levine, A., Monnelly, G., Martel, F., Morgan, E., Woosley, S. E., Cline, T., Braga, J., Manchanda, R., Pizzichini, G., Takagishi, K., and Yamauchi, M. (2005). Global Characteristics of X-Ray Flashes and X-Ray-Rich Gamma-Ray Bursts Observed by HETE-2. *ApJ*, 629:311–327.
- Salvaterra, R. and Chincarini, G. (2007). The Gamma-Ray Burst Luminosity Function in the Light of the Swift 2 Year Data. *ApJL*, 656:L49–L52.
- Salvaterra, R., Della Valle, M., Campana, S., Chincarini, G., Covino, S., D’Avanzo, P., Fernandez-Soto, A., Guidorzi, C., and et al (2009a). GRB 090423 reveals an exploding star at the epoch of re-ionization. *ArXiv:astro-ph/0906.1578*.
- Salvaterra, R., Guidorzi, C., Campana, S., Chincarini, G., and Tagliaferri, G. (2009b). Evidence for luminosity evolution of long gamma-ray bursts in Swift data. *MNRAS*, pages 602–+.
- Sari, R., Piran, T., and Narayan, R. (1998). Spectra and Light Curves of Gamma-Ray Burst Afterglows. *ApJL*, 497:L17+.
- Savaglio, S. (2006). GRBs as cosmological probes and cosmic chemical evolution. *New Journal of Physics*, 8:195–+.
- Savaglio, S., Fall, S. M., and Fiore, F. (2003). Heavy-Element Abundances and Dust Depletions in the Host Galaxies of Three Gamma-Ray Bursts. *ApJ*, 585:638–646.
- Savaglio, S., Glazebrook, K., and Le Borgne, D. (2008). The Galaxy Population Hosting Gamma-Ray Bursts. *ArXiv e-prints*, 803.
- Spergel, D. N., Verde, L., Peiris, H. V., Komatsu, E., Nolte, M. R., Bennett, C. L., Halpern, M., Hinshaw, G., Jarosik, N., Kogut, A., Limon, M., Meyer, S. S., Page, L., Tucker, G. S., Weiland, J. L., Wollack, E., and Wright, E. L. (2003). First-Year Wilkinson Microwave Anisotropy Probe (WMAP) Observations: Determination of Cosmological Parameters. *ApJS*, 148:175–194.
- Springel, V., White, S. D. M., Jenkins, A., Frenk, C. S., Yoshida, N., Gao, L., Navarro, J., Thacker, R., Croton, D., Helly, J., Peacock, J. A., Cole, S., Thomas, P., Couchman, H., Evrard, A., Colberg, J., and Pearce, F. (2005). Simulations of the formation, evolution and clustering of galaxies and quasars. *Nature*, 435:629–636.
- Stanek, K. Z., Gnedin, O. Y., Beacom, J. F., Gould, A. P., Johnson, J. A., Kollmeier, J. A., Modjaz, M., Pinsonneault, M. H., Pogge, R., and Weinberg, D. H. (2006). Protecting Life in the Milky Way: Metals Keep the GRBs Away. *Acta Astronomica*, 56:333–345.

- Stanek, K. Z., Matheson, T., Garnavich, P. M., Martini, P., Berlind, P., Caldwell, N., Challis, P., Brown, W. R., Schild, R., Krisciunas, K., Calkins, M. L., Lee, J. C., Hathi, N., Jansen, R. A., Windhorst, R., Echevarria, L., Eisenstein, D. J., Pindor, B., Olszewski, E. W., Harding, P., Holland, S. T., and Bersier, D. (2003). Spectroscopic Discovery of the Supernova 2003dh Associated with GRB 030329. *ApJL*, 591:L17–L20.
- Subrahmanyan, R., Kulkarni, S. R., Berger, E., and Frail, D. A. (2001). GRB 011121: radio observations. *GRB Coordinates Network*, 1156:1–+.
- Tanvir, N. R. and Levan, A. J. (2007). The population of GRB hosts. *ArXiv e-prints*.
- Tanvir et al. (2009). A glimpse of the end of the dark ages: the gamma-ray burst of 23 April 2009 at redshift 8.3. *ArXiv:astro-ph/0906.1577*.
- Tavani, M., Barbiellini, G., Argan, A., Basset, M., Boffelli, F., Bulgarelli, A., Caraveo, P., Chen, A., Costa, E., De Paris, G., Del Monte, E., Di Cocco, G., Donnarumma, I., Feroci, M., Fiorini, M., Foggetta, L., Froyland, T., Frutti, M., Fuschino, F., Galli, M., Gianotti, F., Giuliani, A., Labanti, C., Lapshov, I., Lazzarotto, F., Liello, F., Lipari, P., Longo, F., Marisaldi, M., Mastropietro, M., Mattaini, E., Mauri, F., Mereghetti, S., Morelli, E., Morselli, A., Pacciani, L., Pellizzoni, A., Perotti, F., Picozza, P., Pittori, C., Pontoni, C., Porrovecchio, G., Prest, M., Pucella, G., Rapisarda, M., Rossi, E., Rubini, A., Soffitta, P., Traci, A., Trifoglio, M., Trois, A., Vallazza, E., Vercellone, S., Zambra, A., and Zanello, D. (2006). The AGILE mission and its scientific instrument. In *Society of Photo-Optical Instrumentation Engineers (SPIE) Conference Series*, volume 6266 of *Society of Photo-Optical Instrumentation Engineers (SPIE) Conference Series*.
- Taylor, G. B., Frail, D. A., Beasley, A. J., and Kulkarni, S. R. (1998). GRB980703 very long baseline interferometry. *GRB Coordinates Network*, 152:1–+.
- Thompson, D. J. (2004). GLAST: GeV astronomy in a multiwavelength context. *New Astronomy Review*, 48:543–549.
- Totani, T. (1997). Cosmological Gamma-Ray Bursts and Evolution of Galaxies. *ApJL*, 486:L71.
- Totani, T., Kawai, N., Kosugi, G., Aoki, K., Yamada, T., Iye, M., Ohta, K., and Hattori, T. (2006). Implications for Cosmic Reionization from the Optical Afterglow Spectrum of the Gamma-Ray Burst 050904 at $z = 6.3$. *Astronomical Society of Japan*, 58:485–498.
- Tremonti, C. A., Heckman, T. M., Kauffmann, G., Brinchmann, J., Charlot, S., White, S. D. M., Seibert, M., Peng, E. W., Schlegel, D. J., Uomoto, A., Fukugita, M., and Brinkmann, J. (2004). The Origin of the Mass-Metallicity Relation: Insights from 53,000 Star-forming Galaxies in the Sloan Digital Sky Survey. *ApJ*, 613:898–913.
- Ubertini, P., Lebrun, F., Di Cocco, G., Bazzano, A., Bird, A. J., Broenstad, K., Goldwurm, A., La Rosa, G., Labanti, C., Laurent, P., Mirabel, I. F., Quadrini, E. M., Ramsey, B., Reglero, V., Sabau, L., Sacco, B., Staubert, R., Vigroux, L., Weisskopf, M. C., and Zdziarski, A. A. (2003). IBIS: The Imager on-board INTEGRAL. *A&A*, 411:L131–L139.
- van Paradijs, J., Kouveliotou, C., and Wijers, R. A. M. J. (2000). Gamma-Ray Burst Afterglows. *ARA&A*, 38:379–425.
- Vaughan, S., Willingale, R., O’Brien, P. T., Osborne, J. P., Reeves, J. N., Levan, A. J., Watson, M. G., Tedds, J. A., Watson, D., Santos-Lleó, M., Rodríguez-Pascual, P. M., and Schartel, N. (2004). The Discovery of an Evolving Dust-scattered X-Ray Halo around GRB 031203. *ApJL*, 603:L5–L8.
- Virgili, F. J., Zhang, B., Troja, E., and O’Brien, P. (2009). Type I gamma-ray bursts: Constraints from Monte Carlo simulations. In Meegan, C., Kouveliotou, C., and Gehrels, N., editors, *American Institute of Physics Conference Series*, volume 1133 of *American Institute of Physics Conference Series*, pages 118–120.
- Vreeswijk, P. M., Ellison, S. L., Ledoux, C., Wijers, R. A. M. J., Fynbo, J. P. U., Møller, P., Henden, A., Hjorth, J., Masi, G., Rol, E., Jensen, B. L., Tanvir, N., Levan, A., Castro Cerón, J. M., Gorosabel, J., Castro-Tirado, A. J., Fruchter, A. S., Kouveliotou, C., Burud, I., Rhoads, J., Masetti, N., Palazzi, E., Pian, E., Pedersen, H., Kaper, L., Gilmore, A., Kilmartin, P., Buckle, J. V., Seigar, M. S., Hartmann, D. H., Lindsay, K., and van den Heuvel, E. P. J. (2004). The host of GRB 030323 at $z=3.372$: A very high column density DLA system with a low metallicity. *A&A*, 419:927–940.

- Wainwright, C., Berger, E., and Penprase, B. E. (2007). A Morphological Study of Gamma-Ray Burst Host Galaxies. *ApJ*, 657:367–377.
- Wang, J., De Lucia, G., Kitzbichler, M. G., and White, S. D. M. (2008). The dependence of galaxy formation on cosmological parameters: can we distinguish between the WMAP1 and WMAP3 parameter sets? *MNRAS*, 384:1301–1315.
- Watson, D., Fynbo, J. P. U., Thöne, C. C., and Sollerman, J. (2007). No supernovae detected in two long-duration gamma-ray bursts. *Royal Society of London Philosophical Transactions Series A*, 365:1269–1275.
- Waxman, E., Kulkarni, S. R., and Frail, D. A. (1998). Implications of the Radio Afterglow from the Gamma-Ray Burst of 1997 May 8. *ApJ*, 497:288–+.
- Wijers, R. A. M. J., Bloom, J. S., Bagla, J. S., and Natarajan, P. (1998). Gamma-ray bursts from stellar remnants - Probing the universe at high redshift. *MNRAS*, 294:L13–L17.
- Willingale, R., O’Brien, P. T., Osborne, J. P., Godet, O., Page, K. L., Goad, M. R., Burrows, D. N., Zhang, B., Rol, E., Gehrels, N., and Chincarini, G. (2007). Testing the Standard Fireball Model of Gamma-Ray Bursts Using Late X-Ray Afterglows Measured by Swift. *ApJ*, 662:1093–1110.
- Wolf, C. and Podsiadlowski, P. (2007). The metallicity dependence of the long-duration gamma-ray burst rate from host galaxy luminosities. *MNRAS*, 375:1049–1058.
- Woosley, S. E. and Heger, A. (2006). The Progenitor Stars of Gamma-Ray Bursts. *ApJ*, 637:914–921.
- Yamaoka, H., Ayani, K., and Itagaki, K. (2004). GRB 041006: precise astrometry. *GRB Coordinates Network*, 2781:1–+.
- Yoon, S.-C., Langer, N., Cantiello, M., Woosley, S. E., and Glatzmaier, G. A. (2008). Evolution of Progenitor Stars of Type Ibc Supernovae and Long Gamma-Ray Bursts. In *IAU Symposium*, volume 250 of *IAU Symposium*, pages 231–236.
- Yoon, S.-C., Langer, N., and Norman, C. (2006). Single star progenitors of long gamma-ray bursts. I. Model grids and redshift dependent GRB rate. *A&A*, 460:199–208.
- Zhang, B. (2006). Astrophysics: A burst of new ideas. *Nature*, 444:1010–1011.
- Zhang, B. (2007). Gamma-Ray Bursts in the Swift Era. *Chinese Journal of Astronomy and Astrophysics*, 7:1–50.
- Zhang, B. and Mészáros, P. (2004). Gamma-Ray Bursts: progress, problems & prospects. *International Journal of Modern Physics A*, 19:2385–2472.
- Zucca, E., Ilbert, O., Bardelli, S., Tresse, L., Zamorani, G., Arnouts, S., Pozzetti, L., Bolzonella, M., McCracken, H. J., Bottini, D., Garilli, B., Le Brun, V., Le Fèvre, O., Maccagni, D., Picat, J. P., Scaramella, R., Scodreggio, M., Vettolani, G., Zanichelli, A., Adami, C., Arnaboldi, M., Cappi, A., Charlot, S., Ciliegi, P., Contini, T., Foucaud, S., Franzetti, P., Gavignaud, L., Guzzo, L., Iovino, A., Marano, B., Marinoni, C., Mazure, A., Meneux, B., Merighi, R., Paltani, S., Pellò, R., Pollo, A., Radovich, M., Bondi, M., Bongiorno, A., Busarello, G., Cucciati, O., Gregorini, L., Lamareille, F., Mathez, G., Mellier, Y., Merluzzi, P., Ripepi, V., and Rizzo, D. (2006). The VIMOS VLT Deep Survey. Evolution of the luminosity functions by galaxy type up to $z = 1.5$ from first epoch data. *A&A*, 455:879–890.